A STUDY OF THE PERFORMANCE OF DIAMOND WIRE IN HARD NATURAL STONE

by

Paul William Butler - Smith

Submitted to the University of Cape Town in fulfilment of the requirements for the Degree of Master of Science in Engineering

Date 30 September 1997

ABSTRACT

Diamond wire has been developed as a flexible cutting tool and is used by the natural stone industry for the quarrying of blocks and for subsequent squaring, slabbing and shaping operations in the stone yard. The performance of diamond wire depends on how its beads wear and the optimum life is achieved when the diamond particles are consumed in a desired manner from the periphery of each bead. This thesis covers diamond related aspects which influence the performance of diamond wire.

An investigation is made of the wear of diamond particles in the bead matrix and a comparison is made with diamond particle wear found in other diamond tools. Bead matrix wear progressions are described, pertaining to diamond wire sawing operating conditions.

An equation of chip thickness in relation to the cutting action of a diamond segment is derived and chip thicknesses are determined for wire sawing operating parameters used in different stone types. The sawability and abrasivity properties of stone are evaluated and are compared with corresponding results of diamond wire life.

Formulae are derived for the approximation of the length of cut and area sawn in quarrying and stationary wire sawing applications and for the forces acting on a bead over a constant cutting radius. A method of testing single diamond beads is

used for comparative assessments of different diamond grades and the effects of applied load, cutting velocity and cutting rate are examined in relation to bead wear. High speed video imaging is used to analyse the dynamics of diamond wire in operation and the problems associated with uneven bead wear.

ACKNOWLEDGEMENTS

I would like to extend my sincere thanks and appreciation to:

Associate Professor J. Gryzagoridis for his valued guidance in the work carried out for this thesis.

Associate Professor R. B. Tait for his assistance with the scanning electron microscopy of diamond wire beads.

Mr L. Watkins and Mr A. Warburton for preparing the diamond wire test beads and manufacturing the single bead testing apparatus.

Mr E. N. Von Guerard for his assistance in providing the facilities for single bead testing.

and to my wife Jen for her understanding
frequent field trips.

TABLE OF CONTENTS

LIST OF ILLUSTRATIONS

Page

List of Plates

List of Figures

List of Tables

List of Graphs

CHAPTER 1

A BACKGROUND TO DIAMOND WIRE

1.1 Early developments in diamond tool manufacture

The increasing success of diamond tools in natural stone and construction applications can largely be attributed to the continuing development of diamond abrasive products and the methods which bond diamond into suitable cutting tool elements. The origins of this technology can be traced back to 1751, when the drill bit was first described by Diderot (1), followed by Hermann's successful patent application in 1854 for various derivatives of single point diamond cutting tools for stone. The diamond circular saw blade was later designed by Fromholt (1) in 1885 and further developed by Jacquin (2).

Early tools were manufactured using natural diamonds of polycrystalline structure, which were set by hand in various configurations onto the cutting elements of the tool. With ensuing development, circular saw blades, used in the early part of this century, consisted of hardened and tensioned steel discs with cast steel sockets set around the periphery. Rounded diamonds, referred to as carbonada of up to 0,8 carats in mass, were individually hand set into a hole in each socket drilled just large enough to accept the diamond. Each socket was firmly gripped with a set of copper jaws through which an electric current was passed for a few seconds to soften the steel and secure the diamond. Normally about 0,75 mm of diamond protruded from the socket (3).

Poor tool performance resulting from rapid wear of the sockets and premature loss of the diamonds prompted the development of metal powder matrix technology in the late 1930's for bonding diamond to the tool. Industrial grade natural diamond particles that were appropriately sized, were homogeneously mixed with predominantly bronze based powders and cold pressed into the required segment form. The segments were sintered under pressure at temperatures determined by the melting point of the metal powder, normally in an inert or oxygen reducing atmosphere to minimise the risk of graphitising the diamond (which occurs at temperatures above 900 degrees Celsius with oxygen present). The sintered segments were then braised onto the steel body of the tool. Studies of stone cutting mechanisms indicated that the removal of a smaller volume of material per pass at a faster cutting rate was more efficient and produced superior finishes than taking deep cuts (4).

Once it was realised that diamond was just another crystal form of carbon, various attempts were made to convert carbon into diamond. Claims of success in diamond synthesis in the late 1800's and the early 1900's by Hannay (5), Parsons (6) and others were proven false by data which were later established. In 1938 Rossini and Jessup (7) calculated the theoretical pressure-temperature equilibrium for the graphite-diamond transition up to 1300 degrees Celsius. Applying results of measurements of the coefficient of expansion of diamond, Berman and Simon (8) found that a linear extrapolation above 1200 Kelvin, as shown in Figure 1.1, would best meet the conditions for the formation of diamond.

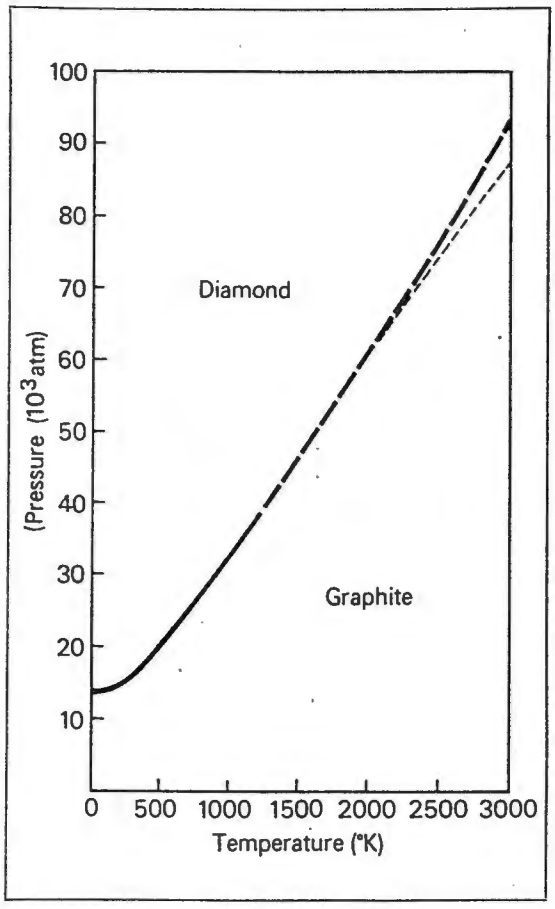

Figure 1.1 Pressure temperature diagram of the diamond graphite equilibrium (8)

Leipunskii (9) argued that the formation of diamond from graphite in the solid state would take place at a minimum temperature of 2000 Kelvin and a pressure of around 6000 MPa. By using a suitable solvent for carbon it would be possible to obtain diamond at a lower temperature and a correspondingly lower pressure. Carbon is soluble in many metals and most notably, iron. The solubility which increases with temperature rises to about 9 percent in iron at 2200 degrees Celsius. If the solution is cooled, carbon will be deposited as graphite at pressures below the equilibrium curve and as diamond at pressures above the curve. The pioneering work by Bridgman (10) in 1946 on a high pressure

apparatus, made it possible to achieve these conditions and results of experiments in which diamond was repeatedly formed were published in 1955. In 1963, Bundy (11) published results of experiments on the melting temperature of graphite as a function of pressure and these were later confirmed by Fateeva and Vereshchagin (12). See Figure 1.2 (13).

The commercial introduction of synthetic diamond products in the late 1950's and subsequent improvements in manufacturing and processing techniques has lead to significant improvements in tool life. It is now possible for properties such as crystal size, shape and toughness (resistance to fracture) to be engineered into a product.

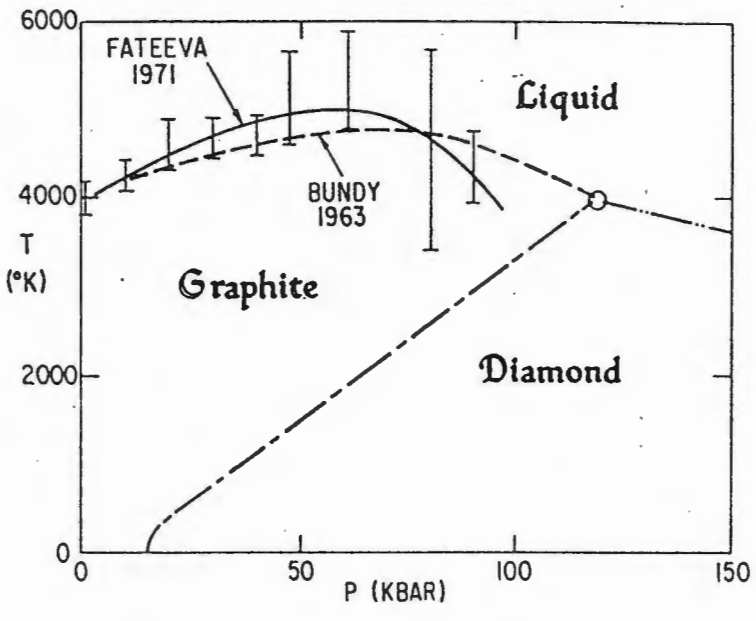

Figure 1.2 The melting temperature of graphite as a function of pressure (13)

1.2 The development of diamond wire

The quarrying of calcareous rock for decorative applications is usually carried out by cutting or controlled splitting methods opposed to explosive techniques which cause severe cracking of the deposit. Helical wire sawing was a widely used cutting method in marble quarries. The system consisted of a helical steel cable driven by a pulley and used siliceous sand or steel shot as the abrasive which was continuously fed into the cut at appropriate points. The system however was not ideal as the helical cable, sometimes stretching for kilometres over numerous pulleys, had a high wear rate and required frequent replacement. It was also difficult to recycle the large quantities of loose abrasive used for cutting. Based on the successful performance of diamond in circular sawing applications of natural stone, research was initiated on diamond wire as a replacement for the helical wire system.

Impregnated Diamond Products and their owners, Bath and Portland Stone Firms Ltd. claimed to have run a confidential research project (4) between 1955 and 1957, to test the idea of diamond wire sawing but they were unsuccessful in their attempts. Prowse (14) from the United Kingdom based company Triefus, initiated experimental work in marble quarries, in Carrara, Italy in 1968, with diamond wire made up using a steel cable which was threaded alternately with diamond beads and spacers. The diamond beads consisted of steel tubes which were electroplated using nickel to retain the diamond. Various tests yielded some interesting data from the cuts that were carried out. Realising the potential of this concept for sawing in quarries, other diamond toolmaking firms started research into diamond wire sawing. Various field trials were carried out with diamond wires

and a number of methods of spacing the beads were evaluated. These consisted of assemblies as shown in Figure 1.3 using:-

(i) loose rubber sleeves positioned between each bead,
(ii) cotter pins which were inserted through the cable in front and behind each bead thereby locking them into position,
(iii) springs located between each bead and cotter pins inserted through the cable every few beads, so as to locate an assembly of beads and springs,
(iv) springs and crimps, the crimps performing the same function as the cotter pins mentioned in (iii) above.

The latter arrangement proved the most successful and various derivatives of this type were manufactured and tested. After reducing wire breakage problems which were initially experienced, by rigorous assessment of different cable designs, diamond wire sawing gradually became accepted in marble quarries since 1978. Large savings over the helical wire systems were reported from ensuing evaluations (15).

Most diamond wire manufactures standardised on an electroplated bead of approximately 6 mm in length with an external diameter of around 10 mm, threaded onto a cable of approximately 5 mm in diameter. Typically thirty beads are used per metre of diamond wire for marble applications.

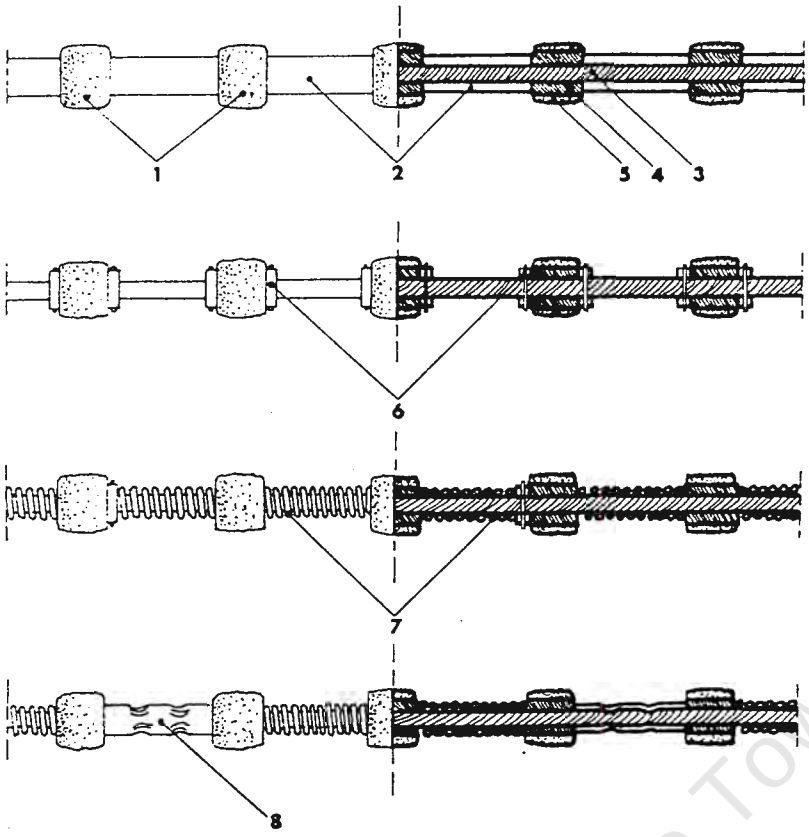

Key	
1	Bead
2	Spacer
3	Wire cable
4	Inner sleeve
5	Diamond layer
6	Cotter pin
7	Spring
8	Crimp

Figure 1.3 Early diamond wire designs (4)

Prior to the developments in marble quarries, wire sawing had not been seriously considered in the quarrying of siliceous material. A number of cutting and splitting techniques have been employed with varying levels of success in the primary operation of separating blocks of stone from the deposit and in the secondary operation of further reducing the blocks into manageable sizes. Due to its simplicity of use, thermal lancing, which works on the principle of spalling rock through localised heating, became one of the more popular methods used in the primary quarrying operations. Explosive techniques such as controlled blasting have also been widely employed and together with drilling, is still extensively used for the reduction of stone blocks of this material type. In some quarries, slot drilling, which produces a slot by drilling a series of overlapping holes in the rock, has been preferred in the primary operation. This technique produces a much wider cut, than that made by diamond wire sawing which, together with thermal

lancing and various explosive methods, damage the material beyond the cut, resulting in wastage of predominantly saleable material.

The success of diamond wire in marble quarries provided sufficient incentive to research its potential in the cutting of the much harder and more abrasive siliceous rock. However the loose spacer system was found unsuitable for the cutting of these materials, particularly granites having high quartz constituents, as rapid abrasive wear was encountered between the bead and cable (16). Diamond electroplated beads were also found unsuitable as the single layer of diamonds wore away rapidly, resulting in a short tool life. To overcome the problems of abrasion of the cable, diamond wires were developed using either injection moulded plastic or vulcanised rubber, which fully covers the cable and fixes the beads into position, thus eliminating any direct contact between the cable and the abrasive rock and between the bead and cable, as shown in Plate 1.1.

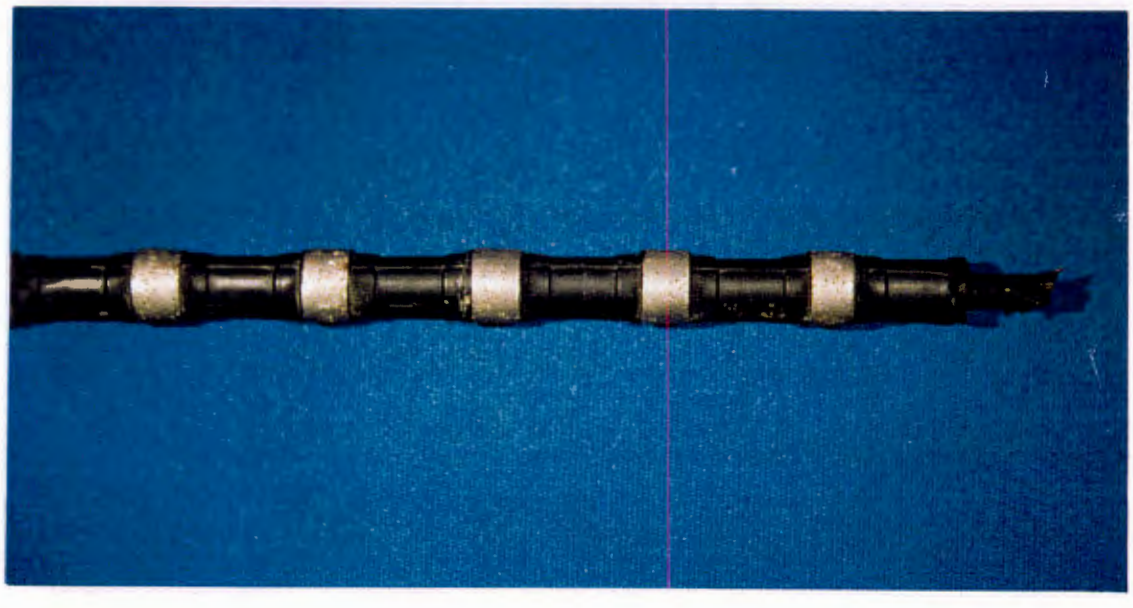

Plate 1.1 Diamond wire using the vulcanised rubber spacer system

The rapid wear of diamond electroplated beads was addressed by developing beads using diamond matrix sintering technology, similar to that used in the manufacture of diamond drill bits and diamond saw blades. In the manufacture of diamond wire beads, a matrix consisting of a mixture of diamond grit and metal powder is sintered in a hot pressing process onto the periphery of a steel sleeve, to produce the bead. Initial trials took place in granite quarries around the middle of the 1980's and good results were reported in the sawing of a number of siliceous materials (17). Diamond toolmakers have found that for most quarrying applications of this type of material, the best size of the sintered diamond bead is in the same order of the electroplated beads used for marble quarrying (an outer diameter of between 10 mm and 12 mm with a length in the region of 7 mm, threaded onto a cable of between 5 mm and 6 mm in diameter).

The attributes of the more popular techniques used in the quarrying of siliceous materials compared with those of diamond wire sawing are shown in Table 1.1.

Attribute / Method	Quarry yield	Productivity	Universality	Ease of operation	Noise pollution	Safety
Torch cutting	-	-	- -	+	- -	-
Classical explosive	- -	+	+	+	-	-
Smooth blasting	-	o	-	- -	-	-
Slot drilling	+	-	+	-	o	+
Diamond wire	+	+	+	o	+	o

Key	+	o	-	- -
	Advantage	Insignificant effect	Disadvantage	Negative or inhibitory criteria

Table 1.1 The attributes of methods employed in the quarrying of siliceous rock (18)

The overall performance of diamond wire has progressively improved by further development. Improved cutting rates and tool life have been achieved by developing sintered beads for use in specific materials by selecting a suitable diamond product and bond metal to attain a desired wear balance. Diamond wires using sintered beads have become well established in sawing applications of siliceous rock and wire sawing has become the preferred method of primary extraction for materials having finely dispersed mineral constituents, such as gabbro. Diamond wire sawing has become particularly beneficial where the yield of material from a quarry is of primary importance (19) as it produces flat smooth faces with a minimum of material wastage over large surface areas, as shown in Plates 1. 2 and 1. 3.

Plate 1. 2 Diamond wire sawing a bench of approximately 3 metres high in a granite quarry in Namaqaland

Plate 1.3 A gabbro rock face in excess of 300^2 metres, cut with diamond wire in a quarry near Rustenburg

While the diamond wire consisting of electroplated beads (spaced with springs and crimps) is still used to some extent in the sawing of calcareous materials, for example where rapid cutting rates are required, diamond wire using sintered beads bonded to the cable or for some marble applications, mounted with springs, have become increasingly popular and are now widely used due to their improved wear characteristics.

Designs of injection moulded polymer and vulcanised rubber bead mounting systems have been enhanced by improving the shear strength of the polymer and rubber, their adhesion to the metallic components and their flexibility. Improvements have also been made by a general reduction of the cross sectional area between beads, which is desirable in order to carry the flushing water and

silt debris in the cut. Wire breakages have been reduced by developing cable designs to accommodate the bending over small radii, experienced in a number of applications and improving the screw and sleeve type crimps which are used to join the wire.

Improvements to diamond wire sawing machines have also contributed to the reliability and performance of diamond wire. Slow start up and shut down facilities on wire sawing machines have reduced the frequency of breakage of the wire cable during transitionary periods. Improvements to the control systems of diamond wire saws have had a positive effect on diamond wire life by keeping the wire tension, and therefore the load on the wire beads, more constant during operation. This has been achieved by incorporating traverse rate, wire speed and cutting power control into diamond wire saws. (Wire speed and traverse rate are controlled by rotational and linear displacement of the drive pulley respectively through either amperage control in the case of an electric drive or pressure control when a hydraulic motor is used).

Diamond wire sawing is also used in the squaring and slabbing of siliceous blocks in the stone yard (see Plate 1.4). This has lead to increased efficiencies in the subsequent processes of cutting and polishing the material. With the availability of numerical control systems from the machine tool industry, multi-axis diamond wire profiling machines have been designed which enable intricate profiles to be cut in natural stone much more efficiently than the previously used circular sawing and grinding methods.

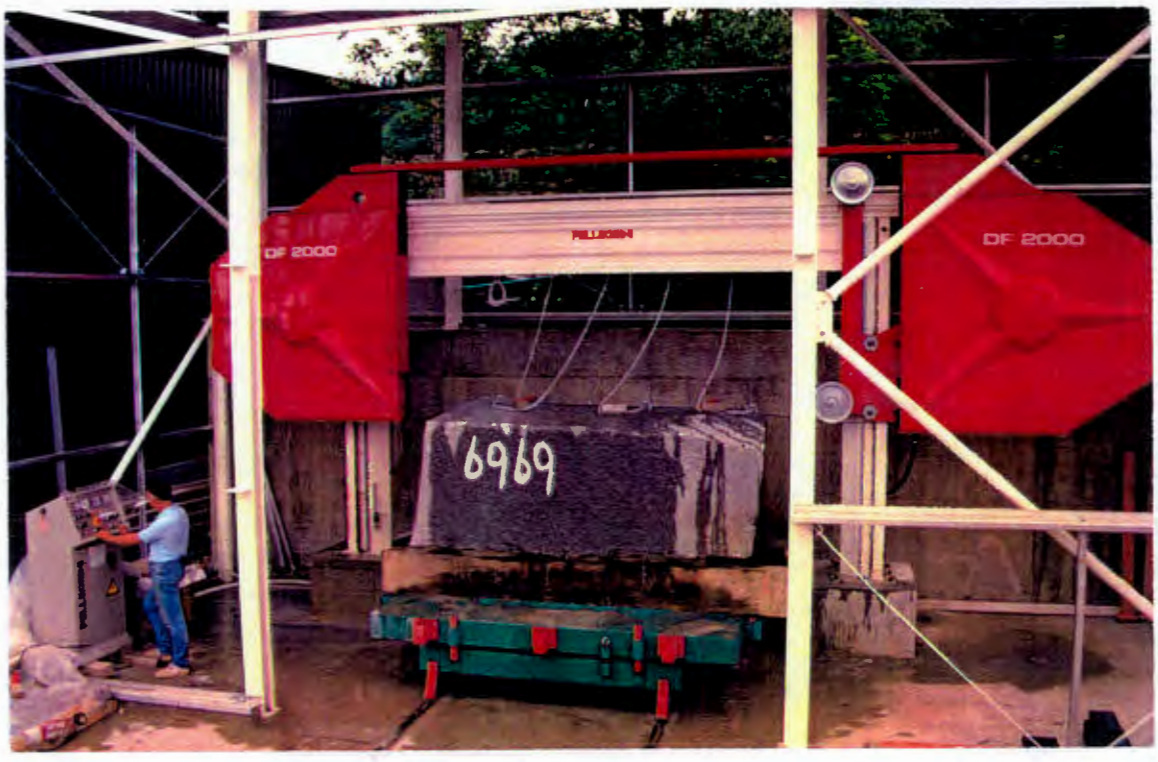

Plate 1.4 Diamond wire sawing of granite in a stone yard

1.3 The wear behaviour of diamond particles in a sintered tool matrix

The diamond and bond matrix which forms the cutting element of the tool is manufactured by moulding a carefully prepared mixture of diamond particles and metal powder into a required shape using a hot sintering process. Key factors in the design of the matrix are the choice and concentration of diamond and the metal powder that forms the bond. The selection is determined by the intended application in which the cutting forces and the material being cut are important considerations.

The matrix is designed to enable a number of diamond particles to be in contact with the material being worked at any one time, with each particle exhibiting an

individual life cycle. Under the correct conditions, the matrix has a self sharpening characteristic, as diamond particles are lost through abrasive wear, new particles progressively emerge from the matrix. Wear of the matrix is thus characterised by the balance achieved between the wear of each diamond particle and its retention by the bond material.

Buttner (20), studied the wear of diamond matrices when cutting natural stone and proposed that a diamond particle has four stages in its life cycle. These are initial coverage by the bond material, diamond particle exposure resulting from the erosion of the matrix, wear exhibited by the diamond particle during cutting and finally, erosion of the matrix to a point where the diamond particle is pulled out. He stated that under ideal conditions of operation, the load on the diamond particle results in controlled fracture whereby it eventually breaks down and presents new cutting points.

Alexandrov et.al. (21) evaluated the wear of diamond particles on a grinding apparatus and described the abrasive wear of a particle once it had emerged, as a steady growth of a 'bluntness area' on the grain, in the presence of characteristic grooves or furrows coinciding with the direction of grinding. This was followed by spalling of the particle in which the working surface underwent a major change, accompanied by the disappearance of the bluntness area.

Bailey and Bullen (22), in a study of diamond particle wear in circular sawing, classified four states of wear as; a good diamond, a diamond with wear flat, a rough diamond and a diamond having wear flat and rough. The results of their research showed that the wear behaviour of diamond particles was affected by the impact of the diamond particles with the work piece, which is dependent on

the rotational speed, and the forces on the diamond particles induced by direct mechanical loading.

Mamalis, et.al. (23) monitored the way in which diamond particles wore using a one segment sawing apparatus and categorised three wear states as, a particle without significant wear, a particle exhibiting a flattened area and a broken or fractured particle. It was found that, when sawing Colombo Red granite, a major proportion of particles were either fractured or flattened and when sawing the easier to cut Impala granite, the number of diamond particles without significant wear was higher. In fair agreement with Bailey and Bullen (15), Mamalis, et.al. concluded that the predominance of fractured particles was as a result of impact loading with cleavage fracturing caused by shock waves travelling through the particle.

In assessments of the wear behaviour of segments of a circular saw, Ertingshausen (24) suggested two hypotheses to explain diamond particle wear.

(i) As sawing progresses, the newly exposed diamond particles develop wear flats, causing cutting forces to increase which results in fracturing of the diamond particles. The diamond particles are then reduced in the form of splinters.
(ii) The points of newly exposed diamond break off after initial contact with the workpiece. Wear flats then develop and the particle is pulled out of the bond in this state, when the cutting forces exceed the strength of the anchorage.

Tonshoff and Warnecke (25) realised that in diamond tools such as circular saws and grinding wheels, the cutting edges of the diamond particles are not all

located at the same height, but are statistically distributed. The wear of diamond particles has been attributed to the combination of friction, compressive loads and associated local heating.

Wright (26) looked at the height of protrusion of diamond particles from the matrix during their working lives in circular sawing. He observed that with some particles, after initial fracture which reduced the protrusion, their working height was subsequently attained after a certain period of operation, as a result of a higher wear rate of the matrix in relation to the diamond particle. In later work, Wright, et. al. (27) studied the wear progression of diamond particles on a laboratory drill rig by observing their height of protrusion from the matrix over accumulated distances drilled in Pennant sandstone and Cornish Grey granite. It was found that in the more abrasive sandstone, the predominant wear mode was erosion of the bond material around the diamond, which resulted in the diamond particle being lost soon after fracturing. In the granite however, the breakdown of a diamond particle occurred at an earlier stage but it remained in the matrix for longer.

Miller and Ball, (28) carried out detailed examinations of the wear of the diamond matrix in drilling experiments and identified two different sequences of diamond particle wear. At sub-optimal loads, i.e. where the rate of penetration of the bit decreased steadily for a given applied load, newly exposed diamond particles tended to develop large wear flats. This phenomena was also observed on diamond particles that had fractured. At loads where the rate of penetration remained steady for a given applied load, it was found that the sharp edges of newly exposed diamond particles became rounded. This led to transitory wear flats which broke up by micro fracturing, with possible cyclical repetition of these

two stages. Complete fracture ultimately reduced the diamond particle to splinters and its eventual loss from the matrix.

The wear flat surface of diamond particles exhibited striations with grooves of varying depths, orientated in the direction of travel. Steps were also evident on the surface, approximately transverse to the direction of travel and these eventually contributed to the micro fracture of the diamond particle at loads above the sub-optimal transition.

1.4 The selection criteria for diamond and the bond material in sintered cutting tools

The testing and evaluation of industrial diamond abrasives is continually being carried out by the major producers, resulting in improvements of product and the criteria used for selection. It has been recognised that the diamond particle size, the impact strength and thermal stability have a major effect on the way the particles behaves in an application, therefore indices have been derived to rank these properties.

1.4.1 Diamond type

(i) Natural diamond

The early diamond abrasive products were of natural origin and different characteristics were obtained by processing industrial grade diamond by crushing, sizing and sorting the diamond grit into categories of shape. The

thermal stability of natural diamond is somewhat higher than synthetic diamond, allowing matrix sintering temperatures of 1300 degrees Celsius to be reached without danger of graphitisation. Natural diamond particles are generally of irregular shape which makes them particularly suitable for applications where particle retention is important, such as with diamond electroplated tools.

(ii) Synthetic diamond

The morphology of synthetic diamond crystals can be controlled to an extent in the manufacturing process which enables diamond particles, having known properties such as thermal stability and impact strength, to be produced. High quality synthetic diamond consisting of regular crystalline particles having few inclusions, allow matrix sintering temperatures of 1100 degrees Celsius to be used without danger of graphitisation. Some lower grades having irregular shapes and greater amounts of inclusions will start to graphitise at temperatures below 1100 degrees Celsius. The consistency of synthetic diamond products is achieved by processing and grading the diamond grit produced, into categories of size, strength, shape and inclusions.

Synthetic diamond producers have based their technology on either exclusively using nickel or cobalt based solvents and although each producer claimed particular benefits of their products, no direct comparison was made on any differences that might exist in the particle wear behaviour. The recent availability of products manufactured with both types of solvent from one producer facilitated a direct comparison between the two product types (29) and the findings have enhanced the selection criteria of synthetic diamond.

1.4.2 Diamond particle strength

One of the foremost techniques used to quantify the strength of a diamond product was the Friartester developed by Belling and Dyer (30) which determines the resistance to impact of a diamond grit sample by subjecting it to a number of controlled blows by a ball in a capsule. The sample's friability value is related to the mass of non-fractured particles which remain after the test to the mass of fractured particles. Tests are carried out to obtain the sample's friability value at room temperature, referred to as the toughness index (TI) value and at elevated temperatures, typically at 900 and 1100 degrees Celsius, to obtain the thermal toughness index (TTI) values.

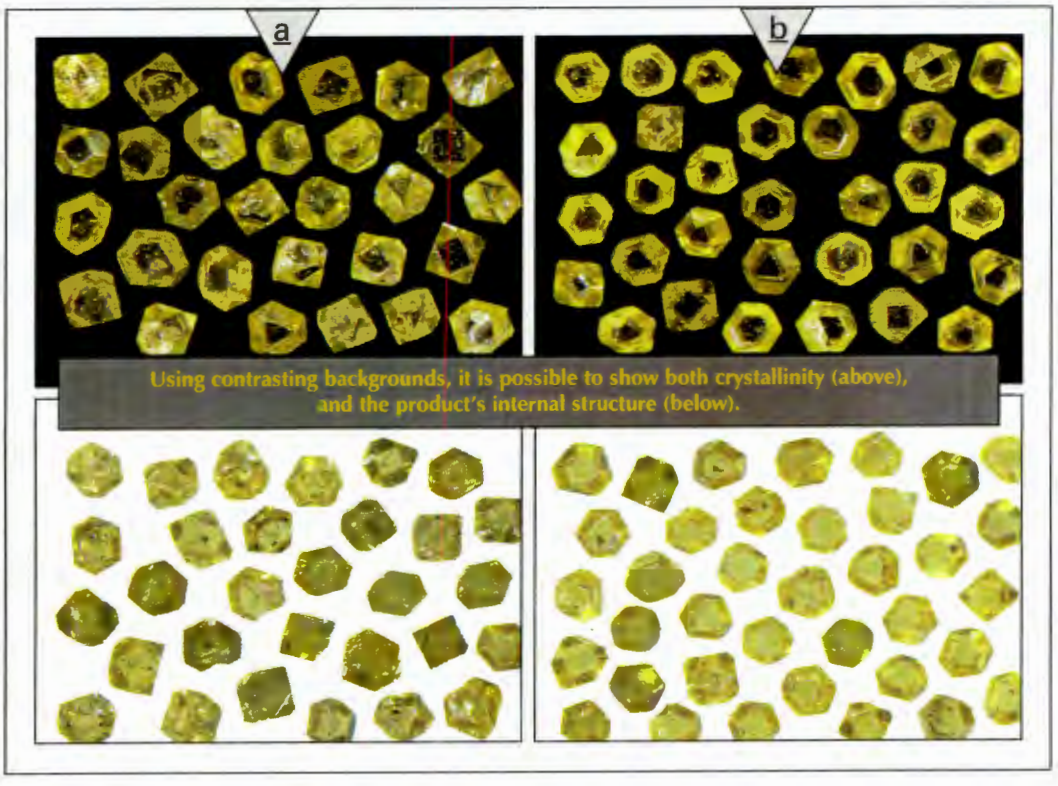

Key	a	SDA 85+ from synthesis process using cobalt based solvent
	b	SDB 1085 from synthesis process using nickel based solvent

Plate 1.5 Synthetic diamond products from different synthesis process having similar TI strengths but with visual dissimilarities (29)

The limitations of the friability test relating to product performance, are highlighted by the fact that while the friability index values of certain synthetic diamond grades may be similar, they may visually look different, as can be seen from Plate 1.5. It was suspected that behavioural differences existed between the two synthetic diamond types, particularly as the characteristics of the inclusions are different and therefore further classification was desirable in order to better define the product.

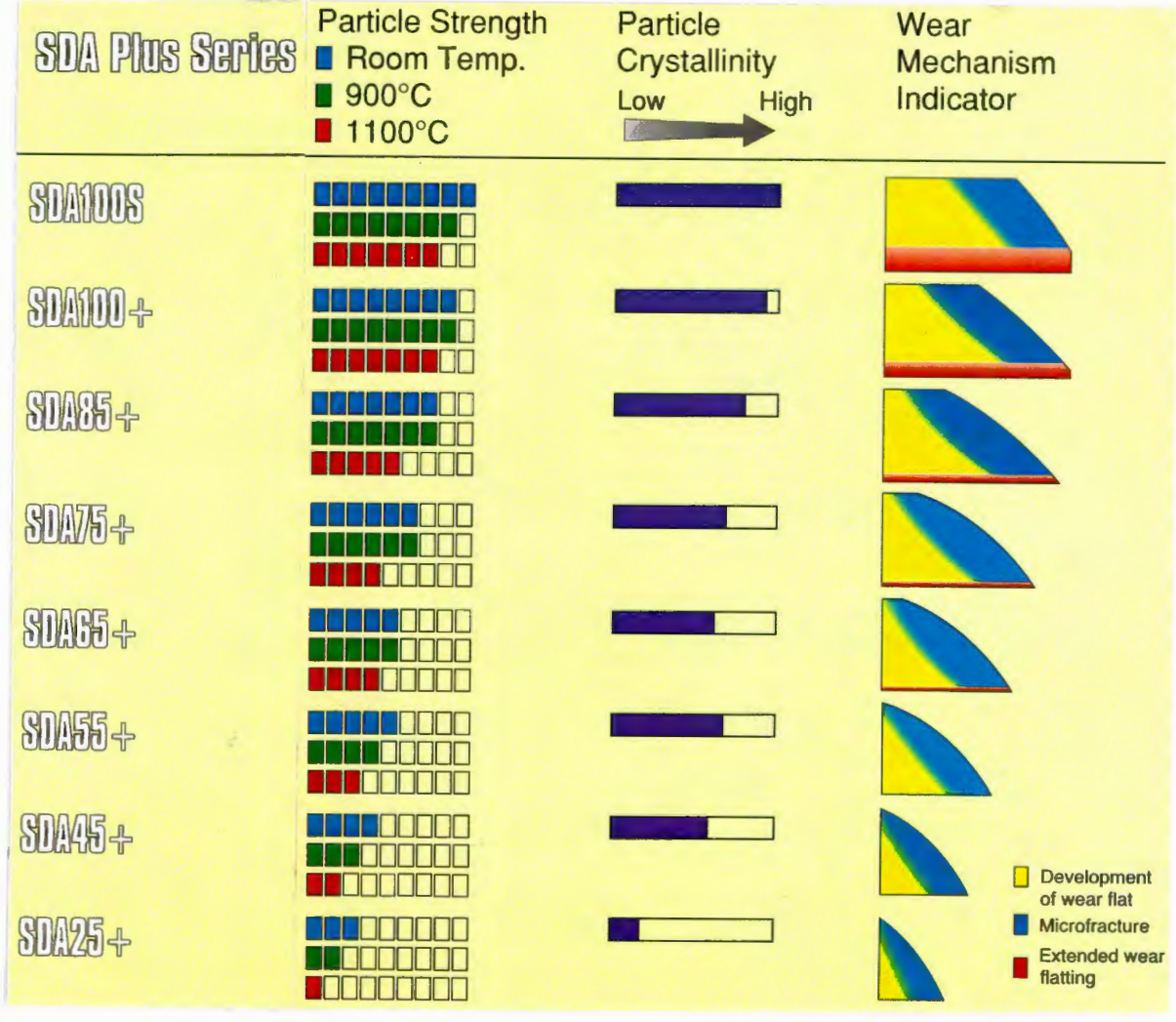

Figure 1.4 Diamond classification indices (29)

Davis et. al. (29) produced three diamond classification indices comprising of a diamond particle strength index at ambient and elevated temperatures, a particle cystallinity scale and a wear mechanism indicator (see Figure 1.4). While the absolute values are not indicated, the indices provide a relative ranking for the products.

1.4.3 Diamond particle structure

In order to quantify the diamond particle characteristics, it is necessary to define its structure. The particle structure can be described by size, shape, surface texture and the inclusions present.

(i) Particle size

Diamond particles are sized by using precision electroformed sieves to the American National Standards Institute (ANSI) and the Federation Europeene des Fabricants de Produits Abrasifs (FEPA) specifications, both designations being equivalent. Diamond products for sawing and drilling applications, according to the ANSI, are specified in US mesh size. The relationship between mesh size, the FEPA designation and the number of particles per carat are shown in Appendix 1.

A fundamental relationship exists between the compressive strength of diamond grit and particle size, with smaller crystals exhibiting higher strengths (31). In a bond matrix, this relationship combines with a number of other factors which influence the selection of grit size. As the diamond particle size reduces, the number of particles per carat increases and correspondingly the number of

cutting points in a matrix. Considering a certain applied load, the increased number of cutting points has the effect of reducing the average cutting forces that each particle experiences. Therefore the wear rate tends to reduce with reducing particle size (32).

The size of grit also affects the height of protrusion of the particle from the matrix since the protrusion height is reduced with smaller particle size. The particle's height of protrusion affects the productivity of the tool in operation. If the particle protrusion is insufficient, too little clearance will exist between the diamond matrix and the workpiece for efficient chip storage and removal which results in a high bond wear. Below a minimum critical particle size, the wear rate of the bond increases with reducing diamond size (25).

The choice of diamond grit size is dependent on the workpiece material (33). As a guide for sawing applications, 20/30 US mesh is generally recommended for cutting sedimentary materials (e.g.. limestone, sandstone), 30/40 US mesh for cutting calcareous materials of medium hardness (e.g.. marble) and 40/50 US mesh for harder siliceous materials (e.g. granites, gabbros). Harder stone types such as those having a high quartz content, would require finer diamond sizes.

Diamond toolmakers normally select a diamond grit size to best suit the application and the performance requirements of their tool design so mixed particle sizes of different diamond products are not uncommon.

(ii) Particle shape

Synthetic diamond particles range from regular cubo-octahedral shapes having smooth faces and well defined edges to irregular and angular shapes as shown in Plate 1.6. These shapes define the crystallinity of the diamond particle (34). The relationship between crystal shape and strength is well known, with the less regular and angular shapes exhibiting lower strengths. This is due to reductions in cross sectional areas on which the cutting forces act and stress raisers caused by asperities or acute corner angles. The shape of the particle will also influence its retention by the bond, with the irregular shapes being easier to retain, such as the case with natural diamond particles.

(iii) Diamond surface texture

The surface characteristics of a diamond particle, which range from smooth and flat to irregular and microcracked surfaces, relates to crystallinity. Large irregularities would affect the edge definition of the crystal and therefore shape. Localised surface irregularities form stress raisers which affect the strength of the diamond particle.

Synthetic diamond particles can be used as sintered or, to enhance retention characteristics in the bond, the surfaces can be modified either before or during the tool making process. Surface modification is carried out by either coating the diamond surface with metals such as titanium, chromium, niobium, molybdenum or tantalum, or by a diamond particle's in-situ reaction with carbon solvents in the bond at elevated temperatures during the matrix sintering process (36).

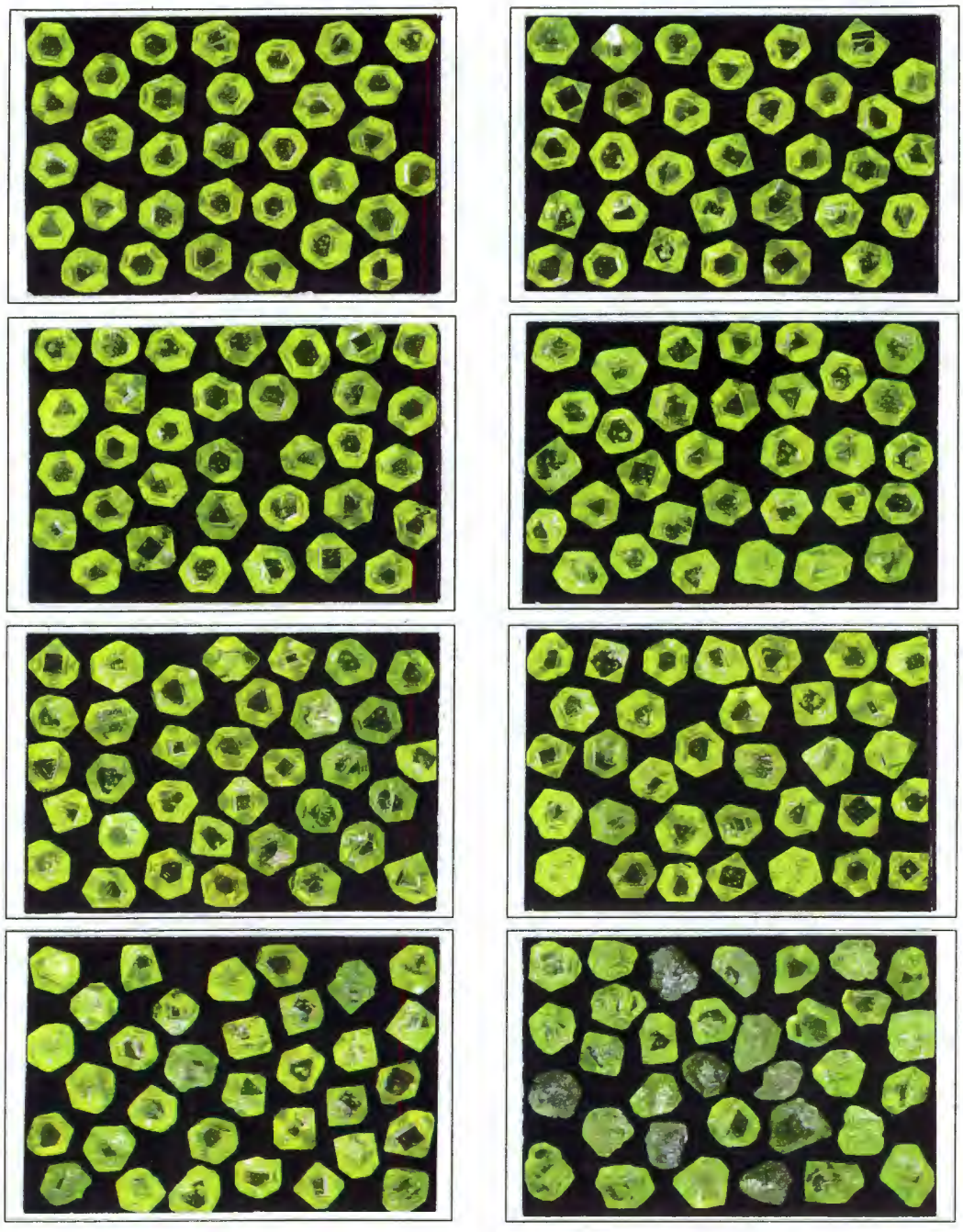

Plate 1.6 Synthetic diamond particle shapes in a product range (35)

(iv) Inclusions

The inclusions in synthetic diamond particles, which are mostly metallic, become trapped during the synthesis process. They are either fine orientated inclusions as found in the product which is manufactured using the cobalt based synthesis

process or finely distributed as in the product resulting from the nickel based synthesis process. The presence of inclusions affect the properties and wear behaviour of the diamond particle (29). The inclusions are more compressible than diamond and under sufficient compressive loads, allow the diamond particle to locally deform, causing stress concentrations, which lead to fracture. This is particularly apparent when the inclusion is close to the diamond particle's surface. The thermal stability of the diamond particle is also affected since it is dependent on the size, shape, position and number of inclusions.

1.4.4 Diamond particle wear

Studies of the wear behaviour of diamond particles in a sintered matrix, referred to in Section 1.3, have shown that the duration that a given particle remains in each wear state (without significant wear, wear flatting and microfracturing) is dependent on the cumulative effects of the cutting forces. These forces include normal and tangential components as well as impact loading. In operation, the useful life of the diamond particle can be defined by the length of time it remains at its working height in each wear state. If a particle is selected with insufficient strength to withstand the effects of the cutting forces in an application, it will remain in the wear flat state for a short period only, and then rapidly microfracture reducing its height of protrusion from the matrix. Conversely, if a particle is selected having too high a strength for an application where the cutting forces are low, the particle will reach its working height and remain in the wear flat state for an extended duration, referred to as extended wear flatting, and ultimately become dislodged in that state as a result of matrix erosion. Should a high percentage of particles on the surface of a diamond tool be in the wear flat state,

the tool will effectively be blunt and stall. When this occurs it is unlikely that the tool will rapidly revert to the free cutting state under normal operating conditions.

The wear mechanism indicator (see Figure 1.4) provides a relative ranking of the expected individual and cumulative durations of wear flat and microfracture wear states for each product under a range of load conditions. The indicator includes the extended wear flat state which is exhibited when the operating loads are below a critical value.

The wear behaviour of synthetic diamond products having similar strengths but with different crystal structures can be compared by their breakdown response curves as shown in Figure 1.5. While some differences can be observed between the wear response curves of the two products, it is interesting to note the product produced using nickel based solvents has a greater tendency to extended wear flatting.

1.4.5 Diamond concentration

The industry refers to diamond grit concentration as the mass of diamond per unit volume of bond material. Diamond concentration is linearly scaled, with 100 concentration being 4.4 carats per cm^3 of bond material. Typical concentrations for diamond wire sawing range from 25 to 45, depending on the application and material type to be sawn. Decreasing the diamond concentration increases the load per particle for a given applied load, so it is important that concentration is considered in conjunction with the strength characteristics of the diamond product being used. Higher concentrations increase tool life but the increased number of cutting points increase the power requirements to drive the tool (25).

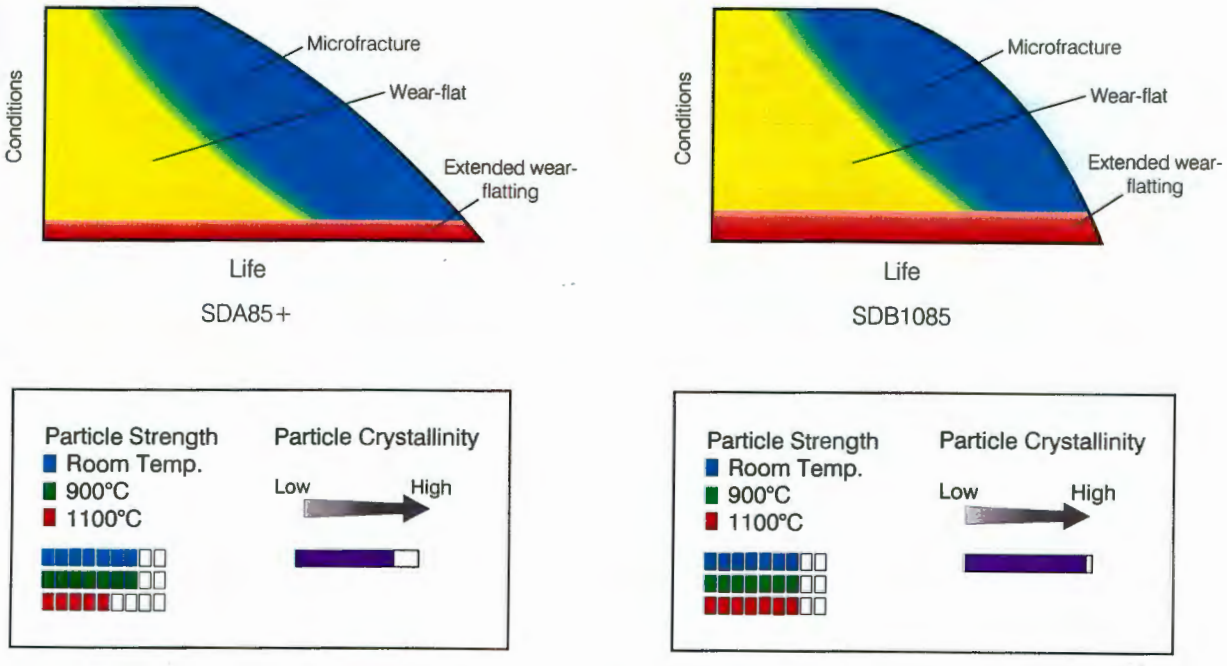

Figure 1.5 Breakdown response curves for SDA 85+ and SDB 1085 (29)

1.4.6 Characteristics of the diamond bond material

The primary function of the bond matrix is to provide support for the diamond particles during their working lives. This is achieved by selecting a bond material that has sufficient strength to constrain the particles during operation while eroding at a rate which is compatible with the diamond loss.

The wear resistance of the bond metal must correspond to the abrasiveness of the workpiece in order to achieve the desired wear balance with the diamond particles being used. A bond metal having too high a wear resistance for the required application will not allow sufficient diamond particle protrusion and cause extended wear flatting, whereas bond metals having too high a wear

resistance will erode faster than the diamond loss and result in diamond particles being pulled out of the matrix prematurely.

Bond metals based on copper, bronze, tungsten, tungsten carbides and cobalt are popular for diamond matrices for most sawing applications. The relationship between hardness and relative resistance to wear of popular bond metals has been determined in a vapour blast test (37). Matrix wear is also dependent on the amount of debris present and diamond wire sawing generally has a high silt concentration in the cut, compared to say circular sawing, as a result of the arc of contact with the workpiece material being typically much longer. For this reason, cobalt or cobalt bronze based bonds having a relatively high wear resistance are generally preferred.

The retention of diamond particles is dependent on factors such as their shape and surface characteristics and the properties of the bond metal. The means of retention can either be purely mechanical by bond encapsulation, which occurs when there is no surface reaction between the diamond and matrix, or by chemical bonding where an atomic or braised type surface reaction takes place at the diamond bond interface. An atomic chemical bond occurs when a solid state chemical reaction takes place at the metal diamond interface, resulting in the formation of a thin carbide layer without degrading the diamond (38). The retention of the particle by the braising type of reaction is attributed to a liquid phase formation which wets the diamond and when it has cooled, firmly anchors the particle in place. The braise reaction is typically evident in the cobalt based bonds used for diamond wire beads.

1.5 Assessment of the effect of stone properties on diamond tool performance

Diamond tools having sintered diamond segments are used in cutting and drilling of natural stone for architectural, monumental, decorative and engineering applications. Those commonly used in dimension stone[1] applications can be classified basically by their constituents, into the following groups (39).

(i) Siliceous rock which includes the basic rock group containing 45 - 52 % silica, including gabbro and basalt, the intermediate rock group containing 52 - 66 % silica including syenite and the acid rock with more than 66 % silica and includes true granite.

(ii) Calcareous rock containing significant amounts of calcium carbonate and includes metamorphisized deposits such as marble and sedimentary deposits such as travertine (tufa).

With the realisation that the performance of a diamond tool is dependent on the material being worked, efforts were made to ascertain the properties of rock which facilitate its machinability and therefore influence the life of the tool. Research into the derivation of machinability indices for the materials commonly encountered in drilling and sawing applications was approached with the intention of addressing the specific characteristics of each of these applications.

In studies of drill bit performance in different materials, investigations were made into the properties of rock which enabled the penetrating and cutting action of the

1. The term dimension stone is used by industry to describe naturally occurring rock that is shaped into blocks, slabs and other units of specific configuration.

drill bit segment to take place. Efforts to derive a drillabality index were based on the rate of penetration in a given rock type for a particular drilling system.

Paone and Bruce (40) in studies of penetration rates in eight different types of rock claimed that a relationship existed between the rate of penetration by a diamond core bit and the drilling strength of the rock, which at first approximation approaches the compressive strength of the rock.

In measurements of the relationship between the drillability and physical properties of rock such as hardness, specific disintegration (volume of rock broken per unit input of work), Young's modulus and sonic velocity, Gstalder and Raynal (41) stated that the drillability of rock cannot be defined in an absolute manner by a single quantity or measured by a single test. However, rock hardness, which could be determined through mechanical means or from sonic velocity measurements, could be a useful quantity to predict drilling performance if consideration be given to the type of bit used and the drilling parameters employed.

Singh (42) found that, in assessments of drillability using statistical regression analyses on results from tests with a microbit, no single physical or mechanical property of rock is directly connected to drillability but postulated that the failure mechanism of rock is related to its hardness, strength properties, abrasiveness, grain size and shape and nature of the bond between individual particles.

Fei, et. al., (43) developed a groove cutting method to evaluate drillability. The apparatus consisted of an impregnated diamond test rod which was used to simulate the diamond drill bit. Using a set of experimental conditions, the test rod

is applied to the periphery of a core sample while it is being rotated, which produces a groove as shown in Figure 1.6. Rock samples were found to have groove depths which related to drilling performance and it was concluded that this method was suitable as a means to determine the drillability of rocks. In addition, the wear of the diamond test rod could be determined from its reduction in mass as a result of the test and this could be used to indicate the abrasivity of the rock sample.

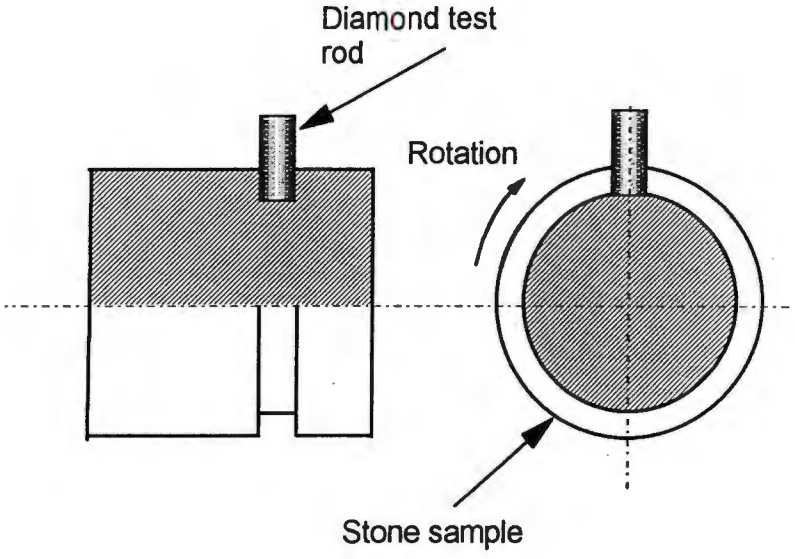

Figure 1.6 Drillability apparatus (43)

Cassapi, Ambrose and Waller (44) investigated the performance of two drill bit designs in Swedish granite and sandstone. It was found that the diamond concentration affected the drilling performance. The rate of pennetration of the drill bits appeared to be greatly influenced by both hardness and physical strength of the stone, whereas the abrasivity of the stone affected the cutting efficiency, through the wear of the matrix. The wear of the matrix influences the rate of new diamond exposure.

A number of tests were evaluated to determine the properties of stone which affect the performance of diamond circular saws. A practical test was sought to be able to predict diamond segment wear in the sawing of a particular stone workpiece and to rank stone in terms of its sawability.

Copeman and Ford (45) realised that petrographical analyses of stone samples were inadequate in providing data on the sawability of stone but suggested that mineralogical factors such as the amount of free quartz present would have a bearing.

In his work, Burgess (46) interpreted sawability as the life of the saw blade, cutting at a constant rate in various stone types. An attempt was made to correlate the wear of the circular saw blade segments with properties of workpiece materials. This was achieved by carrying out sawing tests on several types of granites for which the physical and mechanical properties were obtained. A Shore scleroscope was used to measure the hardness of the stone samples and an abrasion resistance test was developed which measures the ease of removing the surface of a stone sample with a dry rotating lap and loose abrasive. Based on the results of the sawing tests and incorporating the above parameters, a semi-empirical relationship was derived and a sawability ranking of stone was determined.

Wright and Cassapi (47) ran circular sawing tests in different stone types and carried out an analysis on the mechanical properties of representative samples using the Shore scleroscope hardness test, the National Coal Board (UK) cone

indentor hardness test, the Carchar abrasiveness test and tensile and compressive strength tests. No meaningful correlation was found.

In order to evaluate the sawability of stone, Wright and Cassapi set up a circular sawing test bed with load cells to measure the vertical and tangential forces produced from sawing. A direct relationship was found between the measured cutting forces and specific wear of the blade in the test materials. Based on these findings, they built a miniature circular saw apparatus, as shown in Plate 1.7, which uses a disc with a rim of diamond electroplated to the perimeter, making it possible to take high resolution measurements of cutting torque, loads and blade speed. A reasonably close correlation of the measured normal cutting force or the work done in removing material (the area under the power vs. time curve, measured in watts / second) with blade wear was established for different stone types, thus providing a means of determining diamond wear of the blade segments in relation to sawability.

After establishing that the Carchar test machine was inadequate for measuring abrasivity of different stones within the same group, Wright (48) developed an abrasivity test apparatus based on the Carchar test but by employing an enlarged bronze stylus which is traversed across the stone sample as shown in Plate 1.8. A good correlation was reported between the abrasivity values obtained from the wear area of the stylus (measured in mm^2) and saw blade life for the stone samples tested.

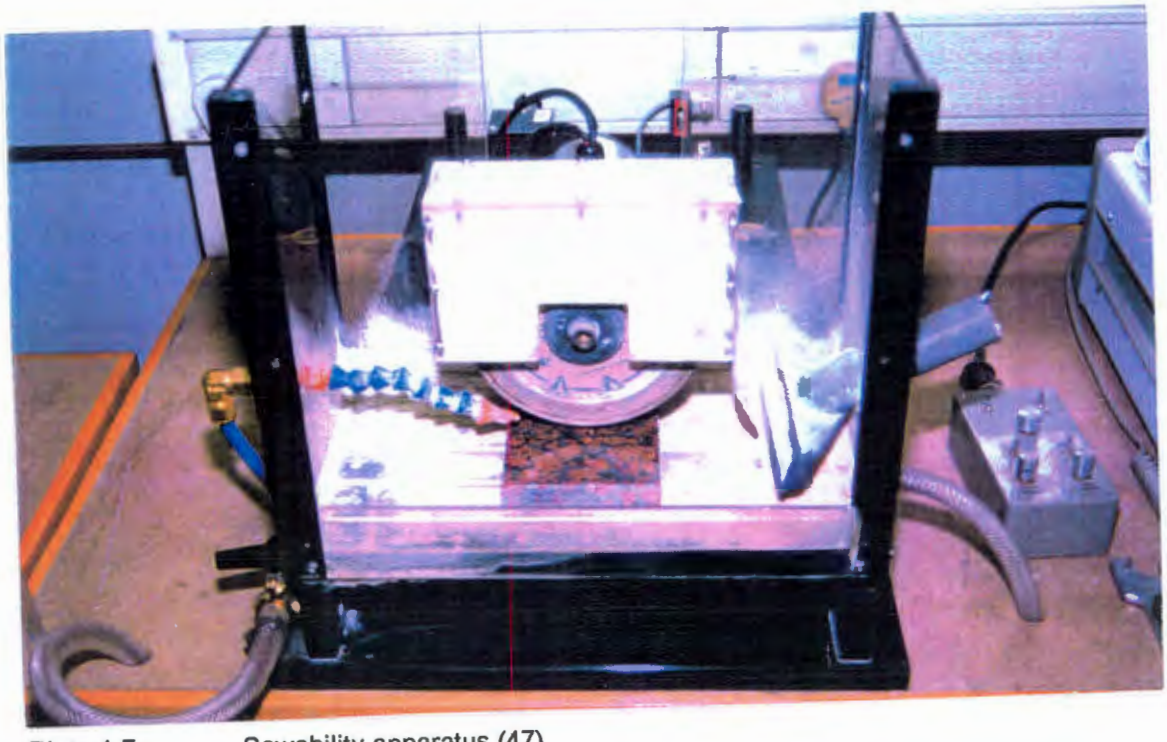

Plate 1.7 Sawability apparatus (47)

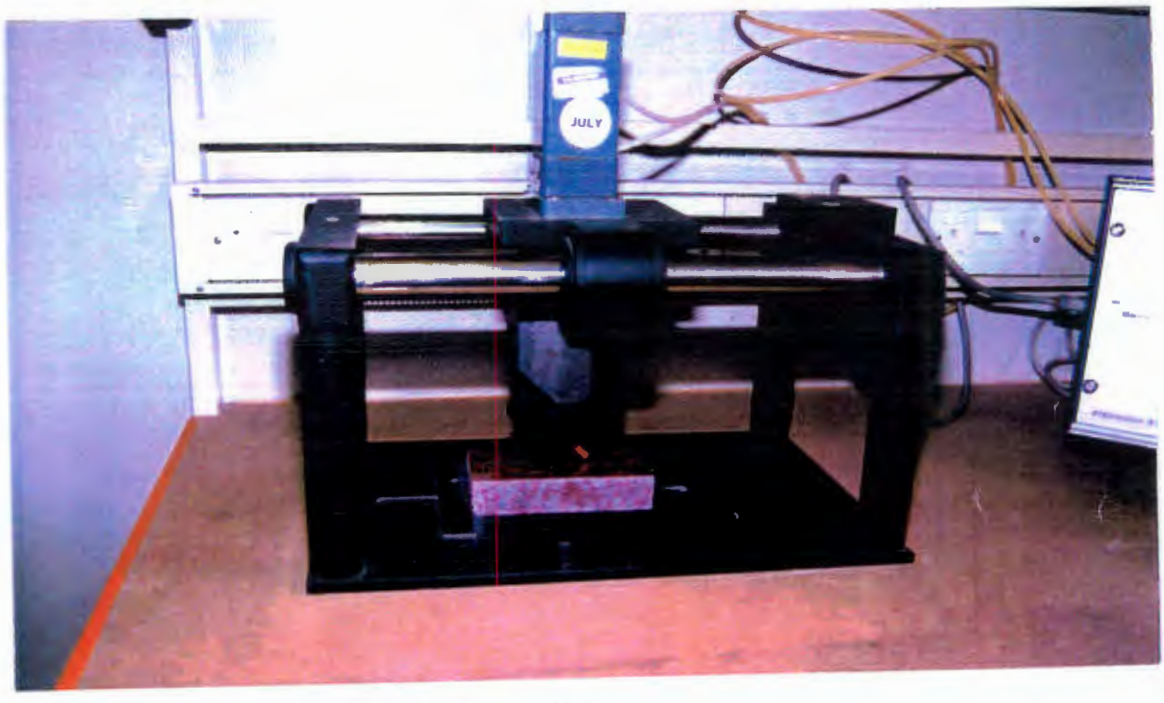

Plate 1.8 Abrasivity test apparatus (48)

1.6 Performance assessments of diamond wire sawing

Reports on diamond wire sawing tests in the field (49)(50)(51) have provided data on the life of diamond wire and cutting rates achieved in various material types. Work has also been published on the effects of parameters such as wire speed and cutting rates on diamond wire life in laboratory conditions by the following authors.

Tonshoff and Panhorst (52) studied the performance of diamond wire using diamond electroplated beads on an laboratory wire saw apparatus. It was found that the volumetric wear of the bead was approximately proportional to the relative cut depth in the granite test material. Relative cut depth was obtained from the proportionality of depth of cut at a measured point to the total depth of cut at the end of the cutting element's life. It was also found that the cutting forces and wear of the cutting elements increased with increasing feed rates.

In experiments on stationary wire sawing of granite, Wright (53) found that diamond wire life reduces with increasing cutting rates, with the trend becoming more pronounced as the length of cut reduces. In agreement with Tonshoff (52) the horizontal cutting forces (acting along the length of the wire) were found to be approximately a factor of ten below the corresponding vertical forces (acting in the normal direction on the wire). Both vertical and horizontal cutting forces were found to increase with cutting rate over an equal length of cut. Within the constraints of the machine, the life of the diamond wire was found to improve as the cutting speed was increased between 20 and 32 ms^{-1}.

In laboratory evaluations of diamond wire bead performance, Bortolussi et. al. (54) found that both cutting rate and specific wear increase with load. High cutting rates were accompanied by accelerated wear with a resulting loss of bead productivity. The cumulative bead mass loss and cumulative area cut showed a diverging trend when tested under different loads. Specific wear of beads were found to increase with load. For a given applied load, average specific wear was found to be approximately constant, except when the bead is new and the initial layer of bond is removed and towards the end of a bead's life, where the wear rate rises considerably.

1.7 Diamond wire rotation

In order to obtain the optimum life from diamond wire, it is necessary for the diamond beads to wear concentrically and evenly around their periphery. This is achieved when the bead's diamond matrix is homogeneous and the entire surface of the bead gets an equal exposure to the workpiece material. The only way this is possible with diamond wires where the beads are fixed to the cable by, for instance, vulcanised rubber or injection moulded plastic, is for the wire to rotate about its polar axis.

Diamond wire rotation is caused by applying a torque to the wire loop during operation. This is achieved by a deliberate misalignment in the system and in the case of stationary wire saws, the pulleys are offset by a few degrees (55). On the stationary wire saw, the pulley from which the wire exits, holds the wire while the receiving pulley induces a torque which causes the wire to rotate. This is a progressive action which is repeated on the upper and lower sides of the pulleys

as they rotate. The effect is shown in Figure 1.7 where the force F_t induced by the tension of the wire can be divided into two components, F_s the side thrust and F_r the force which induces the torque on the wire about the diamond bead radius.

To improve the life of diamond wire, some tool manufacturers recommend twisting the wire a number of turns per unit length in the direction of the lay of the wire cable prior to joining (57) and it was felt that this assists wire rotation (58).

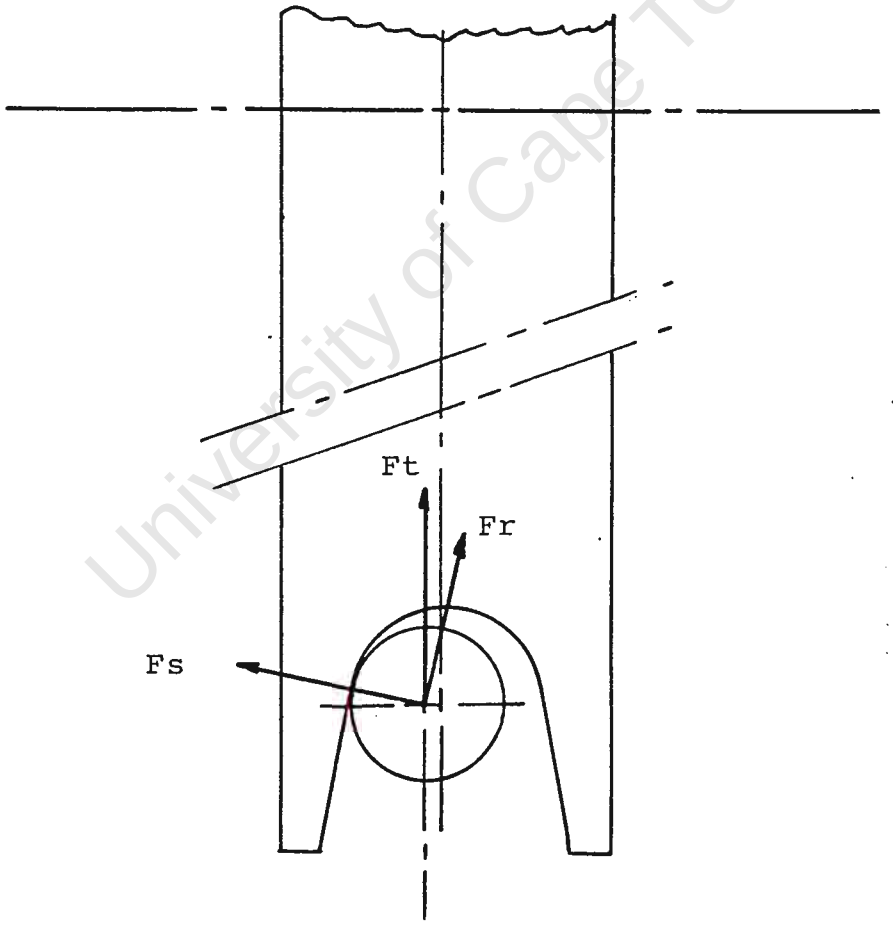

Figure 1.7 Force diagram for diamond wire entering a stationary diamond wire saw pulley

CHAPTER 2

PERFORMANCE RELATED ASPECTS OF THE SINTERED DIAMOND MATRIX

2.1 The wear behaviour of diamond in wire beads

A number of similarities have been observed in the wear behaviour of diamond particles in sintered bond matrices in circular sawing, drilling and grinding of natural stone. While the diamond particles and bond system used in wire sawing beads has been developed using similar constituents and manufacturing techniques to other metal bond diamond tool segments, the contact profile and load cycles are different. A study was carried out by the author on diamond wire beads to ascertain the wear states of diamond particles in wire sawing against the background of diamond particle wear studies in the other applications mentioned above.

2.1.1 Diamond wear states

Diamond wire samples were obtained from quarries in the Bushveld Complex of South Africa, producing a light coloured gabbro from the Rustenburg area (referred to commercially as Impala granite). Beads were separated from the diamond wire samples and individual diamond particles were studied under a scanning electron microscope. The following wear states were evident.

(i) Diamond particles without significant wear

Diamond particles were observed which had emerged from the matrix but clearly below the working height of neighbouring particles, with no comet tail visible as shown in Plate 2.1. Particles exhibiting good edge definition which had reached the working height, displaying the typical matrix supporting comet tails were also evident, as shown in Plate 2.2.

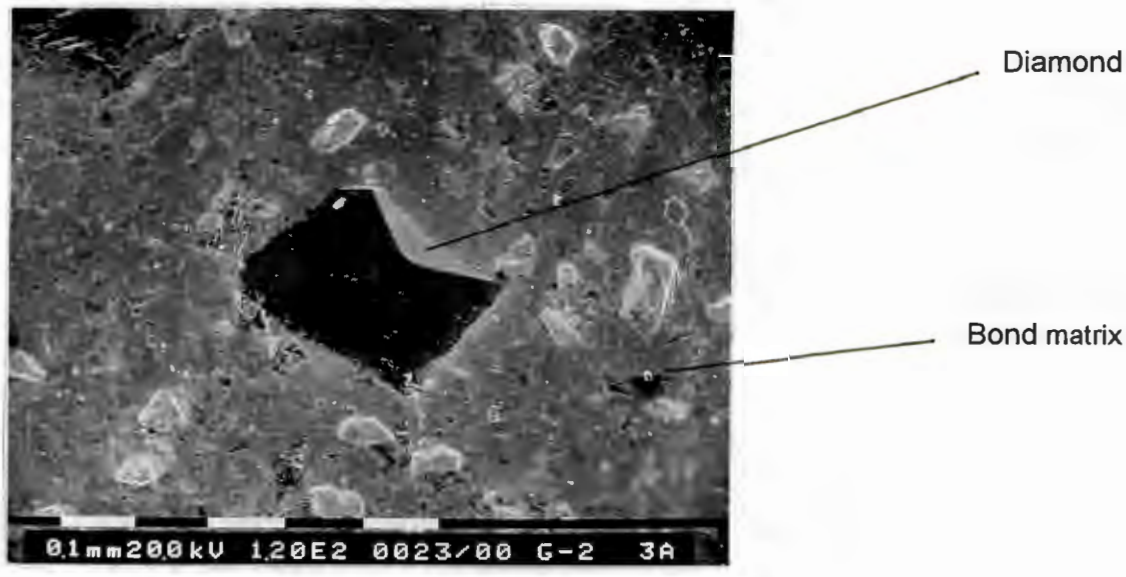

Plate 2.1 Emerging diamond particle

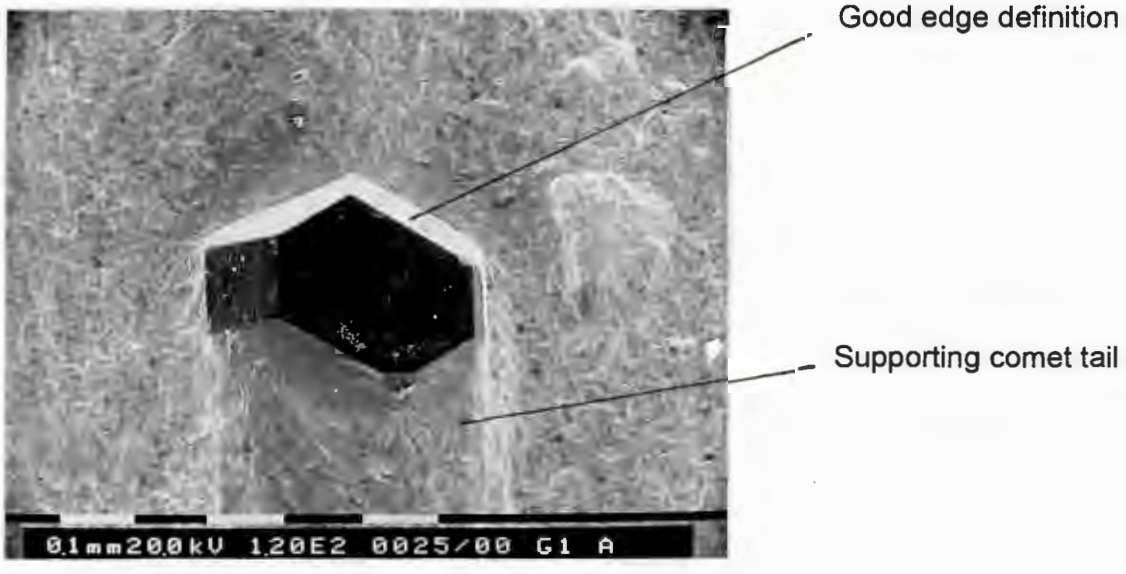

Plate 2.2 Diamond particle at its working height showing good edge definition and supporting comet tail

(ii) Diamond particles with wear flat

Diamond particles in varying stages of wear flatting were evident. Some examples exhibited corner fracturing while others had microfractured to an extent. Where extended wear flatting was observed, in a number of cases it was associated with surface striations running in the direction of travel as shown in Plate 2.3.

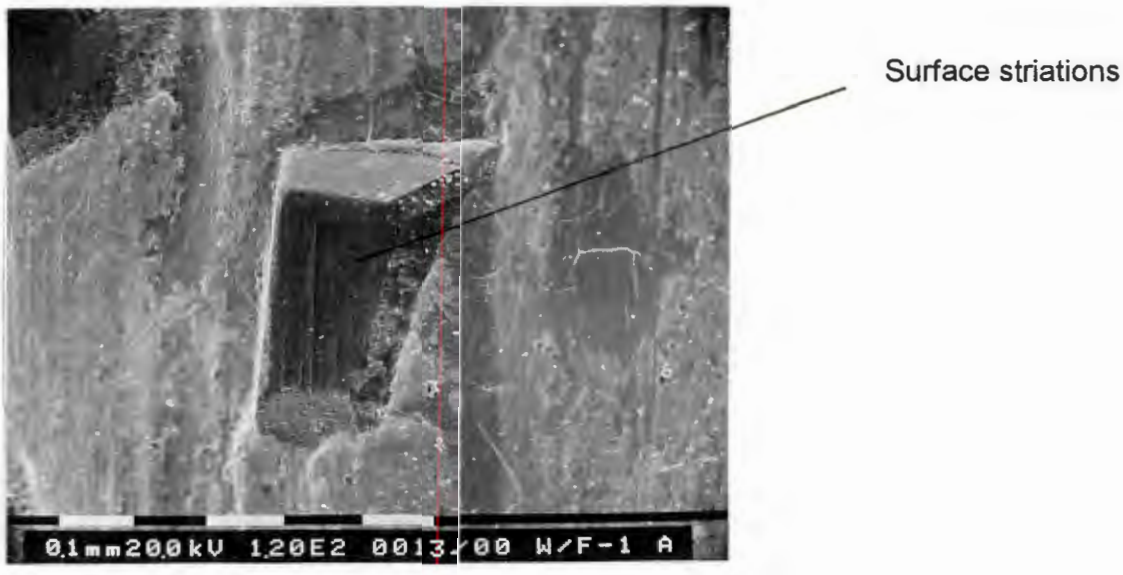

Plate 2.3 Diamond particle exhibiting extended wear flatting and showing surface striations in the direction of travel

(iii) Microfractured diamond particles

Diamond particles in varying states of microfracturing were seen on the bead samples. Plate 2.4 shows the early stages of a microfracture which has been initiated by a chip in the edge of a diamond particle. Plate 2.5 shows a diamond particle which has microfractured but a portion of the particle is still at the

working height above the matrix. Plate 2.6 shows a particle which has almost completely broken down through microfracturing, leaving a small protrusion of the diamond above the matrix.

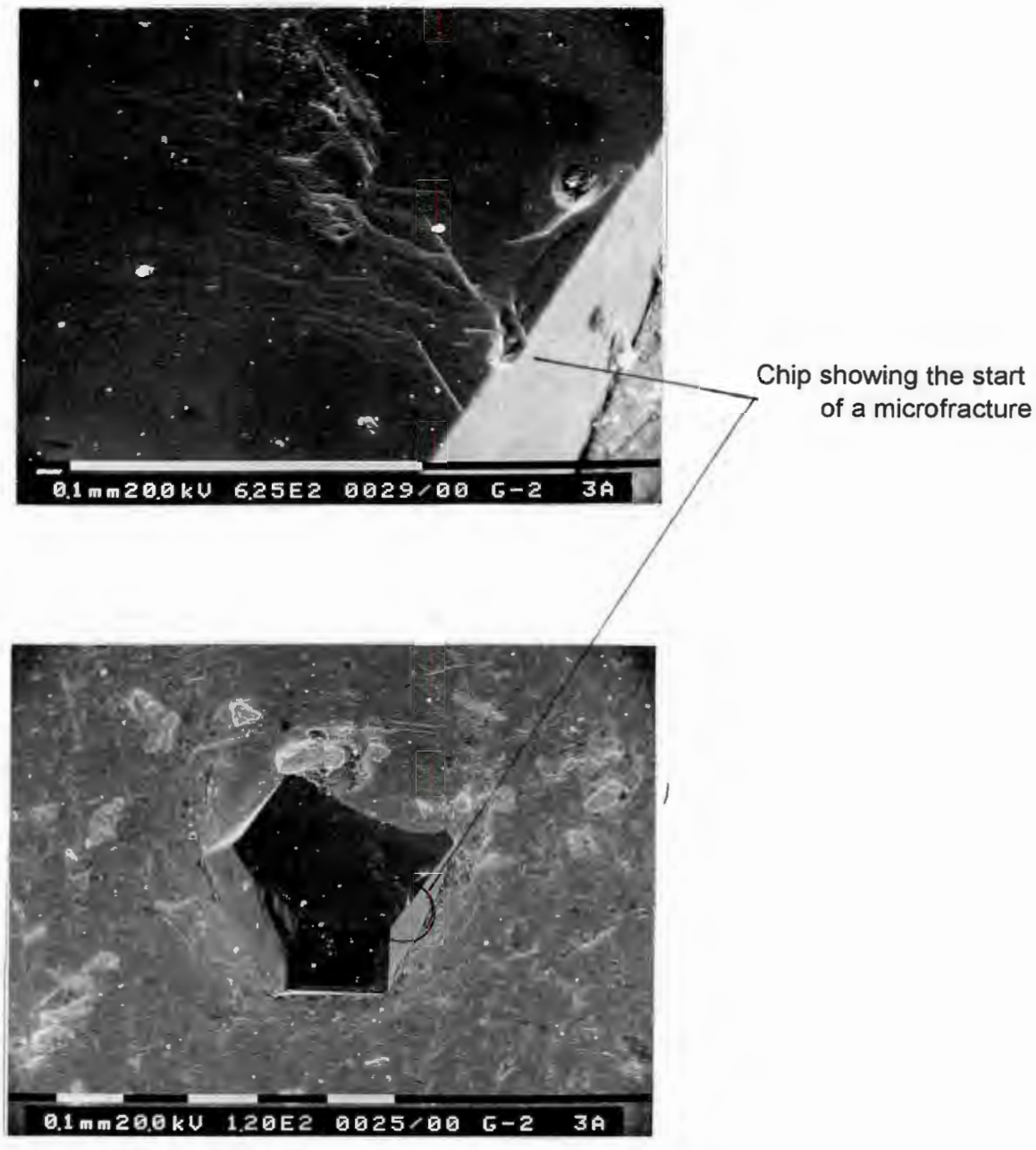

Plate 2.4 Early stages of microfracturing initiated by a chip in the edge of the diamond particle

Plate 2.5 Advanced stages of microfracturing of a diamond particle

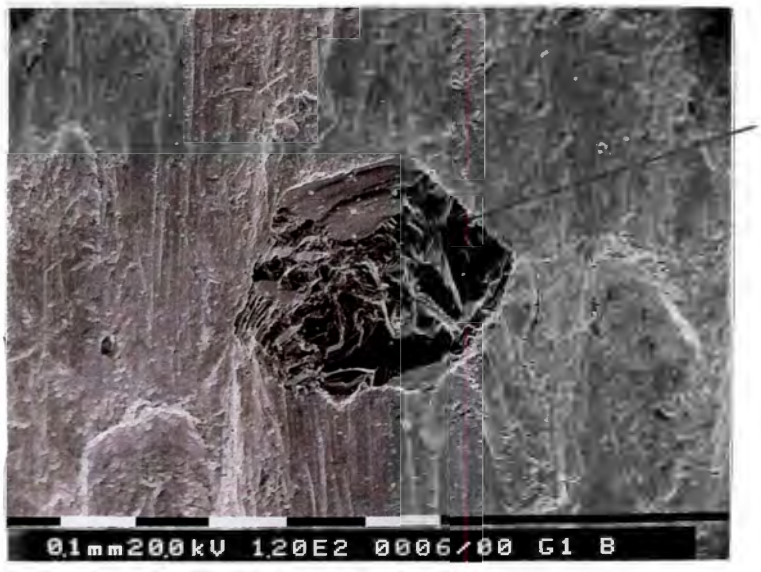

Plate 2.6 Almost complete breakdown of a diamond particle as a result of microfracture

(iv) Hole in the matrix left by diamond pullout

Plate 2.7 shows evidence of a diamond particle lost through pull out from the bead matrix, leaving an impression of its profile in the bond.

Plate 2.7 Imprint left in the matrix by particle pullout

2.2 Diamond wear progression

Beads from diamond wires that had exhibited a free cutting action were compared with beads from diamond wires whose performance had deteriorated to the extent that the cutting action was significantly retarded (see Plates 2.8 and 2.9). The following observations were made.

(i) The bead samples which had exhibited a free cutting action had a predominant number of diamond particles either with no significant wear or in some stage of microfracture. Only a few diamond particles were observed in purely the wear flat state and very little evidence of pull out was observed in the bead samples studied.

(ii) The bead samples which had exhibited poor performance had a large percentage of diamond particles in the extended wear flat state and a

high number of pull outs. This resulted in fewer diamond particles on the surface of the bead.

(iii) The average working height of particles appeared significantly lower in the bead samples which had performed poorly to those in the beads which were free cutting. The diamond particle protrusions however, were not measured.

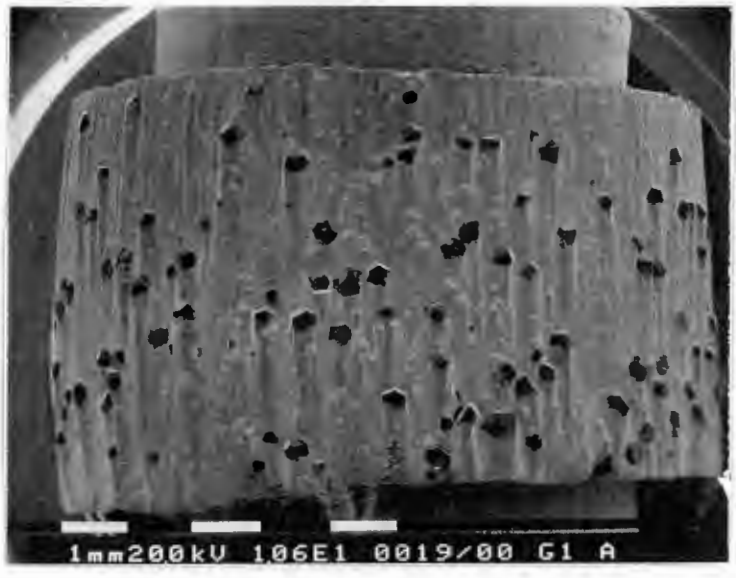

Plate 2.8 Surface of a bead having a free cutting action

Plate 2.9 Bead surface showing extended wear flatting of diamond particles

It is evident from our study that diamond particles in wire beads exhibit similar wear states to those investigations mentioned in the literature. However, as the study was based on an arbitrary point in the life of each diamond particle in a wire sawing application, any differences in the duration of each wear state in the different applications, which has relevance to the overall life of the particle, was not revealed. Based on the observed particle wear states in diamond wire beads, two particle wear progressions are likely.

(i) Under operating conditions of suitable severity to maintain a free cutting action, diamond particles progressively emerge from the matrix and reach working height, undergo a wear flat phase and eventually start to microfracture leading to particle breakdown and loss from the matrix.

(ii) When the operating conditions are not sufficiently severe to maintain a free cutting action, diamond particles progressively emerge from the matrix and reach working height at which stage they start to wear flat. The particles at the working height progressively wear flat and remain in that state for an extended period. This reduces wear of the matrix and retards the emergence of new diamond particles. Eventually the particles are pulled out of the matrix in the extended wear flat state or in some stage of breakdown.

2.3 Diamond retention

Ideally, diamond particles should remain in the matrix until they have reached an advanced stage of breakdown. One of the causes of premature pull out of diamond particles is poor encapsulation by the bond. A number of beads were studied to evaluate the retention of diamond particles by the bond.

While the encapsulation of most particles in various states of wear appeared acceptable, shown by the bond contact with the diamond particle in Plate 2.10, some evidence of poor bonding was identified, as depicted in Plate 2.11. The poor bonding shown here may have been due to a low bond sintering temperature during manufacture and may not necessarily be as a result of the bond materials used. However this cannot be excluded and would certainly result in premature diamond particle loss, thereby reducing the life of the tool.

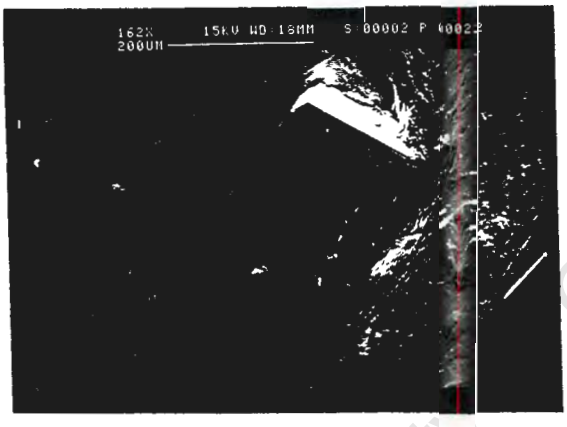

Plate 2.10 Diamond particle showing good retention by the bond

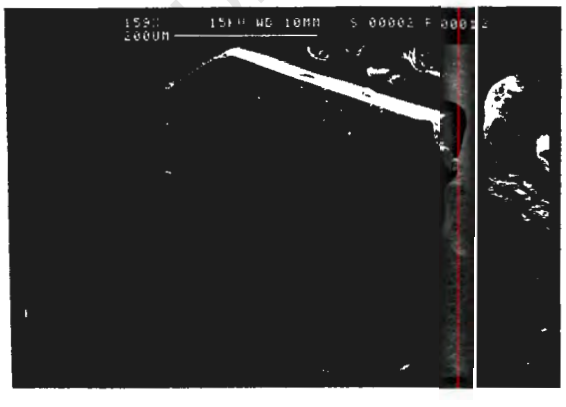

Plate 2.11 Poor retention of a diamond particle by the bond

CHAPTER 3

THE INFLUENCE OF NATURAL STONE PROPERTIES ON DIAMOND WIRE PERFORMANCE

3.1 The calculation of chip thickness

The removal of stone by diamond in a sintered matrix is effected by a progressive scratching sequence of the workpiece at high speed by a perplexity of diamond particles which are statistically distributed on the matrix surface of the tool. An important factor in the mechanics of cutting is the thickness of chip which is produced by each cutting point. With a number of indeterminate cutting edges, an equivalent chip thickness can be found from the kinematic quantities of the tool's cutting velocity, the cutting rate and the length (or depth) of the cut.

By equating the rate at which material is removed from the workpiece, referred to as the external removal rate, to the rate at which the tool is able to cut the material, referred to as the internal removal rate, the equivalent chip thickness can be found. If the external removal rate

$$z_e = b \cdot l_w \cdot v_w \quad \text{.....3.1}$$

and the internal removal rate, for a linear movement of the tool,

$$z_i = h_{eq} \cdot b \cdot v_s \quad \text{.....3.2}$$

then $b \cdot l_w \cdot v_w = h_{eq} \cdot b \cdot v_s$

or $$h_{eq} = \frac{v_w}{v_s} \cdot l_w \quad \text{.....3.3}$$

where

h_{eq} = equivalent chip thickness
b = breadth of cut
l_w = the length of cut
v_w = feed rate
v_s = tool speed

If the cutting action of each particle is considered individually, the mean chip area per particle as shown in Figure 3.1 can be expressed by

$$\overline{b_c} \cdot \overline{h_c} \quad \text{.....3.4}$$

where

$\overline{h_c}$ = the mean chip thickness per particle
$\overline{b_c}$ = the mean chip width per particle

If C is the number of working particles per unit surface area of the tool, then the mean chip area per unit surface area can be given by the expression

$$C \cdot \overline{b_c} \cdot \overline{h_c} \quad \text{.....3.5}$$

For a segmented tool, the effective contact area with the workpiece over the length of the cut, as shown in Figure 3.2, can be given by

$$\frac{l_s}{l_t} \cdot l_w \cdot b \quad \text{.....3.6}$$

where

l_s = the segment length
l_t = the segment pitch

The mean chip area for the effective contact area of the tool can be determined by combining expressions 3.5 and 3.6 and it follows that the equivalent chip thickness

$$h_{eq} = C \cdot \overline{b_c} \cdot \overline{h_c} \cdot \frac{l_s}{l_t} \cdot l_w \quad \text{.....3.7}$$

Substituting equation 3.7 into 3.3 gives

$$C \cdot \overline{b_c} \cdot \overline{h_c} \cdot \frac{l_s}{l_t} \cdot l_w = \frac{v_w}{v_s} \cdot l_w$$

or

$$\overline{h_c} = \frac{v_w \cdot l_t}{C \cdot \overline{b_c} \cdot l_s \cdot v_s} \quad \text{.....3.8}$$

If r is the ratio of the mean chip width $\overline{b_c}$ to mean chip thickness $\overline{h_c}$, then equation 3.8 can be written as

$$\overline{h_c} = \sqrt{\frac{v_w \cdot l_t}{v_s \cdot l_s \cdot C \cdot r}} \quad \text{(after Tonshoff and Warnecke) .....3.9}$$

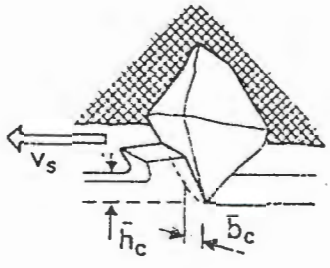

Figure 3.1 Mean chip thickness $\overline{h_c}$ and mean chip width $\overline{b_c}$

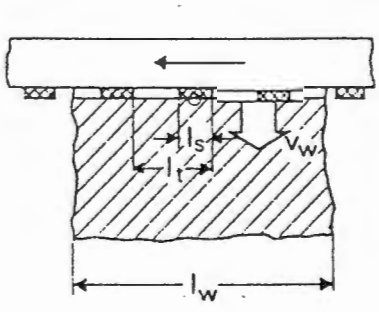

Figure 3.2 Segment length l_s,segment pitch l_t and length of cut l_w

3.2 The relationship of chip thickness to operating conditions for diamond wire sawing

Calculations were made to obtain theoretical chip thicknesses for selected operating conditions on a stationary diamond wire saw. Recommended cutting rates and wire speeds for three chosen materials were used (56) and the ratio **r** of the mean chip width to mean chip thickness was taken from the estimated value by Tonshoff and Warnecke (25). The number of working particles per unit area was based on calculations by Cai (59). The relationship between the mean particle chip thickness and operating variables is given in Appendix 2 and summarised in Table 3.1.

Stone type	v_w mm min^{-1}	l_t mm	v_s m s^{-1}	l_s mm	C**	r*	$\overline{h_c}$ μm
Rustenburg Grey (gabbro)	17.8	20	26	5	1.2	10	0.45
Belfast Black (gabbro)	14.4	20	24	5	1.2	10	0.43
African Red (granite)	10.0	20	20	5	1.2	10	0.38

* (after Tonshoff and Warnecke) ** (after Cai)

Table 3.1 Relationship between chip thickness and diamond wire sawing operating conditions for different siliceous stone samples

For each stone type, a certain diamond wire speed and cutting rate is required to achieve an optimal tool life. The cutting rate is determined by the stone's machinability which is influenced by the characteristics of its mineral constituents, and together with the length of cut, determine the diamond wire feed rate. As the stone type becomes more difficult to cut, the feed rates and wire speeds generally decrease. This has the effect of a reduction in chip thickness corresponding to the reduction in feed rate which is partially offset by an increase in chip thickness corresponding to the reduction in wire speed, according to the relationship defined in equation 3.9 .

3.3 The evaluation of natural stone properties which affect diamond wire life

As with diamond drilling and circular sawing, a practical method was needed to evaluate the properties of stone which affect the life of diamond wire. Based on the work carried out on drillability, sawability and abrasivity it was decided to use the sawability apparatus in the assessment of stone properties which affect diamond bead wear, for the following reasons.

(i) The diamond electroplated disc used for the sawability tests is not as sensitive to influences of the bond matrix as say the diamond test rod used for drillability assessments, so better repeatability was expected.

(ii) The sawability test has been designed to mimic circular sawing, and while the load cycles experienced by the diamond particles differ from those for diamond wire sawing, it was considered not to have a significant effect on the results considering the comparative nature of the test.

(iii) The sawability apparatus is quick and easy to use and requires only a small sample of stone.

The effects of debris as a result of the cutting action, which is expected to be of a higher concentration in the cut for diamond wire sawing than for circular sawing, would however not be adequately highlighted by the sawability test. The abrasivity test was therefore also considered for determining a relationship between the wear of the diamond bead matrix and different stone types.

Diamond wire sawing tests were carried out on selected stone blocks on a stationary wire saw. A comparison was made between the diamond wire life, measured in square metres sawn per metre of wire consumed, in each stone type tested and their sawability and abrasivity values. In order to minimise the effect of different lengths of cut, the stone blocks used were of similar length. Cutting parameters were optimised in each case and data was collected from one diamond wire type for each stone group. For the sawability and abrasivity tests, ten readings were taken in each case and the mean found for each stone sample tested. The results are shown in Appendix 3 and summarised in Table 3.2.

Material description	Material type	Diamond wire life ($m^2\ m^{-1}$)	Mean sawability value ($w\ s^{-1}$)	Mean abrasivity value (mm^2)
White Rhino	Marble	41.2	134.40	1.21
Light Plaisandro	Marble	34.4	185.35	1.03
Rustenburg Grey	Norite	12.6	216.55	2.84
Belfast Black granite	Gabbro	10.1	229.80	2.50
Bitterfontein Green granite	True granite	9.4	247.15	2.87
Zimbabwe Black granite	Gabbro	9.0	308.45	1.93
Juperana	True granite	6.2	311.00	2.94
African Red granite	True granite	6.0	315.95	3.07

Table 3.2 Diamond wire life vs. mean sawability and abrasivity values of siliceous and calcareous stone samples

3.3.1 Analysis of sawability and abrasivity test results

In order to establish a relationship between the sets of variables, the sawability and abrasivity values were plotted against diamond wire life for each stone sample as shown in Graphs 3.1 and 3.2.

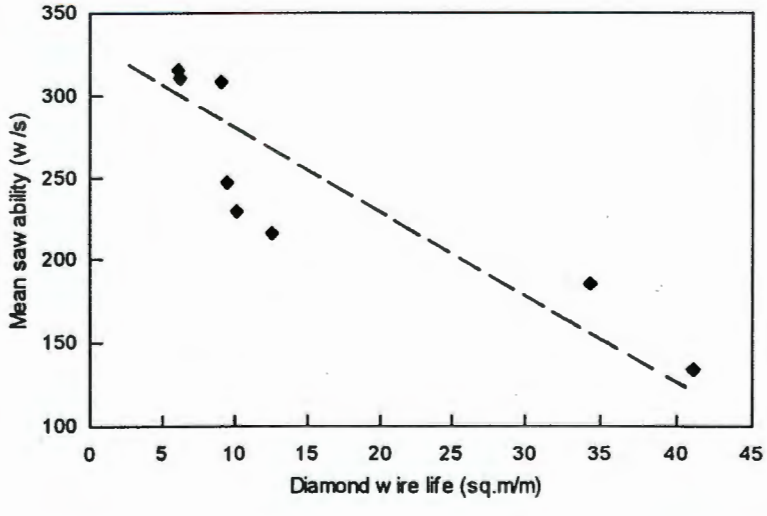

Graph 3.1 X - Y scatter graph of sawability vs. diamond wire life for siliceous and calcareous stone samples

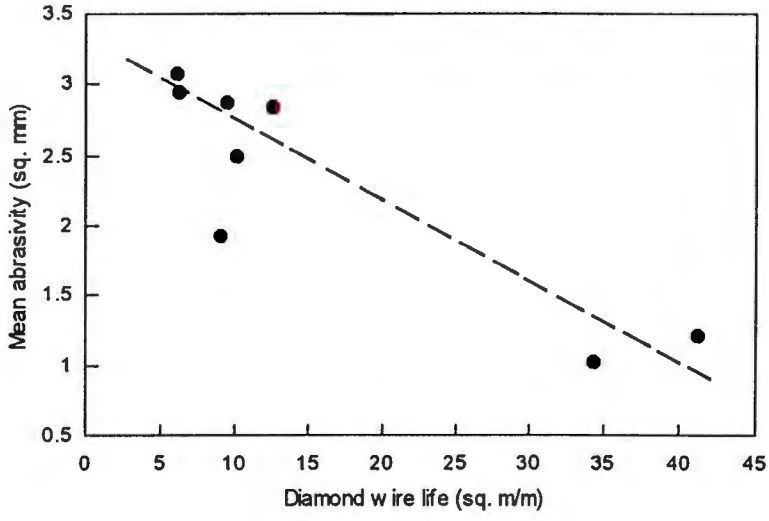

Graph 3.2 X - Y scatter graph of abrasivity vs. diamond wire life for siliceous and calcareous stone samples

A regression analysis was carried out on the data for the stone samples in Table 3.2 and the reliability and the correlation of the sawability and abrasivity values with diamond wire life determined. The results are given in Appendix 3 and summarised in Table 3.3.

	Sawability	Abrasivity
R^2 value	0.77	0.79
Correlation coefficient	-0.88	-0.89

Table 3.3 R^2 value and correlation coefficient of sawability and abrasivity with diamond wire life for siliceous and calcareous stone samples

The proximity of the R^2 values to 1 for sawability and abrasivity show adequate reliability of the data for the set of siliceous and calcareous stone samples when considered together and reasonable negative correlations of sawability and abrasivity with diamond wire life are similarly demonstrated. However, when the R^2 values and correlation coefficients are calculated for just the siliceous stone

samples, the sawability data shows reasonable reliability with a good correlation but the abrasivity data appears unreliable with poor correlation, as shown in Appendix 3 and summarised in Table 3.4.

	Sawability	Abrasivity
R^2 value	0.78	0.08
Correlation coefficient	-0.88	-0.28

Table 3.4 R^2 value and correlation coefficient of sawability and abrasivity with diamond wire life for siliceous stone samples

Based on these findings, the sawability apparatus could be used in determining the sawability characteristics of stone for diamond wire sawing but the reliability of the abrasivity test on its own for this application is suspect, particularly when considering different stone types within a group. The poor correlation may be explained by the fact that the test only measures the abrasivity of stone in its constituted state and does not take into account the abrasive effect of the loose debris in the cut on the bead matrix.

These tests however, only portray the characteristics of stone which influence tool performance and therefore can only be used as a guide in the overall determination of diamond tool life.

CHAPTER 4

THE MECHANICS OF DIAMOND WIRE SAWING

4.1 Diamond wire sawing modes

To effect diamond wire sawing, diamond wire is threaded around the periphery of the material to be cut and joined into a loop. The loop is rotated and traversed through the material in a controlled manner by varying the wire tension in the cutting plane. The configuration is set up depending on the application, the size of cut, the available space and desired result. Two basic modes of cutting are used:

(i) Pull cutting, which is found predominantly in stone quarries and construction applications, uses a single drive pulley configuration. In quarries where the material to be cut forms part of a solid rock formation, two, normally perpendicular intersecting holes are drilled, through which the diamond wire is threaded. Any number of combinations between the vertical and horizontal dimensions of the cutting plane and the pulley centre distance are possible within the system's strength and drive power limits. Guide pulleys are sometimes used to stabilise the wire or to change its direction of travel. In quarry applications, this mode of cutting is characterised by the length of cut which continuously reduces as the cut progresses, as shown schematically in Figure 4.1.

(ii) Push cutting is used predominantly in the stone yard for block slabbing and squaring. Two (or sometimes four) pulleys are used to rotate and traverse a loop of diamond wire through a stone block, as shown schematically in Figure 4.2. One of the pulleys is used to drive the loop while a second rotates freely and maintains a tension on the wire. For

regular block sections (which are commonly encountered), once the wire contact has stabilised in the workpiece material during the initial stage of the cut, the length of the cut is characterised by an arc of contact having a large radius. In regular sections, the length of cut remains fairly constant until the exit stage of the cut is reached.

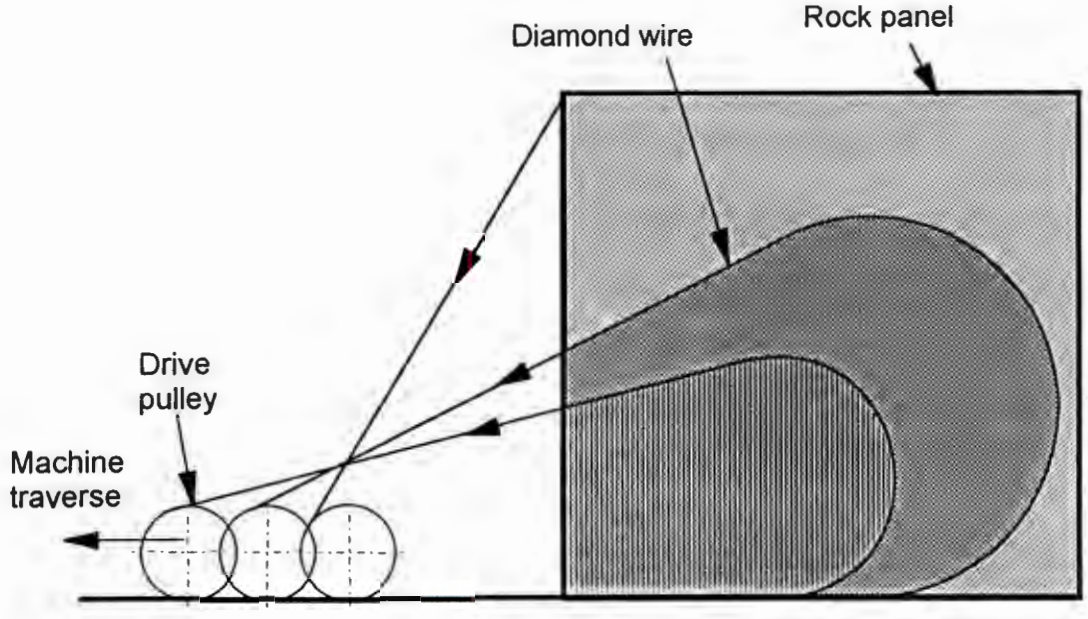

Figure 4.1 Schematic diagram of the pull cutting system

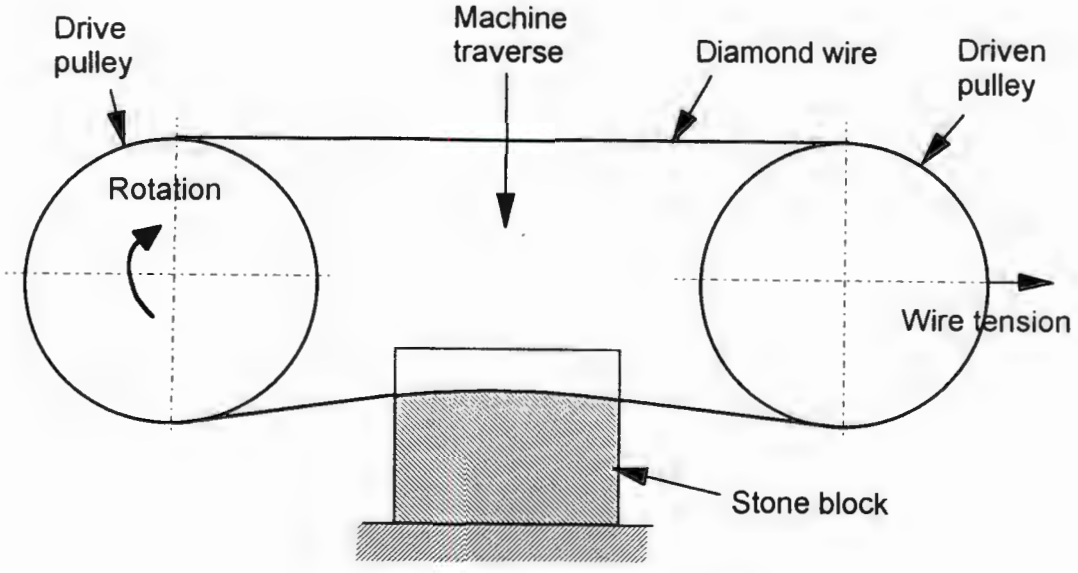

Figure 4.2 Schematic diagram of the push cutting system

4.2 Dimensions of the cut for stationary wire sawing

4.2.1 Determination of the length of cut

For push cutting applications, the length of cut l_c and radius of cut r can be determined directly from the geometric equations of arc length and radius (see Appendix 4). The length of cut

$$l_c = \frac{\pi \cdot r \cdot a}{180} \quad \text{.....4.1}$$

where

a = the circular segment angle defining the arc of contact

and the radius of the cut

$$r = \frac{c^2 + 4h_1^2}{8h_1} \quad \text{.....4.2}$$

where

c = the width of the block
h_1 = the height of curvature

By substituting equation 4.2 into 4.1, the length of cut can be found in terms of the angle of the circular segment and the height of curvature of the arc, which gives

$$l_c = \frac{\pi \cdot a\left(c^2 + 4h_1^2\right)}{1440h_1} \quad \text{.....4.3}$$

From the trigonometric relationship in Figure 4.3, it can be shown that the wire deflection angle

$$\phi = \frac{a}{2}$$

and equation 4.3 may now be written in a more convenient form

$$l_c = \frac{\pi \cdot \phi\left(c^2 + 4h_1^2\right)}{720h_1} \qquad \text{.....4.4}$$

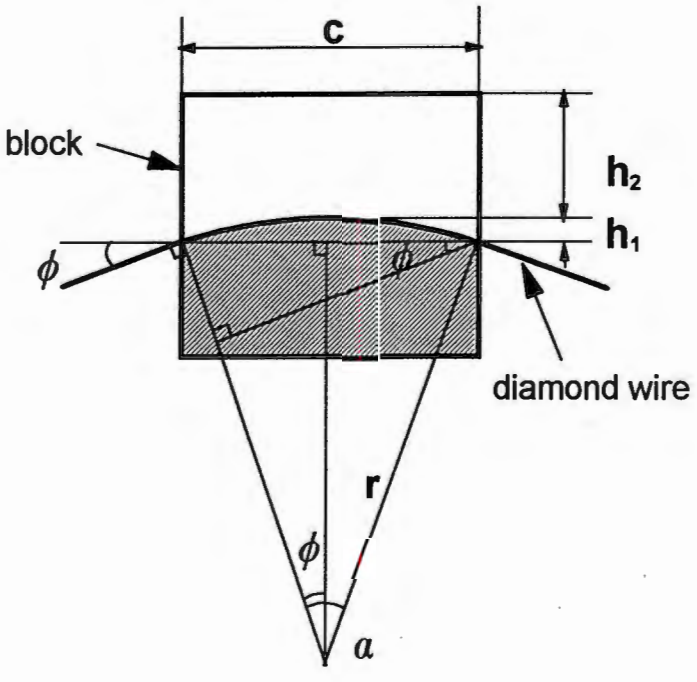

Figure 4.3 Arc of contact for push cutting systems

4.2.2 Determination of the area sawn

If the cutting plane of the workpiece can be defined by the bounds of a regular geometric shape, the area sawn can be readily determined. In the case of a rectangle, once the cut has reached a steady state with a height of curvature h_1, the area sawn is the rectangular area $c \cdot h_1$ less the area under the arc of cut (refer to Figure 4.3 and Appendix 4),

$$a_1 = c \cdot h_1 - \frac{r \cdot l_c - c(r - h_1)}{2} \quad \text{.....4.5}$$

and for any subsequent cutting, the total area cut

$$a_c = c \cdot h_2 + a_1 \quad \text{.....4.6}$$

where

h_2 = the depth of cut from the top of the block to the apex of the cut curvature.

4.3 Dimensions of the cut for quarry wire sawing

The determination of the exact dimensions of the cut in quarry wire sawing is complex due to the number of possible set-ups which determine the cutting geometry. However, the approximate length of the cut and area sawn can be determined if the cutting plane and the arc of contact of the diamond wire with the rock can be geometrically approximated.

4.3.1 Determination of the length of cut

If it is assumed that the cutting arc has a constant radius r_c and for the greatest duration of the cut, $r_c >$ the drive pulley radius (see Figure 4.4a). The length of the arc can be determined from the equation

$$l_c = \frac{\pi \cdot r_c(180 + \phi)}{180} \quad \text{.....4.7}$$

where

ϕ = the diamond wire cutting angle

If we let the centre of radius of the cut from the rock face be l_1 then

$$l_2 = \frac{l_1}{\cos \phi} \quad \text{.....4.8}$$

and it follows that

$$l_3 = r_c \tan \phi \quad \text{.....4.9}$$

The overall length of cut can be determined from

$$l_t = l_1 + l_c + l_2 - l_3$$

$$= l_1 + \frac{\pi \cdot r_c(180 + \phi)}{180} + \frac{l_1}{\cos \phi} - r_c \tan \phi \quad \text{.....4.10}$$

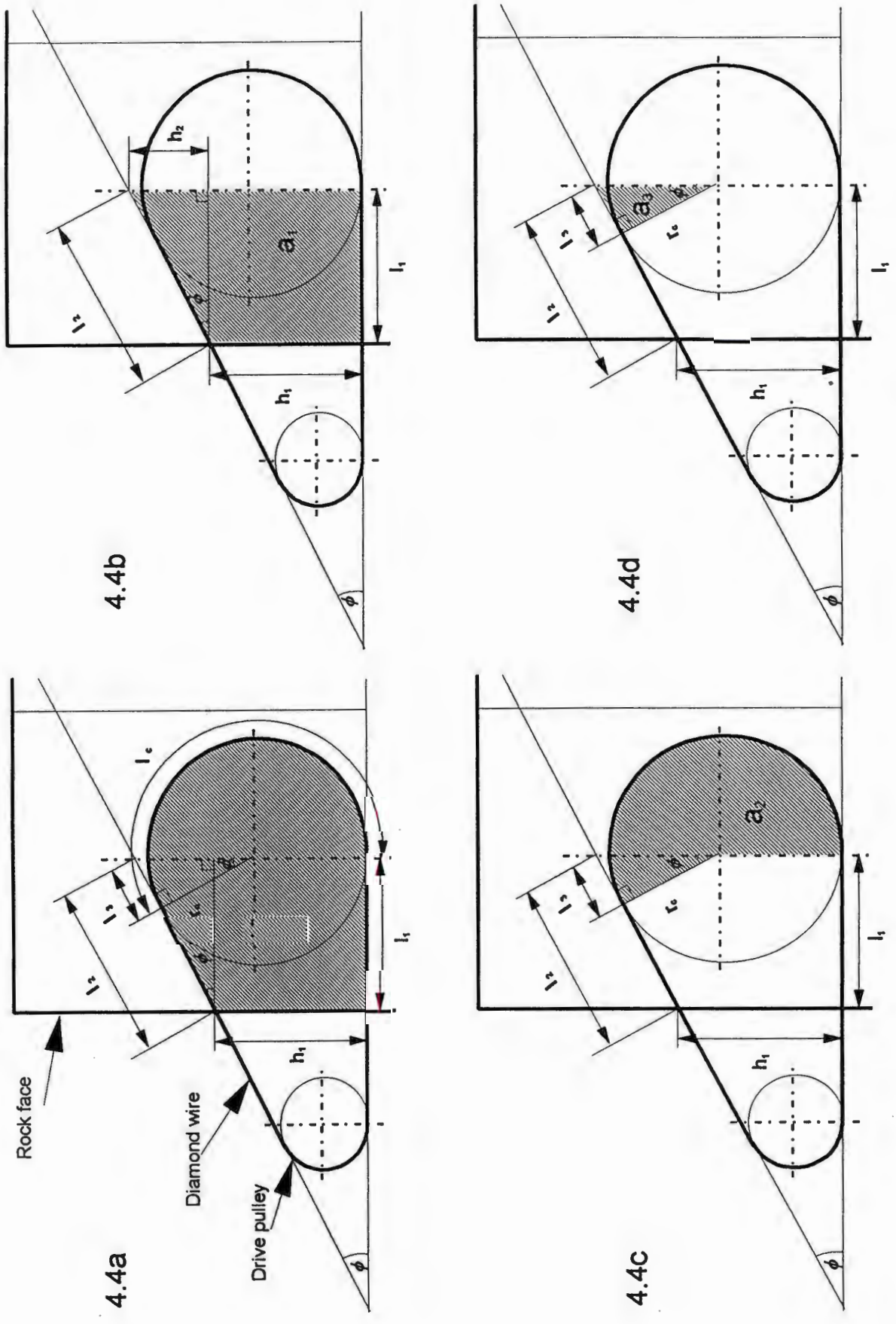

Figure 4.4 Schematic diagrams of the pull cutting system for a pulley radius $\leq$ the radius of cut

Towards the end of cut, when the radius of the cut < the drive pulley radius, the overall length of cut can be similarly calculated. From Figure 4.5a, lengths

$$l_c = \frac{\pi \cdot r_c(180 - \phi)}{180}$$

$$l_2 = \frac{l_1}{\cos\phi} \quad \text{and}$$

$$l_3 = r_c \tan\phi$$

The overall length of the cut can be found from

$$l_t = l_1 + l_c + l_2 + l_3$$

or

$$l_t = l_1 + \frac{\pi \cdot r_c(180 - \phi)}{180} + \frac{l_1}{\cos\phi} + r_c \tan\phi \quad \text{.....4.11}$$

4.3.2 Determination of the area sawn

The overall area to be cut can be determined by dividing it into easily definable geometric shapes. For $r_c \geq$ the drive pulley radius, (Figure 4.4b)

$$a_1 = \frac{l_1(h_1 + h_1 + h_2)}{2}$$

$$= \frac{l_1(2h_1 + l_1 \tan\phi)}{2} \quad \text{.....4.12}$$

where

h_1 = the separation height of the wire at the rock face.

The area of the circular sector (Figure 4.4c)

$$a_2 = \frac{\pi \cdot r_c^2(180 + \phi)}{360} \quad \text{.....4.13}$$

and the triangular area (Figure 4.4d)

$$a_3 = \frac{r_c \cdot l_3}{2}$$

$$= \frac{r_c^2 \tan\phi}{2} \quad \text{.....4.14}$$

The overall area to be cut (Figure 4.4a) is therefore

$$a_t = a_1 + a_2 - a_3$$

$$= \frac{l_1(2h_1 + l_1 \tan\phi)}{2} + \frac{\pi \cdot r_c^2(180 + \phi)}{360} - \frac{r_c^2 \tan\phi}{2} \quad \text{.....4.15}$$

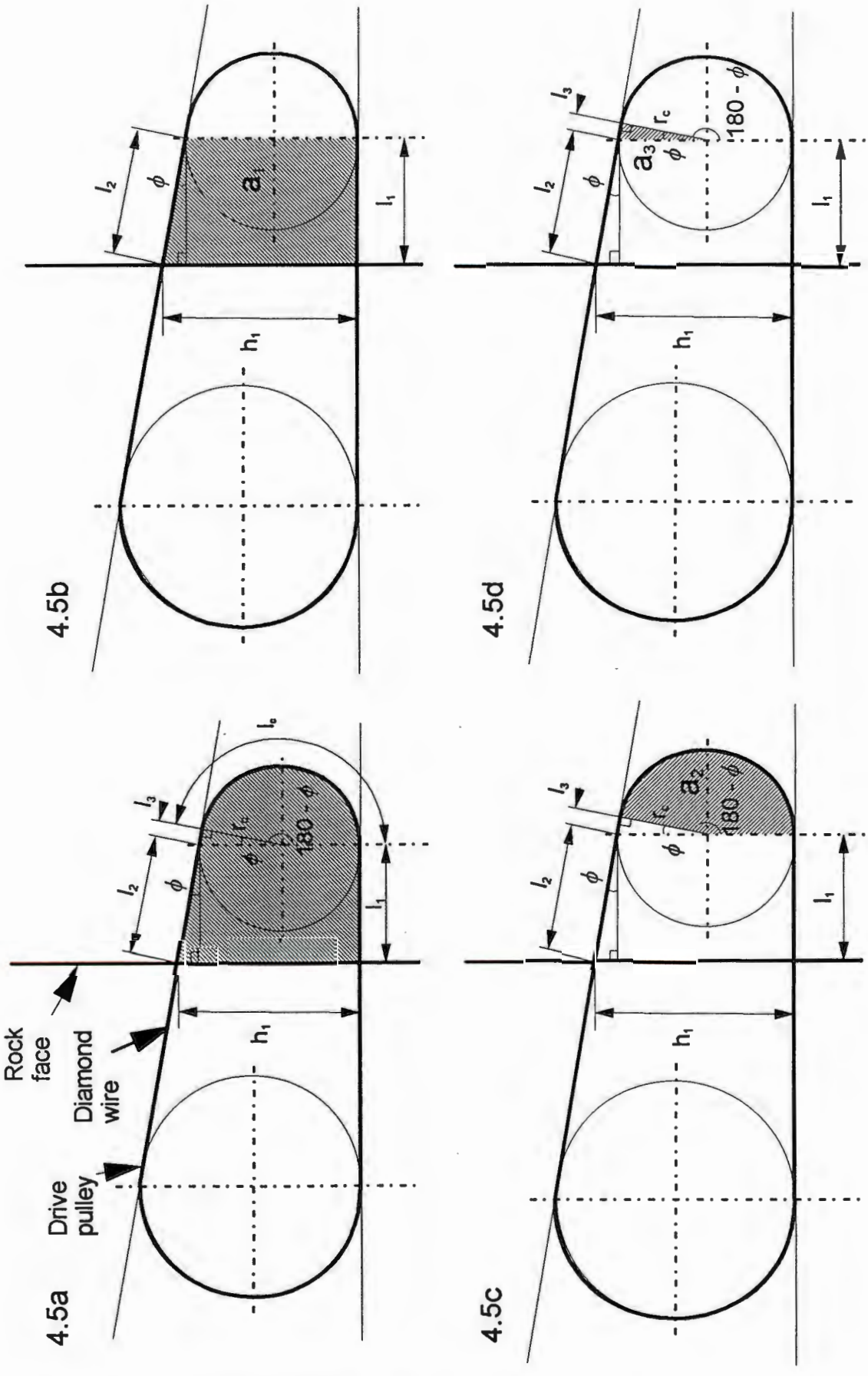

Figure 4.5 Schematic diagrams of a pull cutting system for a pulley radius > the radius of cut

When the radius of the cut $<$ the drive pulley radius, from Figures 4.5b, 4.5c and 4.5d, the areas to be cut can be divided into

$$a_1 = \frac{l_1(2h_1 - l_1 \tan\phi)}{2} \quad \text{.....4.16}$$

$$a_2 = \frac{\pi \cdot r_c^2(180 - \phi)}{360} \quad \text{.....4.17}$$

and

$$a_3 = \frac{r_c^2 \tan\phi}{2} \quad \text{.....4.18}$$

The overall area to be cut can be determined from

$$a_t = a_1 + a_2 + a_3$$

or

$$a_t = \frac{l_1(2h_1 - l_1 \tan\phi)}{2} + \frac{\pi \cdot r_c^2(180 - \phi)}{360} + \frac{r_c^2 \tan\phi}{2} \quad \text{.....4.19}$$

If h_p and l_p are the height and length of the panel to be cut respectively, it follows for either equation 4.15 or 4.19, the area sawn

$$a_c = h_p \cdot l_p - a_t \quad \text{.....4.20}$$

4.4 The determination of forces acting on diamond wire beads over a constant cutting radius

The forces acting on a given diamond wire bead are dependent on the tensions of the wire on each side of the bead and the angular deflection of the wire with the bead's polar axis, as shown in Figure 4.6. If we let θ be the angle between the wire and bead's polar axis at its leading edge and β be the angle between the wire and the bead's polar axis at its trailing edge, then for the cutting geometry shown in Figure 4.3, as the bead enters the cutting arc, θ is determined by the dimension of the cutting radius and $\beta = 0$. For a constant cutting radius, wire angles $\theta = \beta$ and at the exit of the arc, the bead's leading wire angle, $\theta = 0$ with β determined by the dimension of the cutting radius.

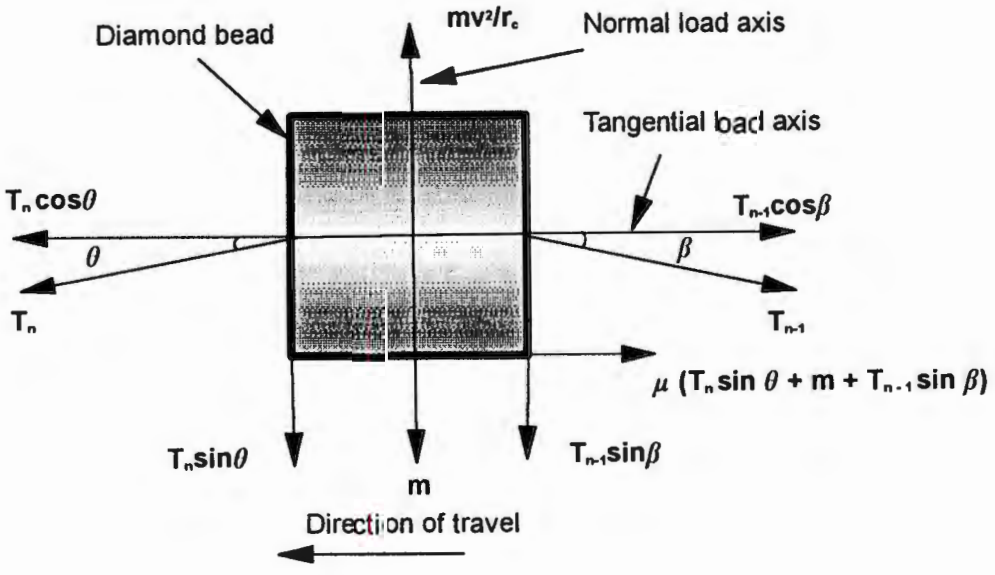

Figure 4.6 Force diagram for a diamond wire sawing bead

If we resolve the normal forces acting on a wire bead on the cutting arc, we get the general expression

$$T_n \sin\theta + m + T_{(n+1)} \sin\beta - \frac{m \cdot v^2}{r_c} \quad \text{.....4.21}$$

where is $\frac{m \cdot v^2}{r_c}$ the centrifugal force acting on the bead assembly at a linear velocity v over the radius of cut r_c

and

T_n = the tension of the wire on the bead's leading edge and
$T_{(n+1)}$ = the tension of the wire on the bead's trailing edge
m = the mass of the bead assembly for one bead pitch

By resolving the components of the forces along the polar axes of a bead on the cutting arc, a general equation can be derived for wire tension across the bead.

$$T_n \cos\theta = \mu(T_n \sin\theta + m + T_{(n+1)} \sin\beta - \frac{m \cdot v^2}{r_c}) + T_{(n+1)} \cos\beta \quad \text{.....4.22}$$

where

μ = the coefficient of friction of the bead with the workpiece material

Considering all the beads along the length the cutting arc, an equation can be derived for the tension of the wire

$$T_1 = \mu(m + T_2 \sin\beta - \frac{m \cdot v^2}{r_c})$$

$$+ \mu(T_2 \sin\beta + m + T_3 \sin\beta - \frac{m \cdot v^2}{r_c}) + \ldots$$

$$+ \mu(T_n \sin\beta + m + T_{(n+1)} \sin\beta - \frac{m \cdot v^2}{r_c}) + \ldots$$

$$+ \mu(T_{(s-1)} \sin\beta + m - \frac{m \cdot v^2}{r_c}) + T_s$$

.....4.23

where

T_1 = the tension on the tight side of the wire between the drive pulley and bead **1** exiting the cutting arc.

T_s = the tension on the slack side of the wire for bead **s** entering the cutting arc.

It follows therefore from equation 4.23 that the tension of the wire reduces progressively over the length of curvature of the cut from $\mathbf{T_1}$ to $\mathbf{T_s}$. A bead traversing over the length of curvature of the cut of constant radius will experience a normal force defined by $\mathbf{T_s}$ and $\mathbf{T_{s-1}}$ in equation 4.22 as it enters the curvature, which will progressively increase to a force defined by $\mathbf{T_1}$ and $\mathbf{T_2}$ as it exits the curvature.

While the approximation of a constant radius holds for most stationary sawing applications, in quarrying applications the cutting arc typically has an increasing radius towards the exit of the cut which tends to reduce the difference in normal forces experienced by a bead between entrance and exit of the cutting arc.

CHAPTER 5

THE EFFECTS OF DIAMOND QUALITY ON DIAMOND WIRE PERFORMANCE

5.1 Conditions affecting diamond bead wear

In the assessments of diamond wire performance discussed earlier, it has been shown that the wear of diamond wire is related to parameters such as load, cutting rate, linear velocity, the type of workpiece material and the length of cut. The performance of diamond wire also depends on its design and the constituents of its bead matrix. The performance is primarily dictated by the way the diamond particles and bond material in the diamond matrix wear. A free cutting action occurs when a suitable wear balance is achieved between the diamond and the bond, allowing the various wear states of each diamond particle to progressively occur. The wear mechanism indicator (Figure 1.4) shows that different diamond grades within a product range, have different wear characteristics and life expectancies.

5.2 Diamond bead test apparatus

Based on these wear characteristics, a study was carried out to investigate the effects of different diamond grades on diamond wire performance. A single bead test apparatus was designed and built to enable different beads to be tested individually under laboratory conditions. The apparatus was configured to facilitate the following.

- A desired load or feed rate could be accurately applied to a bead during cutting.
- Cutting forces could be measured, providing real time traces of the cutting dynamics.
- The bead could be rotated during operation to allow torque measurements to be taken or indexed at a desired rate to ensure even wear of the matrix around its periphery.
- Matrix wear could be determined accurately by measuring the bead mass (or volumetric reduction).
- Microscopy evaluations of a bead's surface could be undertaken at desired stages during a test.

The apparatus consisted of a shaft onto which a diamond bead was mounted and secured by a spacer tube and lock nut. The shaft was free to rotate in bearings mounted in a bracket assembly. The assembly was mounted onto a cutting tool dynamometer so that forces normal to the cutting surface and along the direction of cut of the bead could be measured. The cutting tool dynamometer in turn was fixed to the base of the tool post of a workshop lathe (Plate 5.1).

A constant load or a constant feed rate could be applied to the bead by either bolting the bracket assembly directly onto the cutting tool dynamometer and traversing the tool post at the required rate towards the stone sample or by mounting the bracket assembly onto a pivot arrangement which enabled load to be applied to the bead by a calibrated spring scale. With this configuration, the in-feed rate of the tool post is set to coincide with the cutting rate of the bead.

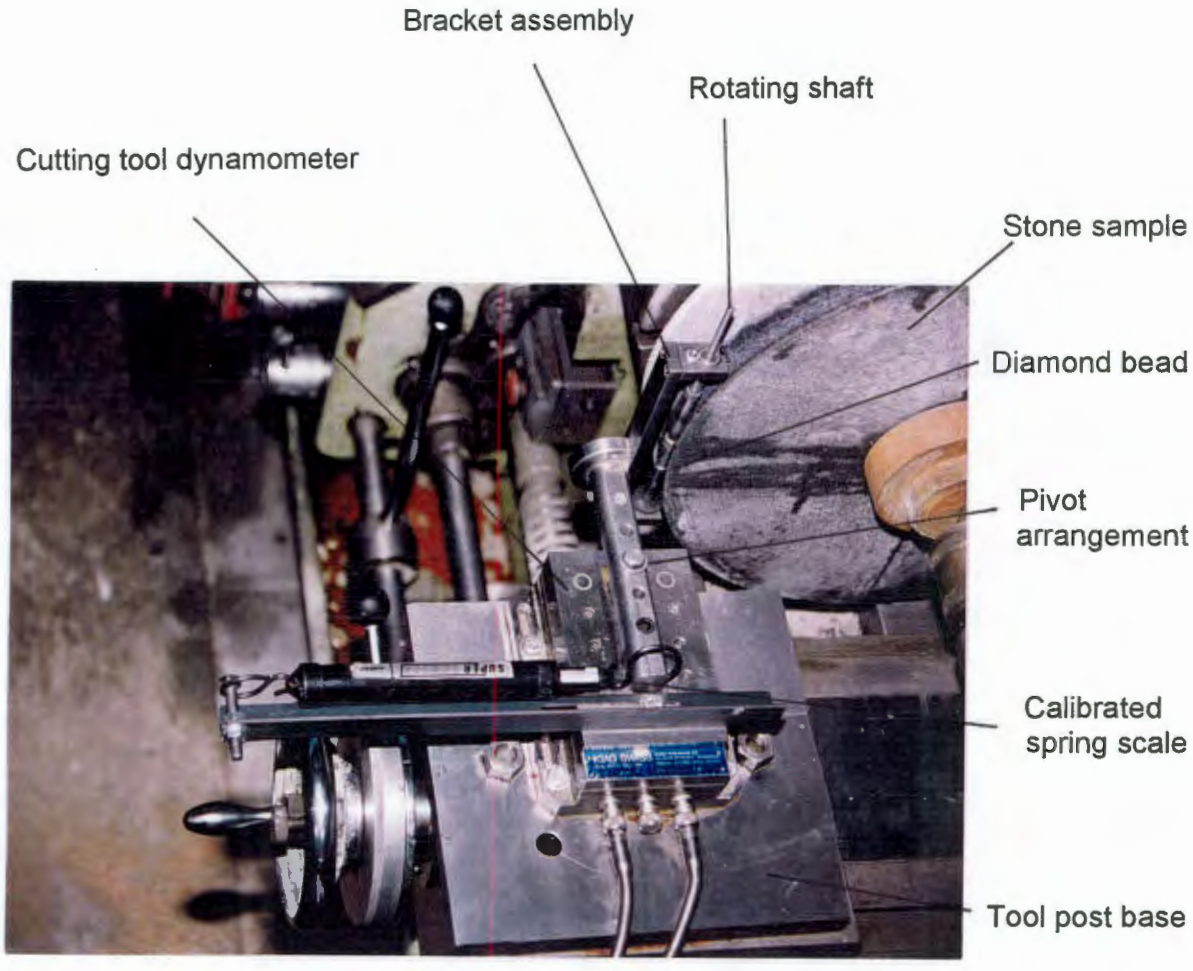

Plate 5.1 Single bead testing apparatus

A pair of charge amplifiers were used to excite two axes of the cutting tool dynamometer and to provide voltage signals which were captured by a storage oscilloscope. Samples of Rustenburg gabbro measuring approximately 41 cm in diameter and 10 cm thick were used for the tests. The sample was clamped between two wooden discs by the lathe end stock and chuck and constrained by the chuck jaws.

Start up effects were minimised by running each bead in the test material for 2 minutes under low load conditions to ensure ample diamond exposure. Adequate surface contact between the bead and the stone samples was ensured by cutting grooves of 5,5 mm radius into circumferences of the stone.

5.3 Diamond selection

Performance tests were carried out on three types of beads each containing a different grade of synthetic diamond grit. Diamond grit of 40/50 US mesh size at 35 concentration in a cobalt bond was used, which is a typical diamond bead matrix specification for the type of stone used. The diamond grades were selected from the De Beers SDA+ products manufactured using cobalt based solvents. Selection was based on the relative strengths and wear characteristics shown in the wear mechanism indicator (Figure 1.4).

- SDA 100+ which is a product containing crystalline diamond particles with good edge definition and blocky shape as shown in Plate 5.2a. The particles exhibit good relative strength and thermal stability factors of 8, 8 and 7 at room temperature, 900 and 1100 degrees Celsius respectively.
- SDA 85+ which exhibits a good crystalinity and contains blocky crystals as shown in Plate 5.2b. The product has a lower strength relative to SDA 100+ and is not as thermally stable with factors of 7, 7 and 5 at room temperature, 900 and 1100 degrees Celsius respectively.
- SDA 75+ which contains fewer cubo-octahedral shapes than the above two products but the particles generally exhibit reasonable crystallinity as shown in Plate 5.2c. The relative strength and thermal stability of the product are lower with factors of 6, 6 and 4 at room temperature, 900 and 1100 degrees Celsius respectively.

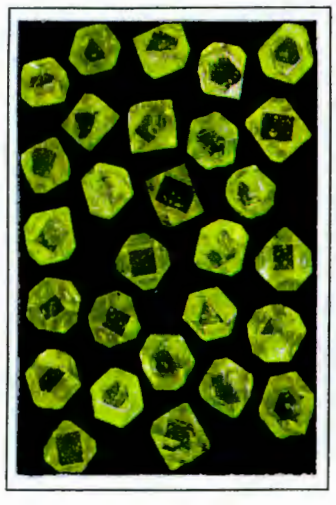

Plate 5.2a SDA 75+ synthetic diamond

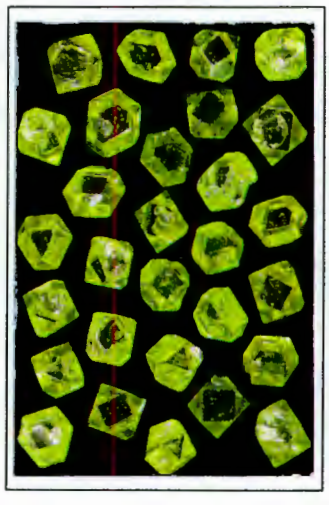

Plate 5.2b SDA 85+ synthetic diamond

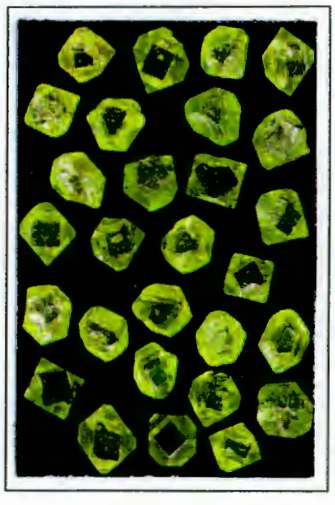

Plate 5.2c SDA 100+ synthetic diamond

5.4 Performance test results

5.4.1 The measurement of cutting forces

Tests were carried out to establish the relationship between the normal force resulting from the applied load and the tangential force as a result of the cutting action of the bead (Figure 4.6). The applied load range was based on the average load per bead determined from diamond wire performance measurements (53) and laboratory bead testing (54). Graph 5.1 shows the relationship of the forces determined from the oscilloscope traces tabulated in Appendix 5. Tests were run at 20 ms^{-1} cutting velocity. Tap water at a flow rate of 0,6 litres per minute was used as the cutting fluid.

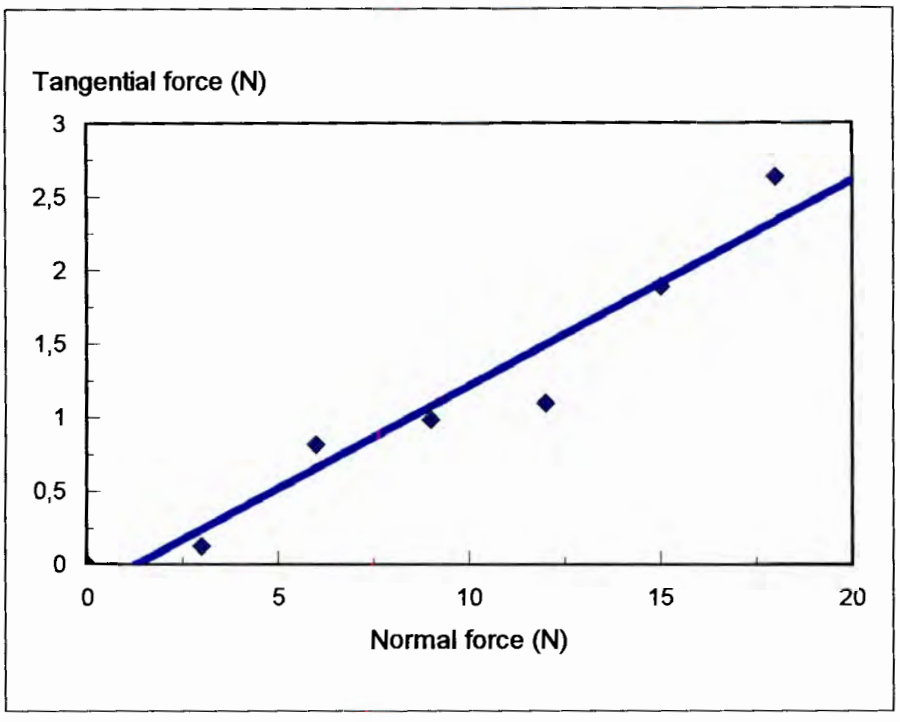

Graph 5.1 The relationship between normal and tangential forces on a diamond wire bead

It can be seen that a linear trend exists between the normal and tangential cutting forces. The tangential force in relation to the corresponding normal force is slightly higher in single bead testing than that measured in stationary wire sawing (52)(53). However the results from these wire sawing tests depict the averaged force components on the beads in contact with the workpiece and not the absolute values on each bead.

5.4.2 The effect of cutting velocity on diamond bead wear

Tests were carried out to assess the effects of diamond grade on bead wear over a range of cutting velocities. A bead was run at a given velocity for 16 minutes in the stone sample with an applied load of 9 N. To ensure even wear of the diamond matrix, the shaft containing the bead was indexed through 90 degrees

every 15 seconds during operation The results of the bead wear rates (see Appendix 6) in relation to cutting velocity are shown in Graph 5.2. The small errors in velocity due to the reducing cutting diameter were not taken into account.

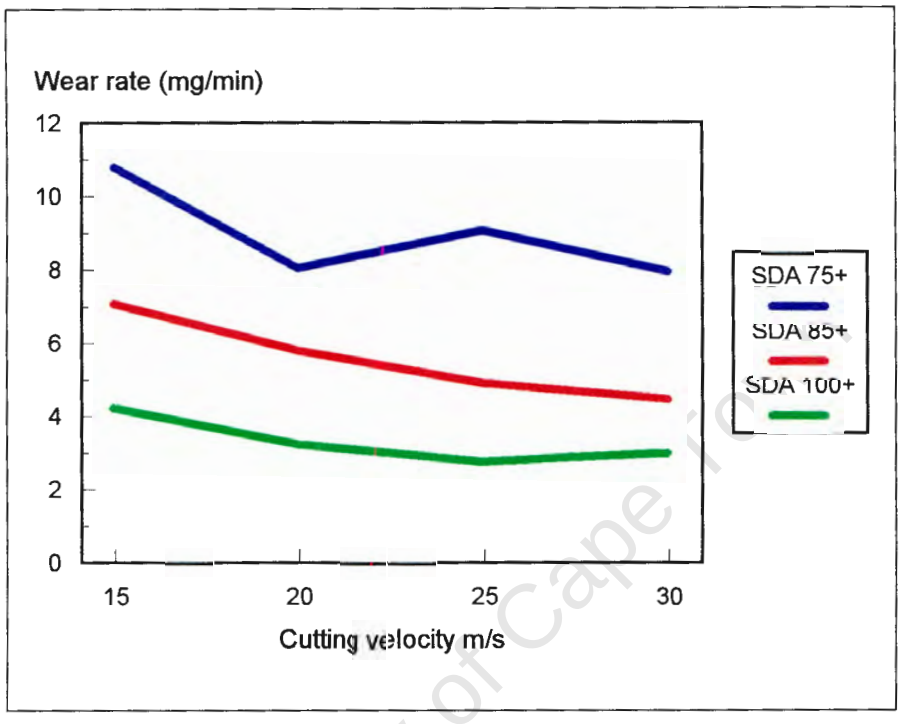

Graph 5.2 Diamond bead wear rates in relation to cutting velocity

Lower wear rates were achieved by the diamond beads containing higher quality diamond. The results for beads using SDA 100+ and SDA 85+ tested at 30 ms^{-1} were characterised by a number of diamond particles which exhibited extended wear flatting, which tended to reduce the wear rates. The findings however are consistent with wire sawing results in the field (57) where too high a cutting velocity for the material being cut causes extended wear flatting of diamond particles in beads.

All subsequent cutting rate and wear tests were carried out at 20 ms^{-1} (ignoring the velocity error referred to in Appendix 6).

5.4.3 The effect of diamond grade on bead cutting performance and wear

Data for the determination of bead cutting performance were obtained from measurements of the depth of the grooves cut into the circumference of the stone sample. Readings were taken after every two minutes of cutting and each test was terminated after 16 minutes. Bead indexing and water flow rates remained as set for the previous tests. The bead was weighed at intervals coinciding with cutting measurements.

While an amount of variance exists with the cutting rate data for the three bead types (refer to Appendix 7), the plots of cumulative area cut vs. time, shown in Graphs 5.3.1 to 5.3.3 indicate typically linear trends. These trends imply constant tendencies in the cutting rates. Increased cutting rates were achieved at higher loads with the beads using the higher diamond grades which can be seen from the steeper gradients in Graph 5.3.3. The cutting rates of beads using SDA 100+ and SDA 85+ tended to reduce at lower loads as the tests progressed which was associated with progressive wear flatting of diamond particles on the surfaces of the beads.

Graph 5.4 shows the averaged cutting rates for the three diamond grades over the range of applied loads. No meaningful differences in cutting rates are evident below 12 N, but a diverging trend for beads using SDA 100+ at higher loads can be seen, with higher cutting rates being exhibited.

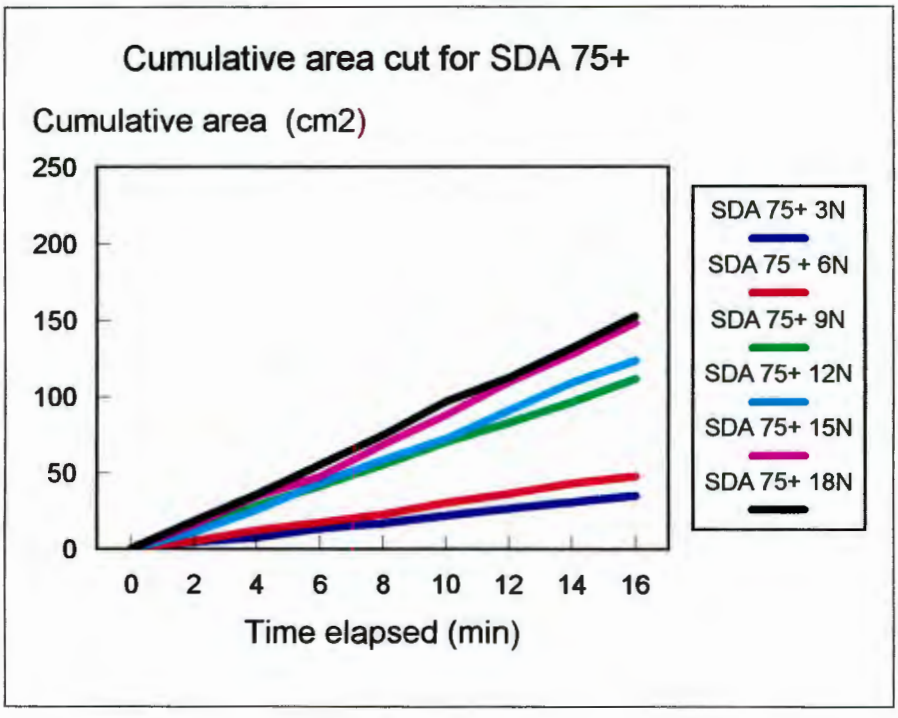

Graph 5.3.1

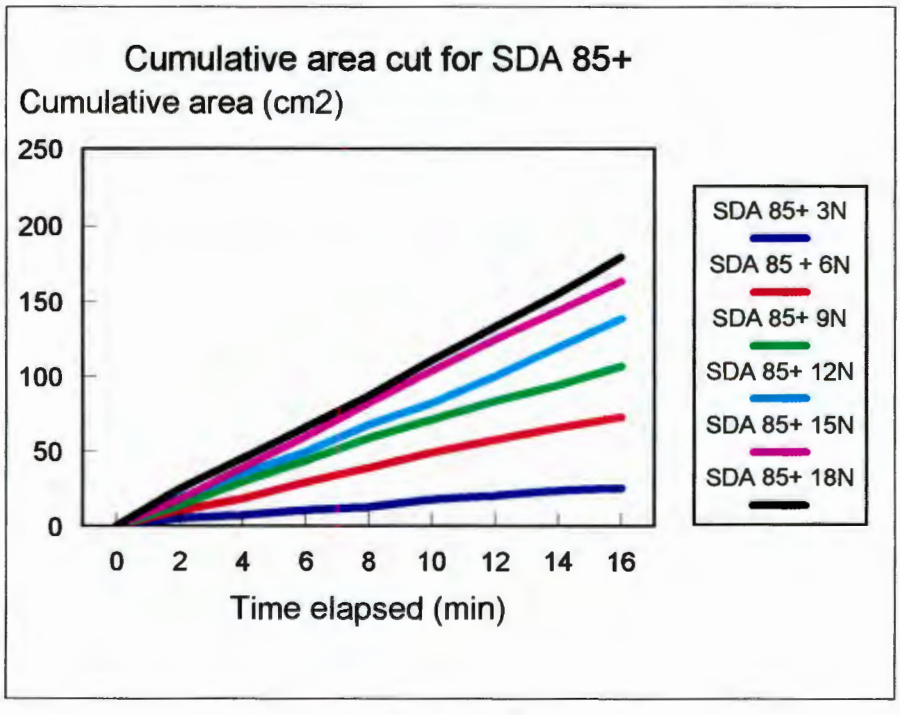

Graph 5.3.2

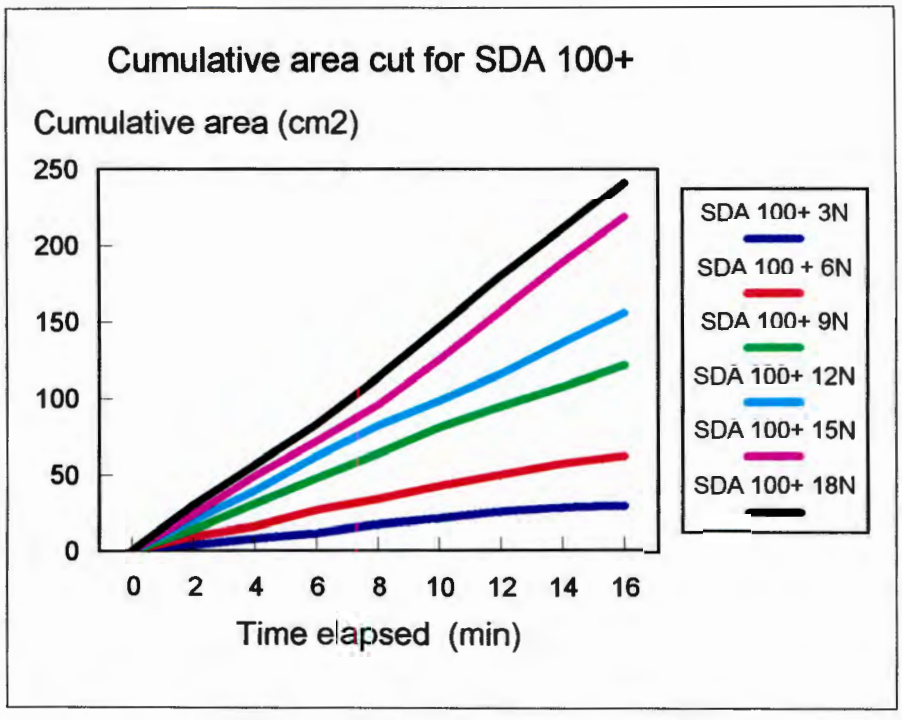

Graph 5.3.3

Graphs 5.3.1 - 5.3.3 Cumulative area cut over elapsed time

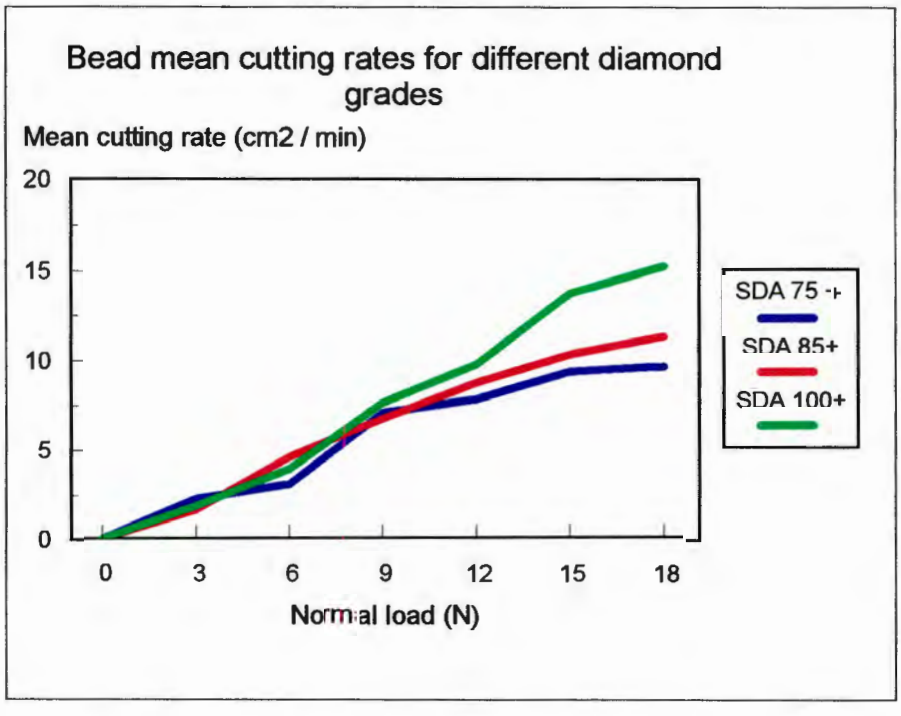

Graph 5.4 Mean cutting rates in relation to applied load

Assuming that the distributions for the sets of results for bead cutting rates are normal and with the bead types being identical other than the diamond used, the Student t-test was used to determine significant differences in the dependent sets of data for each bead type. The Statistica computer software package was employed for the analysis of the data.

Using a 95 percent confidence limit, the t-test analysis of bead cutting rates (see Appendix 10) is summarised in Table 5.1, where the marked values indicate the results which are significantly different at $p < 0,05$.

Diamond type		3 N load	6 N load	9 N load	12 N load	15 N load	18 N load
SDA 75+	p	0,024*	0,002*	0,368	0,141	0,093	0,003*
SDA 85+	t	2,868*	-4,788*	0,963	-1,657	-1,944	-4,478*
SDA 75+	p	0,251	0,053	0,069	0,007*	0,000*	0,000*
SDA 100+	t	1,251	-2,326	-2,142	-3,752*	-7,423*	-9,730*
SDA 85+	p	0,517	0,002*	0,005*	0,054	0,003*	0,000*
SDA 100+	t	-0,683	4,648*	-3,970*	-2,310	-4,480*	-9,773*

Table 5.1 Student t-test results of diamond bead cutting rates where p is the level of significance and t is the variate for the t distribution

Referring to Graph 5.4, the t-test analysis indicates that the cutting rates of beads using the highest and lowest diamond grades selected are not significantly different up to 9 N applied load. The cutting rates of beads become significantly different at higher loads.

The cumulative mass reductions for the three bead types tested are shown in Graphs 5.5.1 to 5.5.3 for the range of applied loads (see Appendix 8). The linear trends in cumulative mass reduction plots indicate constant tendencies in wear rates. Beads using SDA 75+ showed the greatest variation of mass reduction in relation to load, with higher loads substantially increasing the rate of mass reduction, indicated by the steeper gradients in Graph 5.5.1. The beads, in which diamond particles exhibited extended wear flatting at low loads, had low wear rates.

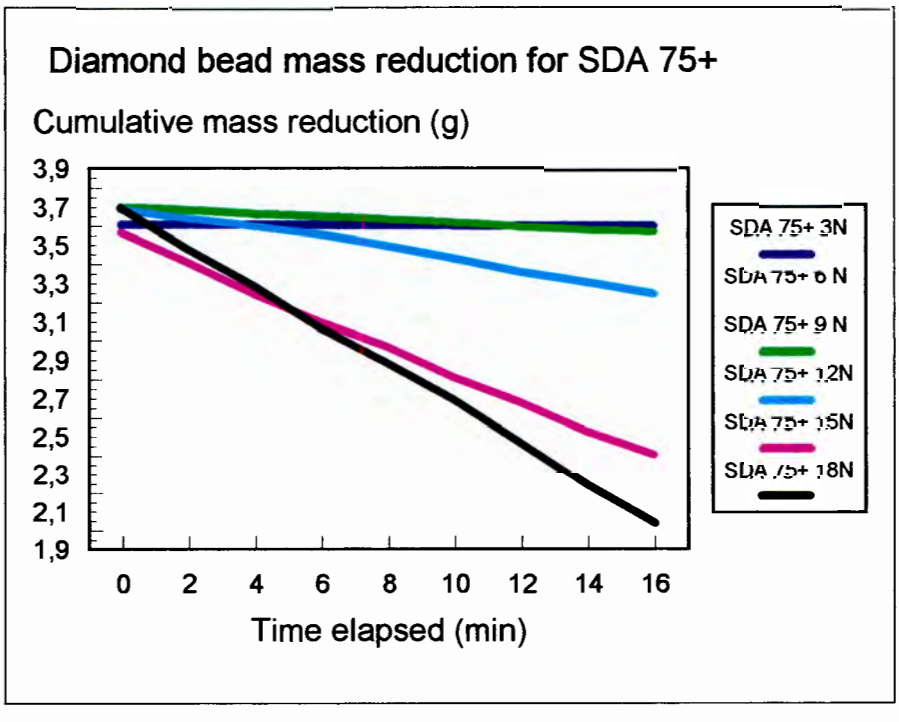

Graph 5.5.1

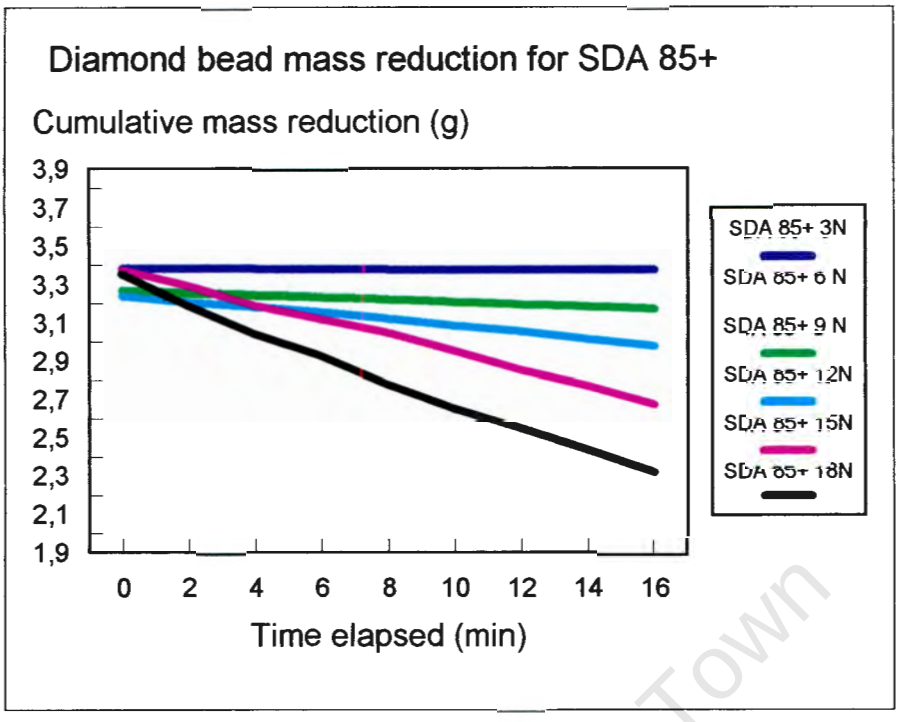

Graph 5.5.2

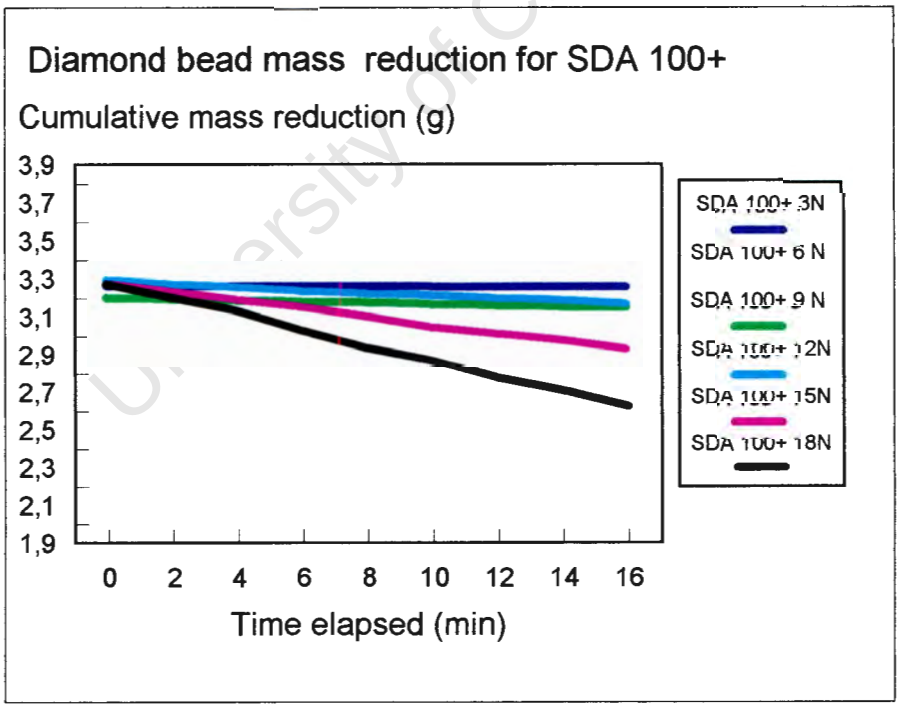

Graph 5.5.3

Graphs 5.5.1 - 5.5.3 Diamond bead cumulative mass reduction over elapsed time

The averaged bead wear rates for the three diamond grades over the range of applied loads are shown in Graph 5.6. Beyond 9 N load, a clear divergence between the averaged wear rates is evident, with beads using the lower grade of diamond exhibiting higher averaged wear rates.

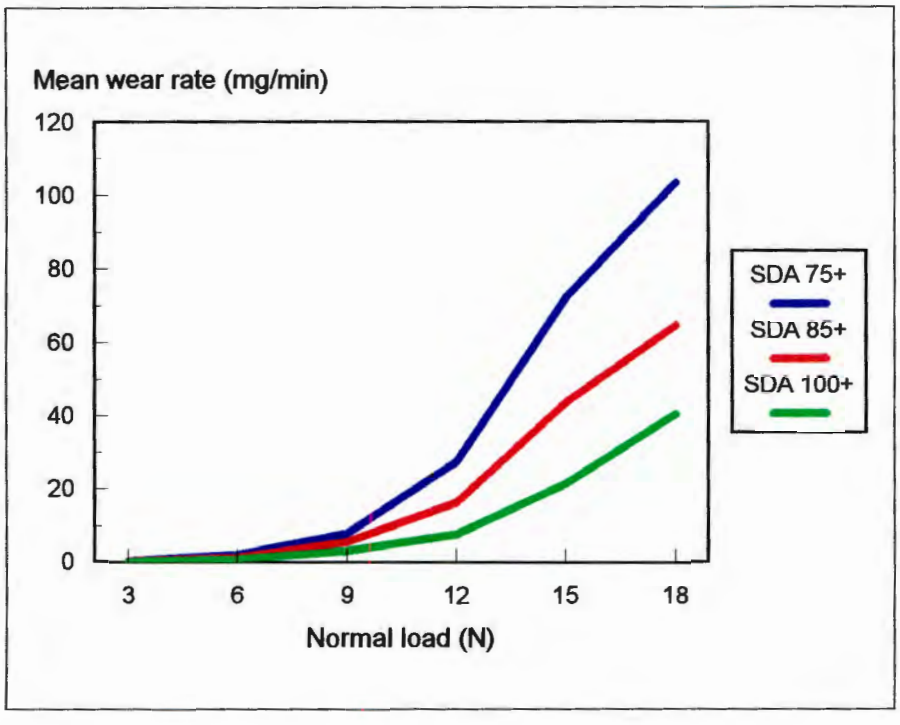

Graph 5.6 Averaged diamond bead wear rates in relation to applied load

Using the same criteria in the Student t-test, an analysis of bead wear rates was carried out (refer to Appendix 11) and the results are summarised in Table 5.2.

Diamond type		3 N load	6 N load	9 N load	12 N load	15 N load	18 N load
SDA 75+	p	0,292	0,009*	0,001*	0,000*	0,000*	0,000*
SDA 85+	t	1,141	3,620*	5,405*	6,711*	8,190*	6,176*
SDA 75+	p	0,000*	0,000*	0,000*	0,000*	0,000*	0,000*
SDA 100+	t	7,470*	9,214*	13,916*	9,343*	16,214*	17,830*
SDA 85+	p	0,006*	0,006*	0,000*	0,001*	0,000*	0,002*
SDA 100+	t	3,904*	3,832*	8,167*	5,933*	8,309*	4,631*

Table 5.2 Student t-test results of diamond bead wear rates

The wear rates for the three bead types are significantly different above 3 N load, as indicated by the diverging trend of average wear rates over the load range tested (see Graph 5.6).

By combining the cutting and wear data, the specific wear rate (mass loss of the bead per unit in area cut) and the productivity, the inverse of specific wear rate, can be evaluated (refer to Appendix 9). The specific wear rates of the beads in Graph 5.7 show similar diverging trends to the averaged wear rates shown in Graph 5.6, with a rapid rise in specific wear associated with load increase. The corresponding bead productivity plots in Graph 5.8 show a rapid reduction in bead productivity down to low levels as the cutting rate rises.

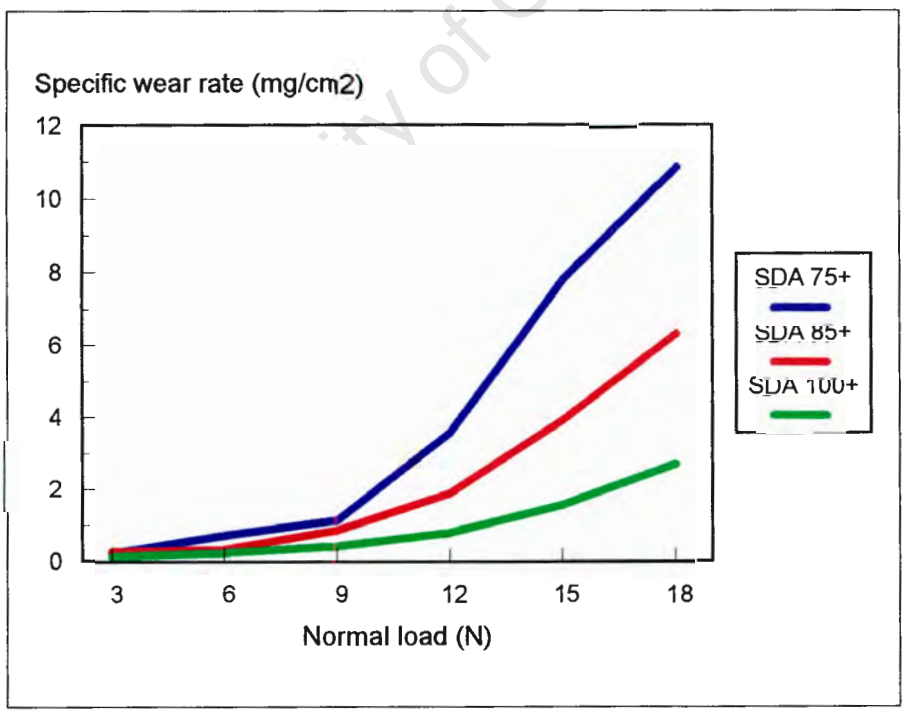

Graph 5.7 Diamond bead specific wear rates in relation to applied load

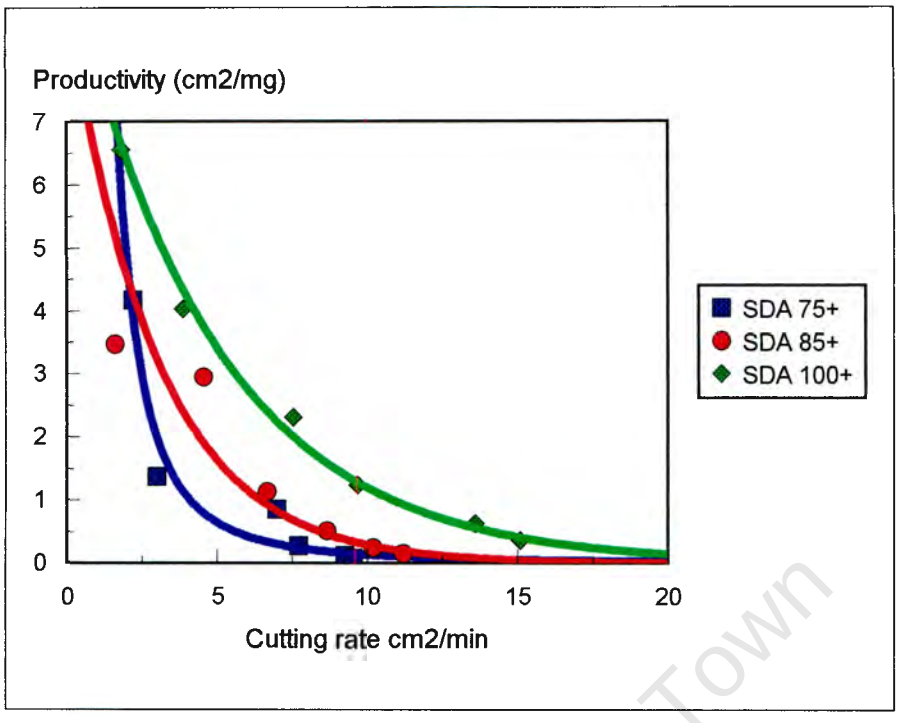

Graph 5.8 Diamond bead productivity vs. cutting rate

5.5 Discussion on diamond bead performance

The results from the single bead tests have shown that diamond bead wear is sensitive to applied load, characterised by accelerated wear as the load is increased. The choice of diamond product has an influence on bead wear rate, with higher quality diamond significantly reducing bead wear. This becomes increasingly apparent at higher loads. A relationship exists between bead wear rate and diamond particle strength as defined by the diamond classification indices (Figure 1.4). At low loads there is a greater tendency for higher quality diamond to exhibit extended wear flatting which reduces the cutting rate as the bead becomes progressively blunt.

Bead cutting rates increase with load and at higher loads it was found that higher quality diamond tends to produce higher cutting rates. High cutting rates are

however at the expense of high wear rates, shown by a rapid fall in the productivity of the bead. The specific wear and productivity attributed to the beads tested, have shown similar trends to reported field results and laboratory tests (54).

CHAPTER 6

THE MEASUREMENT OF DIAMOND WIRE ROTATION

6.1 Diamond bead ovalisation

In order to achieve concentric wear of bonded diamond wires, where the beads are fixed to the wire cable, it is necessary for the wire to rotate about its polar axis during operation. Uneven wear occurs when a certain bead orientation becomes favoured during cutting, which results in an area of preferential wear of the bead's diamond matrix. Wire samples collected from the field have indicated that once ovalisation starts, it progressively spreads to a number of adjacent beads along the length of the wire as the wire is used. Plate 6.1 shows an end view of one bead exhibiting concentric wear and one which has ovalised.

Plate 6.1 End view of diamond wire beads showing concentric wear and ovalisation

6.2 The measurement of bead rotational torque

The bead testing apparatus discussed earlier was used to measure the torque required to rotate a single diamond bead under a range of applied loads. Measurements were made with the bead cutting a sample of Rustenburg gabbro a speed of 20 ms^{-1}. The results are given in Appendix 12 and plotted in Graph 6.1.

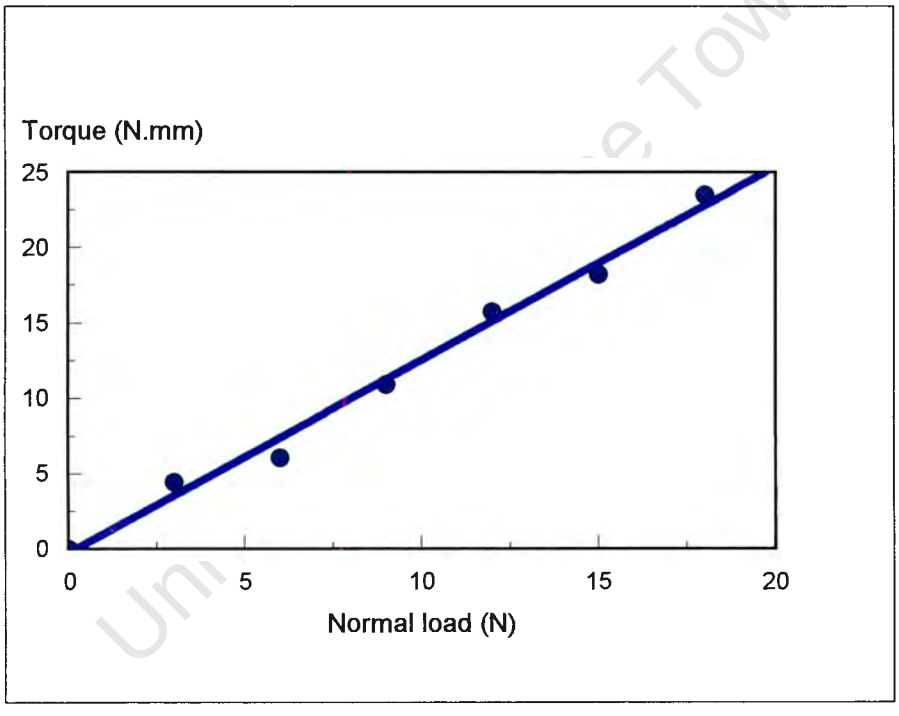

Graph 6.1 Rotational torque vs. applied load for a single diamond bead

It can be seen that the torque required to rotate the bead is linearly dependent on the applied load. With the dependence of cutting rate on applied load (Graph 5.4), it follows that an increasing torque will be required to rotate the bead as the cutting rate is increased.

6.3 The measurement of diamond wire rotation

6.3.1 Free rotation of diamond wire

Tests were carried out on a stationary wire saw on two 20 m lengths of diamond wire, one with injection moulded spacers and the other with vulcanised rubber spacers. Measurements of wire rotation were made with the diamond wire mounted onto the saw but clear of the material to be cut. Wire movement was induced by rotating the machine's pulleys by hand. A mark which was made on the spacer between two beads was followed through a number of cycles of the wire loop and the rotation measured. The results are given in Table 6.1.

Diamond wire type	Bead diameter (mm)	Wire cycles per revolution (360 °)	Direction of rotation along direction of travel
Vulcanised rubber	11,6	16	ccw
Injection moulded plastic	9,8	6	ccw

Table 6.1 Free rotation of different diamond wire types

From the table it can be seen that the wires rotate slowly in a counter clockwise direction viewed along the direction of travel. The direction of rotation was found to correspond to the offset attitude of the machine's pulleys. The smaller bead diameter on the wire with injection moulded plastic spacers would contribute to its higher rotation rate (fewer cycles of the wire loop per revolution of the wire) as the bead would require more revolutions to travel the same linear distance compared to the larger diameter bead (see Figure 1.7). Any torque effects induced by the lay of the cables under tension were not measured.

To study the effects of pre-twisting, the vulcanised wire was repeatedly installed with different amounts of twist, and measurements taken of its rotation. The results are given in Table 6.2.

Twists per 20 m length	Wire cycles per revolution (360 °)
0	16
20	16
60	16

Table 6.2 Diamond wire rotation vs. wire twists

A 20 m length of vulcanised wire was twisted as much as 60 times, however no difference in the rate of rotation could be detected.

6.4 Dynamic measurements of diamond wire rotation

When considering the dynamic measurements of diamond wire rotation, the use of close proximity inductive or magnetic devices for the rotation measurement were discarded in favour of optical techniques. The measurement of the free rotation of diamond wire on a stationary wire saw has shown that the wire rotates slowly in a particular direction which makes wire rotation measurement at a single reference point feasible.

6.4.1 Measurements using a stroboscope

The rotation of the vulcanised diamond wire, sawing a stone block at 20 ms $^{-1}$ velocity on the stationary wire saw, was successfully measured with a

stroboscope and a video camera (see Plate 6.2) using a shutter speed of 800 frames per second. A target made from reflective tape in a step pattern, shown in Figure 6.1, was adhered to the rubber spacer of the vulcanised wire. A leader mark of one metre was painted onto the wire just ahead of the target to assist with video editing (see Plate 6.3).

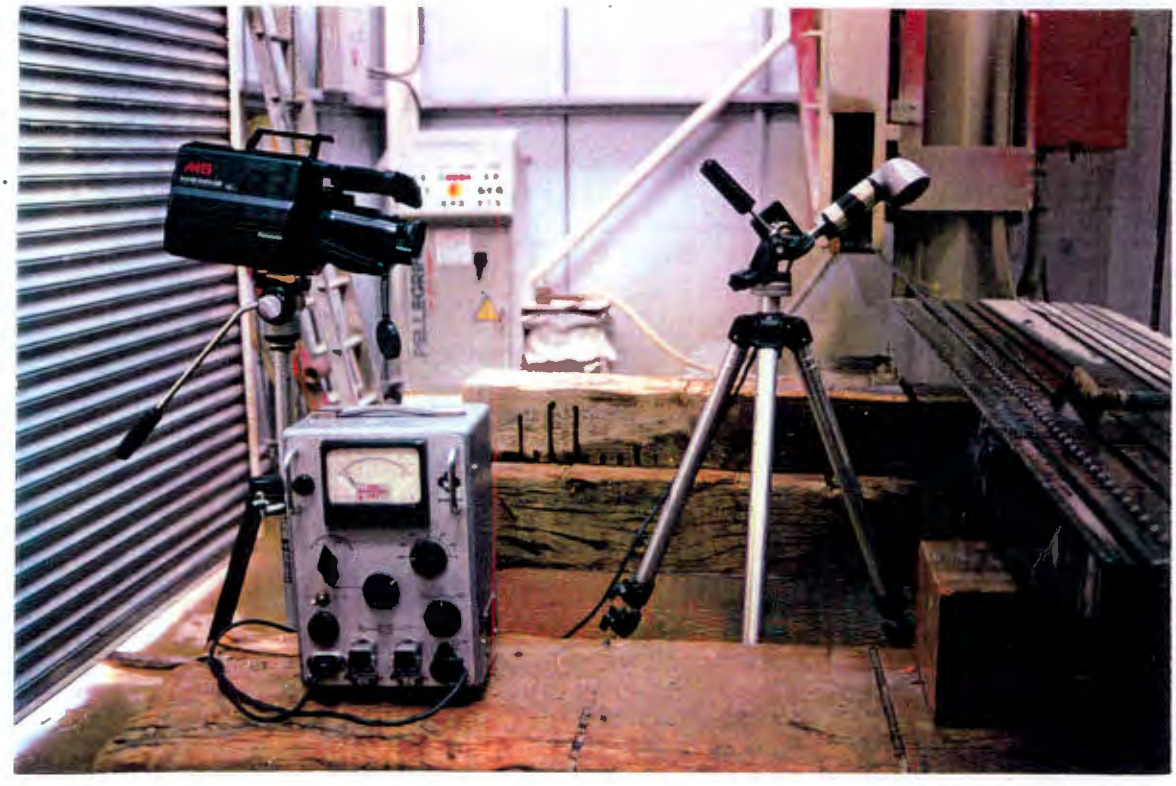

Plate 6.2 Diamond wire rotation measurement using a stroboscope

Although the video images were clear, there was a problem with synchronising the stroboscope with the target at the frequency of approximately one Hertz. Techniques of synchronising the strobe by using a trigger point on the wire were considered but these ideas were discarded in favour of high speed imaging.

6.4.2 High speed video imaging

A NAC HSV 200 high speed video system, incorporating a camera, a tape drive unit, a monitor and a synchronised stroboscope (see Plate 6.4) proved suitable for the analysis of diamond wire rotation. At a wire speed of 20 ms^{-1}, a shutter rate of 200 frames per second provided good image quality with a target position resolution of 100 mm.

The vulcanised diamond wire was inspected to ensure that no beads were ovalised which would influence the results. Tests were carried out on a syenite granite block of 1,5 m in length at cutting rates of 0,75, 1,5 and 2,25 m^2h^{-1}. Rotation was observed just before the wire entered the block as the orientation at this point would have a large influence on the bead orientation in the cut. The video sequence for each test was edited to capture the target for every cycle of rotation of the diamond wire. The results of the diamond wire rotation tests are shown in the photographic sequences in Appendix 13 and summarised in Table 6.3.

Sequence	Cutting rate (m^2h^{-1})	Machine feed rate (mh^{-1})	Wire cycles per revolution (360°)	Direction of rotation
1	0,75	0.5	20	ccw
2	1,5	1	39	ccw
3	2.25	1,5	no wire rotation	none

Table 6.3 Diamond wire rotation at different cutting rates on a stationary wire saw

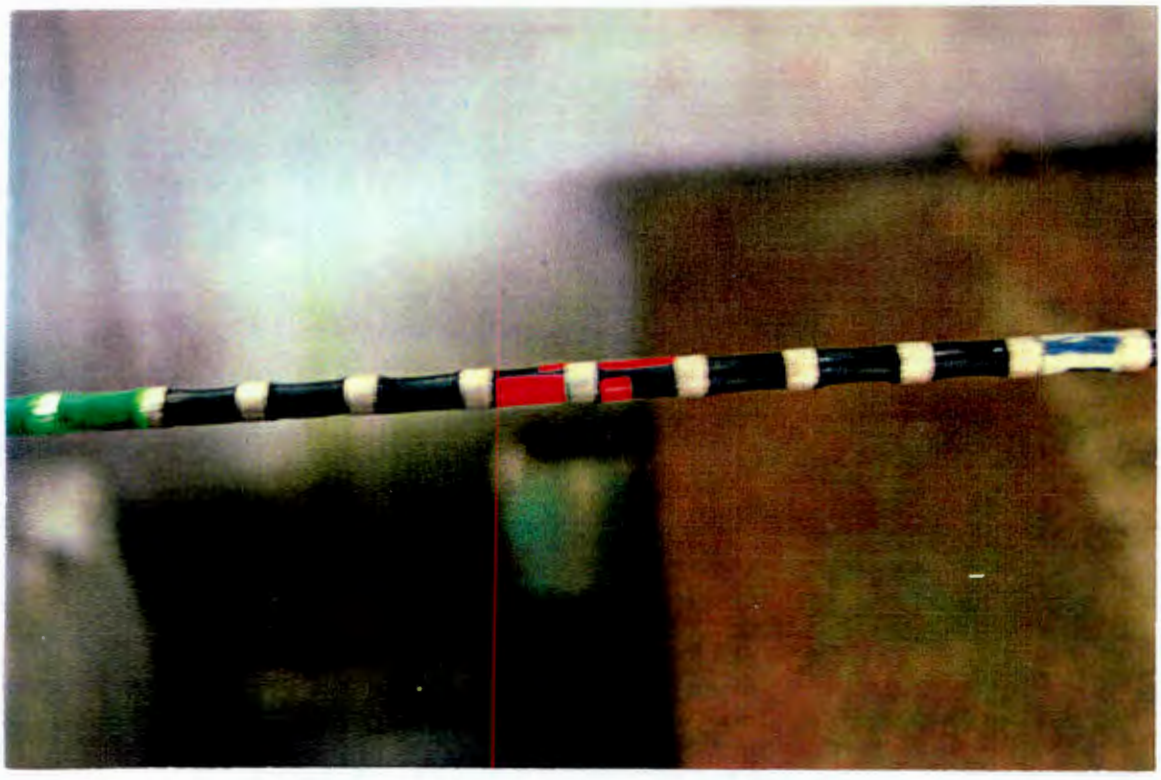

Plate 6.3 Target on the diamond wire for the measurement of rotation

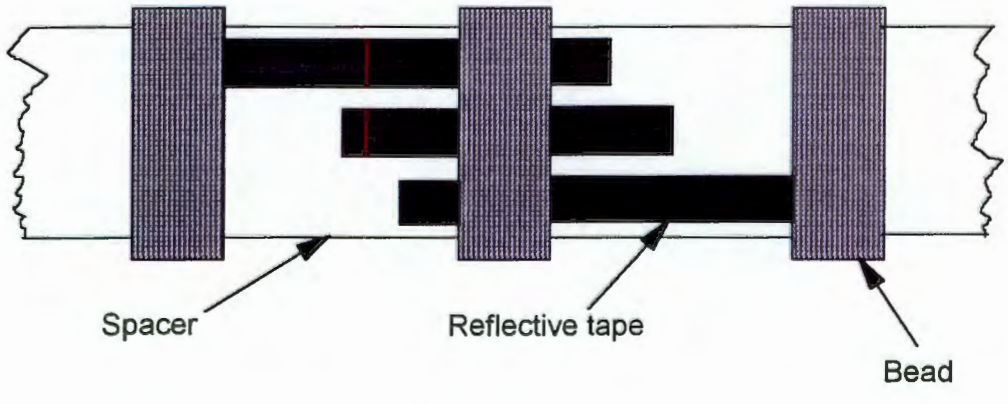

Figure 6.1 Developed section of diamond wire showing the target point for video imaging

Plate 6.4 Diamond wire rotation measurement using high speed video equipment

The target pattern for sequence 1 at 0,75 m^2h^{-1} cutting rate shows that the diamond wire rotates in a counter clockwise direction viewed in the direction of travel, once every 20 cycles of wire movement. Sequence 2 at 1,5 m^2h^{-1} cutting rate shows that the diamond wire rotates by a third of a revolution after 13 cycles and sequence 3 at 2,25 m^2h^{-1} cutting rate shows that no wire rotation takes place. Repeated tests showed little change in wire rotation at the cutting rates considered.

A bead sample was taken from the wire after completing the tests at 0,75 m^2h^{-1} cutting rate and the surface wear was assessed (see Plate 6.5).

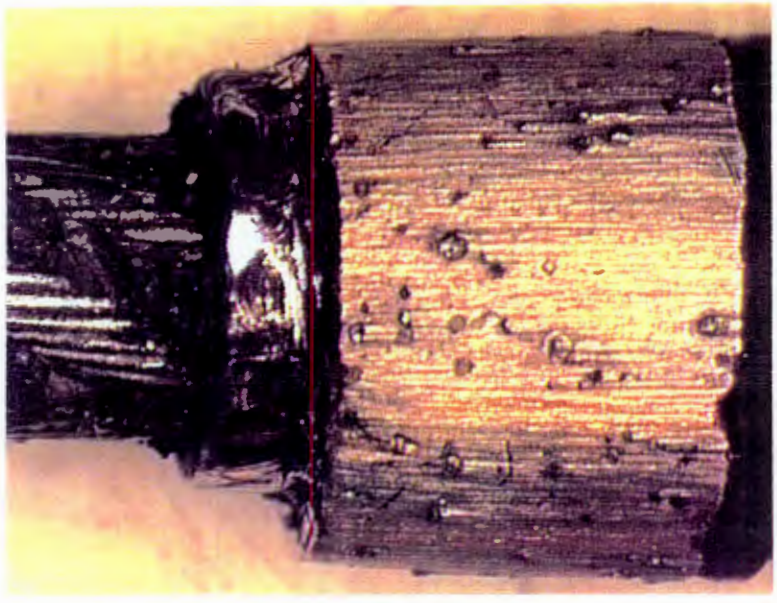

Plate 6.5 Typical wear pattern of a bead's surface after cutting syenite granite at 0,75 m^2h^{-1} on a stationary wire saw

A linear wear pattern is evident on the bead's surface which is orientated axially in the diamond wire's direction of travel.

6.5 Discussion on diamond wire rotation

The diamond wire rotates about its polar axis only partially every cycle in stationary wire sawing which translates into a small angular movement of the bead over the material length being cut. This is verified by the axial wear pattern of the bead's surface shown in Plate 6.5. It could also be possible that no angular movement of the bead takes place during cutting which places great importance on the bead's orientation as it enters the cut. It is expected that the amount of

rotation is dependent on the system's pulley set-up and therefore diamond wire rotation will vary to an extent from machine to machine.

As the cutting rate increases, the amount of wire rotation per cycle reduces and at a point, the resistance to rotation offered by the cut overcomes the torque applied to the wire and the wire stops rotating. Obviously under these conditions the diamond beads would start to ovalise. The pre-twisting of the wire recommended by some diamond tool manufacturers (57) does not in itself cause the wire to rotate about its polar axis as the clockwise moment induced by twisting at one end of the wire equals the anticlockwise moment viewed from the other end and are in equilibrium when the wire is joined.

CHAPTER 7

CONCLUSION

7.1 Concluding discussion and recommendations

It has been established through the literature survey that diamond particles in the matrix of a diamond tool exhibit various wear states, culminating in their eventual breakdown. The wear progression is dependent on the diamond strength and the conditions encountered during cutting. A free cutting action is achieved when a suitable wear balance occurs between the diamond and the bond, allowing the various wear states to take place. The wear states of diamond particles in diamond wire bead matrices were investigated by the author. The investigation has shown that the diamond and matrix wear characteristics are similar to those occurring in other diamond tools.

The life of a diamond tool is dependent on the workpiece material and a number of tests have been developed by researchers to measure the properties of stone which affect the tool's performance. The sawability and abrasivity tests were selected by the author to evaluate the life of diamond wire in different stone workpiece materials. This study has indicated that the sawability test is sufficiently reliable for the prediction of diamond wire life, however the abrasivity test was inconclusive.

Notwithstanding the above, consideration should be given to the abrasivity of stone influencing the wear of the bond matrix, which is not adequately taken into account in the sawability test. A testing method which approximates wire sawing

more closely, by taking into account the load cycles experienced by the beads and the effects of the stone abrasivity and the debris in the cut, would provide a more complete assessment.

Results of laboratory tests and field trials of diamond wire sawing of various stone materials have appeared in the literature. Cutting rate and load measurements have predominantly been based on the cutting performance of a length of diamond wire and bead wear on their diametrical reduction. Single diamond bead testing has been developed to provide a more accurate means of evaluating the cutting performance and wear of diamond wire beads. The author has used this method to evaluate the effects of diamond grades on diamond wire performance. It has been found that bead wear is sensitive to diamond grade, with higher grades experiencing the least wear. Cutting rates also improve with a higher grade of diamond when higher loads are applied.

The single bead testing method proved suitable in evaluating the performance of beads using different diamond grades. However cyclical variances in the wear and cutting data were encountered, which was amplified by the load application mechanism of the apparatus. The quality of data for the assessment of bead wear and cutting rates could be improved with an apparatus for permanent laboratory use, by providing damping to the loading mechanism or by filtering the associated electronic output signals.

It is essential for the diamond wire, incorporating bonded spacers, to rotate about its polar axis during operation to ensure even bead wear. In work carried out by the author, diamond wire rotation has been measured using a stroboscope and a video camera and with high speed video equipment. It was found that the wire

rotation decreases with increasing cutting rate to the point where no wire rotation takes place, which explains the ovalised wear patterns often found on beads in the field.

The high speed video system was found to be suitable for the analysis of diamond wire rotation in the stationary wire sawing application but could have limitations in a quarrying environment. Based on the success of diamond wire rotation measurement with a stroboscope and video camera, it is believed that a sufficiently robust system could be developed for field use.

REFERENCES

1 Hughes, F. H. The Early History of Diamond Tools. Industrial Diamond Review, Nov. 1980, pp 405 - 407

2 Barber, E. and Sanderson, L. Practical Engineering, 8, 1943, pp 244-245

3 Sanderson, L. Practical Engineering, 8, 1943, p60

4 Daniel, P. A. A Brief History of Stone Cutting - Not by Diamond Alone. De Beers Publication, 1994

5 Hannay, J. B. On the Artificial Formation of the Diamond. Proc. Royal Soc., 30, 1880, pp 188 - 189

6 Parsons, C. A. Experiments on the Artificial Production of Diamond. Proc. Royal Soc., 220, 1919, pp 67 - 107

7 Rossini, F. D. and Jessup, R. S. Heat and Free Energy of Formation of Carbon Dioxide and the Transition between Graphite and Diamond. J. Res. Natl. Bur. Stand., 21, 1938, pp 485 - 513

8 Berman, R. and Simon, F. Z. The Graphite Diamond Equilibrium. Electrochemie, 59, 1955, pp 333 - 338

9 Leipunskii, O. I. Synthetic Diamonds. Uspekhii. Khimii., 8, 1939, pp 1519 - 1534

10 Bridgman, P. W. An Experimental Contribution to the Problem of Diamond Synthesis. J. Chem. Phys., 15, 1947, pp 92 - 98

11 Bundy, F. P. Melting of Graphite at Very High Pressure. J. Chem. Phys., 38, 1963, pp 618 - 630

12 Fateeva, N. S. and Vereshchagin, L. F. Concerning the Melting Point of Graphite up to 90 kbar. Pisma Zhur Eks Teor Fiz., 13, 1971, pp 157 - 159

13 Bundy, F. P. The P, T Phase and Reaction Diagram for Elemental Carbon. J. Geo. Res., 85, No B12, Dec. 1980, pp 6930 - 6936

14 Anon. Diamond Wire - Its Origins. Indiaqua, No. 35, 1983, pp 109 - 110

15 Trancu, T. C. Diamond Wire Machine Cuts Marble Quarrying Costs. Industrial Diamond Review, Sep.1980, pp 329 - 331

16 Thoreau, B. Diamond Impregnated Wire for Sawing Hard Abrasive Stones. Industrial Diamond Review, Feb. 1984, pp 94 - 95

17 Anon. Diamond Wire Sawing Increases Quarry Production Five Times. Dimensional Stone, Sep. 1988, pp 22 - 24

18 Butler - Smith, P. W. The Cost Effectiveness of Diamond Wire Sawing in Quarries. Dimension Stone Africa Conference, Mar. 1993

19 Marles, J. T. Norse Saga. Industrial Diamond Review, 1/1990, pp 6 - 7

20 Buttner, A. Diamond Tools and Stone. Industrial Diamond Review, Mar. 1974, pp 89 - 93

21 Alexandrov, V. A., Miflir, D. M. Wear of Synthetic Diamonds and Binder during the Grinding of Natural Rock. Sinteticheskie Almazy 1977, No. 5, pp 36 - 41

22 Bailey, M. W. and Bullen, G. J. Sawing in the Stone and Civil Engineering Industries. Fourth DWMI International Technical Symposium, USA, Nov. 1978

23 Mamalis, A. G., Schulze, R. and Tonshoff H. K. The Slotting of Blocks of Hard Rock with a Diamond Segmented Circular Saw Blade. Industrial Diamond Review, Oct. 1979, pp 356 - 365

24 Ertingshausen, W. Wear Processes in Sawing Hard Stone. Industrial Diamond Review, May 1985, pp 254 - 258

25 Tonshoff, H. K. and Warnecke, G. Research on Stone Sawing. Ultrahard Materials Applications Technology, 1, Ed. Daniel P.,1982, pp 36 - 49

26 Wright, D. N. The Prediction of Diamond Wear in the Sawing of Stone. Industrial Diamond Review, May 1986, pp 213 - 216

27 Wright, D. N., Wilson, S. M., Brown, W. F. and Ovens, U. A Study of Segment Wear on Diamond Impregnated Mining Bits. Drilltorque Conference, South Africa, 1990

28 Miller, D. and Ball, A. The Wear of Diamonds in Impregnated Diamond Bit Drilling. Wear, 141, 1991, pp 311 - 320

29 Davis, P. R., Fish, M. L., Peacock, S. and Wright, D. N. An Indicator System for Saw Grit. Industrial Diamond Review, 56, No. 570, 1996

30 Belling, N. G. and Dyer, H. B. Impact Strength Determination of Diamond Abrasive Grit. Industrial Diamond Information Bureau, London, 1964

31 The Properties of Diamond. Ed. Field, J. E., Academic Press, London, 1979

32 Miller, D. and Ball, A. Rock Drilling with Impregnated Diamond Microbits - an Experimental Study. Int. J. Rock Mech. Min. Sci. and Geomech., 27, No 5, 1990, pp 363 - 371

33 Konstanty, J. The Materials Science of Stone Sawing. Industrial Diamond Review, Jan. 1991, pp 27 - 31

34 De Beers Product Catalogue, SDA Plus Series, 1996

35 De Beers Product Catalogue, SDB Series, 1996

36 Parkinson, D. J. Impregnated Crown Formulation in the '90s. Drilltorque conference, South Africa, 1990

37 Chalkley, J. R. and Thomas, D. M. The Tribological Aspects of Metal Bonded Diamond Grinding Wheels. Powder Metallurgy, 12/1969, pp 582 - 597

38 Anon. Metallurgy of Diamond Tools. Industrial Diamond Review, May 1985, pp 248 - 250

39 Natural Stone Glossary, Stone Federation G.B., London, 1991, p66

40 Paone, J. and Bruce, W. E. Drillability Studies. Report 6324, Bureau of Mines, USA, 1963

41 Gstalder, S. and Raynal, J. Measurement of Some Mechanical Properties of Rocks and their Relationship to Rock Drillability. Petroleum Transactions, Journal of Petroleum Technology, 1966

42 Singh, D. P. The Drillability of Rocks. Miner. Sci. Engng, 5 , No. 3, Jul. 1973, pp 255 - 260

43 Fei, S., Chen, Y., Zhang, J. and Wang, L. Determination of Rock Drillability by a Groove Cutting Method. Drillex '87 Conference, UK., Apr. 1987, pp 47- 52

44 Cassapi, V. B, Ambrose, D. and Waller, M. D. Performance and Wear Characterists in Diamond Core Drilling. Drillex '87 Conference, UK., Apr. 1987, pp 5 - 20

45 Copeman, R. and Ford, I. Geotechnical Aspects of Machining Natural Stones with Diamonds. Diamond Tools in the Stone Industry Conference, Mar. 1969, pp 320 - 325

46 Burgess, R. R. Circular Sawing Granite with Diamond Saw Blades. Proceedings of Fifth Industrial Diamond Seminar, IDA, USA, May 1978, pp 3 - 10

47 Wright, D. N. and Cassapi, V. B. Factors in Calculating Sawability of Stone. Industrial Lubrication and Tribology, Jun. 1985, pp 84 - 89

48 Wright, D. N. and Jennings, M. Guidelines for Sawing Stone. Industrial Diamond Review, 2/1989, pp 70 -75

49 Baisco, G. Diamond Wire for Quarrying Hard Rocks. Industrial Diamond Review, 5/1993, pp 252 - 255

50 Gobbett, J. Diamond Wire in Action. Dimension Stone Africa Conference, Johannesburg, Mar. 1993

51 Daniel, P. More Granites Succumb to Diamond Wire. Industrial Diamond Review, 5/1986, pp 189 - 194

52 Tonshoff, H. K and Panhorst, H. J. Development and Testing of Diamond Wire for the Sawing of Hard Stone. Industrial Diamond Review, Jul. 1974, pp 246 - 251

53 Wright, D. N. The Effect of Parameters on Stationary Wire Sawing Performance. Dimension Stone Africa Conference, Johannesburg, Mar. 1993

54 Bortolussi, A. et. al. Progress in the Knowledge in Granite Cutting with Diamond Wire. Int. Conference on Ground Control in Mining, U. of Wollongong, Jul. 1992

55 Butler - Smith, P.W. A Study of Diamond Wire Rotation. De Beers Report, Aug. 1992

56 Diamant Boart Publication, Cutting Granite with Diamond Wire on Stationary Machines - User Guide, Dec. 1995

57 Diamant Boart Publication, Sawing with Diamond Wire in Granite Quarries - User Guide, Dec. 1995

58 Herbert, S. Diamond Wire Saw-The In Depth Solution. Industrial Diamond Review, 1/1989, pp 11 - 12

59 Cai, O. Comparison Between Shear Stresses in Electodeposited and Sintered Layer Diamond Beads. Diamante Applicazioni and Technologia, 4, 1995, pp 136 - 141

APPENDIX 1

Relationship between sieve size and the number of diamond particles per carat

Sieve size No. US Mesh	Theoretical sieve opening micron	FEPA Size No.	Approx. No. of stones per carat
18	1 000	D1001	110
20	841	D851	180
25	707	D711	310
30	595	D601	510
35	500	D501	860
40	420	D426	1 450
45	354	D356	2 450
50	297	D301	4 100
60	250	D251	6 900
70	210	D213	11 600
80	177	D181	19 500
100	149	D151	32 800
120	125	D126	55 200
140	105	D107	93 000
170	88	D91	156 000
200	74	D76	262 000
230	63	D64	441 000
270	53	D54	742 000
325	44	D46	1 250 000
400	37		

Source: De Beers products chart

APPENDIX 2

Relationship between mean particle chip thickness and diamond wire sawing operating conditions in selected stone types on a stationary wire saw

Stone type	Cut length m	Cutting rate Sq. m / hour	Feed rate mm/min	Bead velocity m/s	Bead pitch mm	Bead length mm	Particles per unit area C / sq. mm	Mean chip width : thickness	Mean chip thickness microns
Rustenberg Grey (gabbro)	1.50	1.60	17.80	29	20	5	1.2	10	0.45
Belfast Black (gabbro)	1.50	1.30	14.40	26	20	5	1.2	10	0.43
African Red (true granite)	1.50	0.90	10.00	23	20	5	1.2	10	0.38

APPENDIX 3

Sawability and abrasivity relationship with diamond wire life for siliceous and calcareous rocks

Stone type	Rock group	Diamond Wire Life (m2/m)	Mean Sawability (w/s)	High Sawability (w/s)	Low Sawability (w/s)	Mean Abrasivity (mm2)	High Abrasivity (mm2)	Low Abrasivity (mm2)
White Rhino	Calcareous	41.20	134.40	144.80	124.00	1.21	1.29	1.13
Light Plaisandro	Calcareous	34.40	185.35	191.44	179.26	1.03	1.07	1.00
Rustenberg Grey	Siliceous	12.60	216.55	226.58	206.52	2.84	2.99	2.70
Belfast Black	Siliceous	10.10	229.80	235.53	224.07	2.50	2.63	2.37
Bitterfontein Green granite	Siliceous	9.40	247.15	260.57	233.63	2.87	3.12	2.62
Zimbabwe Black	Siliceous	9.00	308.45	316.89	300.01	1.93	2.14	1.71
Juperana	Siliceous	6.20	311.00	319.03	302.97	2.94	3.06	2.82
African Red granite	Siliceous	6.00	315.95	322.87	309.03	3.07	3.12	3.01

Analysis of results on siliceous and calcareous rock samples

Sawability Regression Output:	
Constant	311.45
Std Err of Y Est	34.20
R Squared	0.77
No. of Observations	8
Degrees of Freedom	6
X Coefficient(s)	-4.21
Std Err of Coef.	0.95
Correlation	-0.88

Abrasivity Regression Output:	
Constant	3.15
Std Err of Y Est	0.40
R Squared	0.79
No. of Observations	8
Degrees of Freedom	6
X Coefficient(s)	-0.05
Std Err of Coef.	0.01
Correlation	-0.89

Analysis of results on siliceous rock samples

Sawability Regression Output:	
Constant	413.61
Std Err of Y Est	23.95
R Squared	0.78
No. of Observations	6
Degrees of Freedom	4
X Coefficient(s)	-16.00
Std Err of Coef.	4.30
Correlation	-0.88

Abrasivity Regression Output:	
Constant	3.10
Std Err of Y Est	0.45
R Squared	0.08
No. of Observations	6
Degrees of Freedom	4
X Coefficient(s)	-0.05
Std Err of Coef.	0.08
Correlation	-0.28

APPENDIX 4

Standard formulae for a circular segment

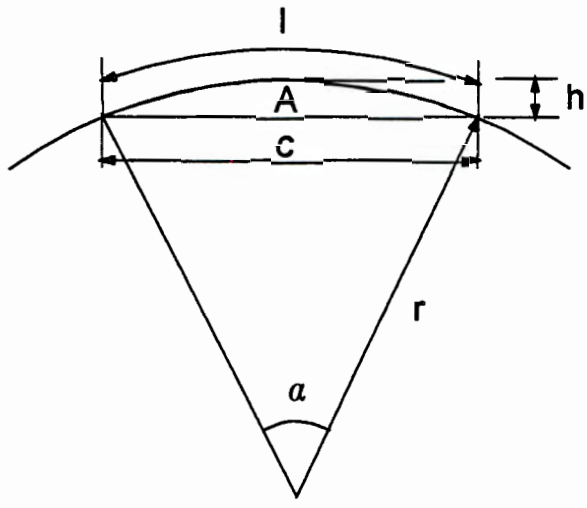

Length of circular arc

$$l = \frac{\pi \cdot r \cdot a}{180}$$

Radius of circular arc

$$r = \frac{c^2 + 4h^2}{8h}$$

Area of circular segment

$$A = \frac{r \cdot l - c(r - h)}{2}$$

Source: Machinery's Handbook, 23 rd ed.,Industrial Press, New York, 1988

APPENDIX 5

Relationship between normal and tangential forces on diamond beads

Fn (N)	Ft (N)
0	0.00
3	0.13
6	0.82
9	0.99
12	1.10
15	1.89
18	2.64

where

Fn is the measured normal force on the bead
Ft is the measured tangential force on the bead

Regression Output:		
Constant		0
Std Err of Y Est		0.256402
R Squared		0.924646
No. of Observations		7
Degrees of Freedom		6
X Coefficient(s)	0.126117	
Std Err of Coef.	0.008959	
Ln / Lt		7.929132

APPENDIX 6

Effects of cutting velocity on bead wear at 9 N applied load

Cutting velocity m/s	SDA 75+ Cum mass loss mg	Wear rate mg/min	SDA 85+ Cum mass loss mg	Wear rate mg/min	SDA 100+ Cum mass loss mg	Wear rate mg/min
15	173.1	10.82	113.7	7.11	68.1	4.26
20	129.7	8.10	93.4	5.84	52.2	3.26
25	146.3	9.14	79.0	4.94	44.5	2.78
30	128.6	8.04	72.1	4.51	48.6	3.04

Data collected after a cutting period of 16 minutes

Velocity error resulting from increasing depth of cut

Stone sample diameter mm	Depth of cut mm	Cutting diameter mm	Linear cutting velocity at 970 rpm	Percentage error of 20 m/s	Percentage error of initial velocity
412	5.5	401	20.37	-1.83	0
412	6	400	20.32	-1.58	-0.25
412	6.5	399	20.26	-1.32	-0.50
412	7	398	20.21	-1.07	-0.75
412	7.5	397	20.16	-0.82	-1.00
412	8	396	20.11	-0.56	-1.25
412	8.5	395	20.06	-0.31	-1.50
412	9	394	20.01	-0.05	-1.75
412	9.5	393	19.96	0.20	-2.00
412	10	392	19.91	0.45	-2.24
412	10.5	391	19.86	0.71	-2.49
412	11	390	19.81	0.96	-2.74
412	11.5	389	19.76	1.22	-2.99

APPENDIX 7

Analysis of diamond bead cutting rates for SDA 75+

Bead	SDA 75+					SDA 75+					SDA 75+				
Load	3 N					6 N					9 N				
Time (min)	Cut depth	Cut area	Cut rate	Cumul cut	Cumul cut	Cut depth	Cut area	Cut rate	Cumul cut	Cumul cut	Cut depth	Cut area	Cut rate	Cumul cut	Cumul cut
	mm	cm2	cm2 / min	area cm2	vol cm3	mm	cm2	cm2 / min	area cm2	vol cm3	mm	cm 2	cm2 / min	area cm2	vol cm3
0	6.10	0.00		0.00	0.00	6.08	0.00	0.00	0.00	0.00	5.96	0.00		0.00	0.00
2	6.29	4.77	2.38	4.77	5.72	6.29	5.27	2.63	5.27	6.32	6.47	12.79	6.40	12.79	15.35
4	6.42	3.26	1.63	8.03	9.63	6.58	7.27	3.63	12.54	15.04	7.10	15.76	7.88	28.56	34.27
6	6.65	5.76	2.88	13.79	16.54	6.78	5.01	2.50	17.54	21.05	7.63	13.22	6.61	41.78	50.13
8	6.79	3.50	1.75	17.29	20.75	7.00	5.50	2.75	23.04	27.65	8.18	13.68	6.84	55.46	66.55
10	6.98	4.75	2.38	22.04	26.45	7.31	7.74	3.87	30.78	36.94	8.79	15.13	7.56	70.59	84.70
12	7.17	4.75	2.37	26.79	32.15	7.55	5.98	2.99	36.77	44.12	9.30	12.61	6.31	83.20	99.84
14	7.35	4.49	2.25	31.28	37.54	7.82	6.72	3.36	43.49	52.19	9.85	13.57	6.78	96.77	116.12
16	7.52	4.24	2.12	35.52	42.62	8.01	4.73	2.36	48.22	57.86	10.46	15.00	7.50	111.77	134.12
Mean cutting rate			2.22					3.01					6.99		
StdS dev.			0.39					0.55					0.59		

Bead	SDA 75+					SDA 75+					SDA 75+				
Load	12 N					15 N					18 N				
Time (min)	Cut depth	Cut area	Cut rate	Cumul cut	Cumul cut	Cut depth	Cut area	Cut rate	Cumul cut	Cumul cut	Cut depth	Cut area	Cut rate	Cumul cut	Cumul cut
	mm	cm 2	cm2 / min	area cm2	vol cm3	mm	cm 2	cm2 / min	area cm2	vol cm3	mm	cm 2	cm2 / min	area cm2	vol cm3
0	5.06	0.00		0.00	0.00	5.08	0.00		0.00	0.00	5.20	0.00		0.00	0.00
2	5.50	11.09	5.55	11.09	13.31	5.73	16.37	8.19	16.37	19.65	5.93	18.37	9.19	18.37	22.05
4	6.10	15.08	7.54	26.17	31.41	6.46	18.33	9.16	34.70	41.64	6.63	17.56	8.78	35.93	43.12
6	6.79	17.29	8.65	43.47	52.16	6.97	12.76	6.38	47.46	56.95	7.40	19.24	9.62	55.17	66.20
8	7.40	15.24	7.62	58.70	70.44	7.83	21.45	10.72	68.91	82.69	8.19	19.66	9.83	74.83	89.80
10	7.96	13.95	6.97	72.65	87.18	8.60	19.12	9.56	88.03	105.64	9.07	21.81	10.91	96.64	115.97
12	8.70	18.37	9.18	91.02	109.22	9.48	21.77	10.88	109.80	131.76	9.70	15.55	7.78	112.20	134.64
14	9.45	18.55	9.27	109.56	131.48	10.21	17.98	8.99	127.78	153.34	10.50	19.68	9.84	131.88	158.25
16	10.02	14.05	7.02	123.61	148.33	11.04	20.36	10.18	148.14	177.77	11.34	20.58	10.29	152.46	182.95
Mean cutting rate			7.73					9.26					9.53		
StdS dev.			1.27					1.48					0.96		

Material diameter	411.72	mm
Average width of cut	12	mm

APPENDIX 7

Analysis of diamond bead cutting rates for SDA 85+

Bead	SDA 85+					SDA 85+					SDA 85+				
Load	3 N					6 N					9 N				
Time (min)	Cut depth	Cut area	Cut rate	Cumul cut	Cumul cut	Cut depth	Cut area	Cut rate	Cumul cut	Cumul cut	Cut depth	Cut area	Cut rate	Cumul cut	Cumul cut
	mm	cm2	cm2 / min	area cm2	vol cm3	mm	cm2	cm2 / min	area cm2	vol cm3	mm	cm 2	cm2 / min	area cm2	vol cm3
0	5.15	0.00		0.00	0.00	5.24	0.00		0.00	0.00	5.25	0.00		0.00	0.00
2	5.36	5.30	2.65	5.30	6.36	5.65	10.34	5.17	10.34	12.40	5.80	13.86	6.93	13.86	16.63
4	5.44	2.02	1.01	7.32	8.78	5.97	8.05	4.03	18.39	22.07	6.43	15.83	7.91	29.69	35.63
6	5.57	3.28	1.64	10.59	12.71	6.40	10.80	5.40	29.19	35.03	7.00	14.28	7.14	43.97	52.76
8	5.66	2.27	1.13	12.86	15.43	6.80	10.03	5.01	39.22	47.06	7.60	14.99	7.49	58.96	70.75
10	5.87	5.29	2.64	18.15	21.77	7.20	10.01	5.00	49.22	59.07	8.10	12.45	6.23	71.41	85.69
12	5.97	2.52	1.26	20.66	24.79	7.54	8.49	4.24	57.71	69.25	8.59	12.17	6.09	83.58	100.30
14	6.10	3.27	1.63	23.93	28.71	7.86	7.98	3.99	65.69	78.83	9.01	10.41	5.21	94.00	112.80
16	6.17	1.76	0.88	25.69	30.82	8.15	7.22	3.61	72.91	87.49	9.53	12.86	6.43	106.86	128.23
Mean cutting rate			1.61					4.56					6.68		
StdS dev.			0.70					0.66					0.87		

Bead	SDA 85+					SDA 85+					SDA 85+				
Load	12 N					15 N					18 N				
Time (min)	Cut depth	Cut area	Cut rate	Cumul cut	Cumul cut	Cut depth	Cut area	Cut rate	Cumul cut	Cumul cut	Cut depth	Cut area	Cut rate	Cumul cut	Cumul cut
	mm	cm 2	cm2 / min	area cm2	vol cm3	mm	cm 2	cm2 / min	area cm2	vol cm3	mm	cm 2	cm2 / min	area cm2	vol cm3
0	5.18	0.00		0.00	0.00	5.42	0.00		0.00	0.00	5.11	0.00		0.00	0.00
2	5.92	18.65	9.32	18.65	22.38	6.13	17.87	8.94	17.87	21.44	6.09	24.69	12.34	24.69	29.62
4	6.57	16.32	8.16	34.97	41.96	6.97	21.06	10.53	38.93	46.72	6.91	20.56	10.28	45.25	54.30
6	7.16	14.77	7.38	49.74	59.68	7.80	20.72	10.36	59.65	71.58	7.73	20.48	10.24	65.73	78.88
8	7.88	17.96	8.98	67.70	81.24	8.71	22.62	11.31	82.27	98.73	8.59	21.39	10.69	87.12	104.54
10	8.46	14.42	7.21	82.12	98.55	9.59	21.78	10.89	104.05	124.86	9.54	23.52	11.76	110.64	132.76
12	9.18	17.85	8.92	99.97	119.96	10.43	20.70	10.35	124.74	149.69	10.44	22.18	11.09	132.81	159.37
14	9.97	19.51	9.75	119.48	143.37	11.20	18.89	9.45	143.64	172.36	11.33	21.83	10.91	154.64	185.57
16	10.75	19.18	9.59	138.66	166.39	12.01	19.79	9.90	163.43	196.12	12.34	24.65	12.33	179.29	215.15
Mean cutting rate			8.67					10.21					11.21		
StdS dev.			0.97					0.77					0.85		

Material diameter	412.13	mm
Average width of cut	12	mm

APPENDIX 7

Analysis of diamond bead cutting rates for SDA 100+

Bead	SDA 100+														
Load	3 N					6 N					9 N				
Time (min)	Cut depth	Cut area	Cut rate	Cumul cut	Cumul cut	Cut depth	Cut area	Cut rate	Cumul cut	Cumul cut	Cut depth	Cut area	Cut rate	Cumul cut	Cumul cut
	mm	cm2	cm2 / min	area cm2	vol cm3	mm	cm2	cm2 / min	area cm2	vol cm3	mm	cm 2	cm2 / min	area cm2	vol cm3
0	5.35	0.00		0.00	0.00	5.30	0.00		0.00	0.00	5.53	0.00		0.00	0.00
2	5.51	4.04	2.02	4.04	4.85	5.68	9.59	4.79	9.59	11.51	6.10	14.36	7.18	14.36	17.23
4	5.68	4.29	2.14	8.33	9.99	5.95	6.80	3.40	16.39	19.67	6.76	16.58	8.29	30.94	37.13
6	5.81	3.28	1.64	11.60	13.92	6.37	10.56	5.28	26.96	32.35	7.42	16.52	8.26	47.46	56.96
8	6.04	5.79	2.90	17.40	20.87	6.65	7.03	3.52	33.99	40.78	8.07	16.22	8.11	63.68	76.42
10	6.19	3.77	1.89	21.17	25.40	6.99	8.52	4.26	42.51	51.01	8.75	16.91	8.46	80.59	96.71
12	6.36	4.27	2.14	25.44	30.53	7.28	7.26	3.63	49.77	59.72	9.30	13.64	6.82	94.23	113.08
14	6.46	2.51	1.26	27.95	33.55	7.56	7.00	3.50	56.77	68.12	9.81	12.61	6.31	106.84	128.21
16	6.51	1.26	0.63	29.21	35.05	7.77	5.24	2.62	62.01	74.41	10.38	14.05	7.03	120.89	145.07
Mean cutting rate			1.83					3.88					7.56		
StdS dev.			0.67					0.83					0.87		

Bead	SDA 100+														
Load	12 N					15 N					18 N				
Time (min)	Cut depth	Cut area	Cut rate	Cumul cut	Cumul cut	Cut depth	Cut area	Cut rate	Cumul cut	Cumul cut	Cut depth	Cut area	Cut rate	Cumul cut	Cumul cut
	mm	cm 2	cm2 / min	area cm2	vol cm3	mm	cm 2	cm2 / min	area cm2	vol cm3	mm	cm 2	cm2 / min	area cm2	vol cm3
0	5.14	0.00		0.00	0.00	4.92	0.00		0.00	0.00	5.01	0.00		0.00	0.00
2	5.93	19.93	9.97	19.93	23.92	5.87	23.91	11.96	23.91	28.69	6.19	29.76	14.88	29.76	35.72
4	6.71	19.60	9.80	39.54	47.44	6.88	25.38	12.69	49.29	59.14	7.23	26.09	13.04	55.85	67.02
6	7.60	22.27	11.14	61.81	74.17	7.78	22.50	11.25	71.79	86.15	8.29	26.45	13.22	82.30	98.76
8	8.40	19.94	9.97	81.75	98.10	8.73	23.64	11.82	95.44	114.52	9.51	30.27	15.13	112.56	135.08
10	9.06	16.39	8.19	98.13	117.76	9.91	29.21	14.61	124.65	149.58	10.83	32.54	16.27	145.10	174.12
12	9.75	17.07	8.54	115.21	138.25	11.19	31.49	15.74	156.14	187.36	12.21	33.78	16.89	178.88	214.66
14	10.58	20.46	10.23	135.67	162.80	12.49	31.77	15.88	187.91	225.49	13.48	30.88	15.44	209.76	251.71
16	11.37	19.39	9.70	155.06	186.07	13.71	29.62	14.81	217.53	261.03	14.79	31.64	15.82	241.39	289.67
Mean cutting rate			9.69					13.60					15.09		
StdS dev.			0.94					1.87					1.36		

Material diameter	412.63	mm
Average width of cut	12	mm

APPENDIX 8

Analysis of diamond bead wear rates for SDA 75+

Bead	SDA 75+				SDA 75+				SDA 75+			
Load	3 N				6 N				9 N			
Time	Mass	Mass loss	Cum loss	Wear rate	Mass	Mass loss	Cum loss	Wear rate	Mass	Mass loss	Cum loss	Wear rate
(min)	(g)	(mg)	(mg)	(mg / min)	(g)	(mg)	(mg)	(mg / min)	(g)	(mg)	(mg)	(mg / min)
0	3.612	0.00	0.00		3.521	0.00	0.00		3.703	0.00	0.00	
2	3.611	1.15	1.15	0.57	3.517	4.20	4.20	2.10	3.688	15.12	15.12	7.56
4	3.610	1.10	2.25	0.55	3.512	4.62	8.82	2.31	3.669	19.28	34.40	9.64
6	3.609	1.05	3.30	0.52	3.508	3.78	12.60	1.89	3.655	13.61	48.01	6.80
8	3.608	1.20	4.50	0.60	3.504	4.62	17.22	2.31	3.639	15.88	63.88	7.94
10	3.607	0.95	5.45	0.47	3.500	3.92	21.14	1.96	3.620	18.90	82.78	9.45
12	3.605	1.10	6.55	0.55	3.495	4.62	25.76	2.31	3.601	19.66	102.44	9.83
14	3.604	1.05	7.60	0.52	3.490	5.18	30.94	2.59	3.585	15.50	117.94	7.75
16	3.604	0.90	8.50	0.45	3.486	4.06	35.00	2.03	3.573	11.72	129.65	5.86
Mean wear rate				0.53				2.19				8.10
StdS dev.				0.05				0.23				1.43

Bead	SDA 75+				SDA 75+				SDA 75+			
Load	12 N				15 N				18 N			
Time	Mass	Mass loss	Cum loss	Wear rate	Mass	Mass loss	Cum loss	Wear rate	Mass	Mass loss	Cum loss	Wear rate
(min)	(g)	(mg)	(mg)	(mg / min)	(g)	(mg)	(mg)	(mg / min)	(g)	(mg)	(mg)	(mg / min)
0	3.692	0.00	0.00		3.569	0.00	0.00		3.700	0.00	0.00	
2	3.642	49.90	49.90	24.95	3.415	154.22	154.22	77.11	3.485	214.64	214.64	107.32
4	3.605	37.20	87.09	18.60	3.248	166.92	321.15	83.46	3.294	191.06	405.70	95.53
6	3.559	46.27	133.36	23.13	3.103	145.15	466.30	72.58	3.073	221.72	627.42	110.86
8	3.500	58.97	192.33	29.48	2.974	128.82	595.12	64.41	2.891	181.62	809.04	90.81
10	3.434	65.32	257.64	32.66	2.814	159.67	754.79	79.83	2.702	188.70	997.74	94.35
12	3.364	70.76	328.41	35.38	2.682	132.45	887.24	66.23	2.473	228.80	1226.53	114.40
14	3.308	55.34	383.75	27.67	2.531	150.60	1037.84	75.30	2.245	228.80	1455.33	114.40
16	3.248	59.88	443.62	29.94	2.410	121.56	1159.40	60.78	2.042	202.85	1658.18	101.42
Mean wear rate				27.73				72.46				103.64
StdS dev.				5.39				7.97				9.40

APPENDIX 8

Analysis of diamond bead wear rates for SDA 85+

Bead	SDA 85+				SDA 85+				SDA 85+			
Load	3 N				6 N				9 N			
Time	Mass	Mass loss	Cum loss	Wear rate	Mass	Mass loss	Cum loss	Wear rate	Mass	Mass loss	Cum loss	Wear rate
(min)	(g)	(mg)	(mg)	(mg / min)	(g)	(mg)	(mg)	(mg / min)	(g)	(mg)	(mg)	(mg / min)
0	3.388	0.00	0.00		3.214	0.00	0.00		3.272	0.00	0.00	
2	3.387	1.05	1.05	0.52	3.211	3.08	3.08	1.54	3.260	11.72	11.72	5.86
4	3.386	1.30	2.35	0.65	3.208	2.94	6.02	1.47	3.248	12.47	24.19	6.24
6	3.384	1.50	3.85	0.75	3.204	3.78	9.80	1.89	3.240	7.94	32.13	3.97
8	3.383	0.90	4.75	0.45	3.200	4.48	14.28	2.24	3.229	11.34	43.47	5.67
10	3.382	0.95	5.70	0.47	3.196	3.36	17.64	1.68	3.215	13.99	57.46	6.99
12	3.382	0.70	6.40	0.35	3.194	2.80	20.44	1.40	3.201	13.61	71.06	6.80
14	3.381	0.50	6.90	0.25	3.191	2.38	22.82	1.19	3.191	9.83	80.89	4.91
16	3.381	0.50	7.40	0.25	3.189	1.82	24.64	0.91	3.179	12.47	93.37	6.24
Mean wear rate				0.46				1.54				5.84
StdS dev.				0.18				0.41				1.00

Bead	SDA 85+				SDA 85+				SDA 85+			
Load	12 N				15 N				18 N			
Time	Mass	Mass loss	Cum loss	Wear rate	Mass	Mass loss	Cum loss	Wear rate	Mass	Mass loss	Cum loss	Wear rate
(min)	(g)	(mg)	(mg)	(mg / min)	(g)	(mg)	(mg)	(mg / min)	(g)	(mg)	(mg)	(mg / min)
0	3.245	0.00	0.00		3.380	0.00	0.00		3.356	0.00	0.00	
2	3.213	31.75	31.75	15.88	3.295	85.28	85.28	42.64	3.196	160.39	160.39	80.20
4	3.189	24.49	56.25	12.25	3.195	99.79	185.07	49.90	3.045	150.96	311.35	75.48
6	3.160	29.03	85.28	14.52	3.124	70.76	255.83	35.38	2.931	113.22	424.57	56.61
8	3.127	32.66	117.94	16.33	3.053	70.76	326.59	35.38	2.783	148.60	573.17	74.30
10	3.090	37.20	155.13	18.60	2.957	96.16	422.76	48.08	2.655	127.37	700.54	63.69
12	3.060	29.94	185.07	14.97	2.856	101.61	524.36	50.80	2.547	108.50	809.04	54.25
14	3.017	42.64	227.71	21.32	2.776	79.83	604.20	39.92	2.438	108.50	917.54	54.25
16	2.980	37.20	264.90	18.60	2.676	99.79	703.99	49.90	2.318	120.29	1037.84	60.15
Mean wear rate				16.56				44.00				64.86
StdS dev.				2.85				6.54				10.38

APPENDIX 8

Analysis of diamond bead wear rates for SDA 100+

Bead	SDA 100+				SDA 100+				SDA 100+			
Load	3 N				6 N				9 N			
Time	Mass	Mass loss	Cum loss	Wear rate	Mass	Mass loss	Cum loss	Wear rate	Mass	Mass loss	Cum loss	Wear rate
(min)	(g)	(mg)	(mg)	(mg / min)	(g)	(mg)	(mg)	(mg / min)	(g)	(mg)	(mg)	(mg / min)
0	3.270	0.00	0.00		3.220	0.00	0.00		3.208	0.00	0.00	
2	3.269	0.95	0.95	0.47	3.218	1.82	1.82	0.91	3.201	6.80	6.80	3.40
4	3.268	0.60	1.55	0.30	3.216	2.52	4.34	1.26	3.194	7.18	13.99	3.59
6	3.268	0.65	2.20	0.32	3.214	1.82	6.16	0.91	3.188	6.05	20.03	3.02
8	3.267	0.70	2.90	0.35	3.212	1.68	7.84	0.84	3.182	6.05	26.08	3.02
10	3.267	0.60	3.50	0.30	3.210	2.52	10.36	1.26	3.174	8.32	34.40	4.16
12	3.266	0.35	3.85	0.17	3.207	2.38	12.74	1.19	3.166	7.18	41.58	3.59
14	3.266	0.30	4.15	0.15	3.206	1.26	14.00	0.63	3.160	6.05	47.63	3.02
16	3.266	0.30	4.45	0.15	3.205	1.40	15.40	0.70	3.156	4.54	52.16	2.27
Mean wear rate				0.28				0.96				3.26
StdS dev.				0.11				0.25				0.56

Bead	SDA 100+				SDA 100+				SDA 100+			
Load	12 N				15 N				18 N			
Time	Mass	Mass loss	Cum loss	Wear rate	Mass	Mass loss	Cum loss	Wear rate	Mass	Mass loss	Cum loss	Wear rate
(min)	(g)	(mg)	(mg)	(mg / min)	(g)	(mg)	(mg)	(mg / min)	(g)	(mg)	(mg)	(mg / min)
0	3.297	0.00	0.00		3.281	0.00	0.00		3.279	0.00	0.00	
2	3.278	19.05	19.05	9.53	3.239	41.73	41.73	20.87	3.206	73.12	73.12	36.56
4	3.263	15.42	34.47	7.71	3.196	43.55	85.28	21.77	3.140	66.04	139.16	33.02
6	3.244	18.14	52.62	9.07	3.159	36.29	121.56	18.14	3.034	106.14	245.31	53.07
8	3.229	15.42	68.04	7.71	3.107	52.62	174.18	26.31	2.944	89.63	334.94	44.82
10	3.219	9.98	78.02	4.99	3.051	56.25	230.43	28.12	2.873	70.76	405.70	35.38
12	3.202	17.24	95.26	8.62	3.018	32.66	263.09	16.33	2.781	91.99	497.69	46.00
14	3.192	9.98	105.24	4.99	2.982	36.29	299.38	18.14	2.711	70.76	568.45	35.38
16	3.172	19.96	125.19	9.98	2.934	47.17	346.55	23.59	2.626	84.91	653.37	42.46
Mean wear rate				7.82				21.66				40.84
StdS dev.				1.92				4.16				6.90

APPENDIX 9

Analysis of diamond bead specific wear rates and productivity

	SDA 75+				SDA 85+				SDA 100+			
	Average	Average	Specific	Productivity	Average	Average	Specific	Productivity	Average	Average	Specific	Productivity
Applied	cutting	wear	wear		cutting	wear	wear		cutting	wear	wear	
load	rate	rate			rate	rate			rate	rate		
N	cm2/min	mg/min	mg/cm2	cm2/mg	cm2/min	mg/min	mg/cm2	cm2/mg	cm2/min	mg/min	mg/cm2	cm2/mg
3	2.22	0.53	0.24	4.18	1.61	0.46	0.29	3.47	1.83	0.28	0.15	6.56
6	3.01	2.19	0.73	1.38	4.56	1.54	0.34	2.96	3.88	0.96	0.25	4.03
9	6.99	8.10	1.16	0.86	6.68	5.84	0.87	1.14	7.56	3.26	0.43	2.32
12	7.73	27.73	3.59	0.28	8.67	16.56	1.91	0.52	9.69	7.82	0.81	1.24
15	9.26	72.46	7.83	0.13	10.21	44.00	3.93	0.25	13.60	21.66	1.59	0.63
18	9.53	103.64	10.88	0.09	11.21	64.86	6.35	0.16	15.09	40.84	2.71	0.37

APPENDIX 10

Student t-test analysis of diamond bead cutting rates over elapsed time

STAT. BASIC STATS	T-test for Dependent Samples (statis01.sta) Marked differences are significant at p < ,05000							
Variable	Mean	Std.Dv.	N	Diff.	Std.Dv. Diff.	t	df	p
N3SDA75P N3SDA75P	2,220000 2,220000	,394462 ,394462	8	0,000000	0,000000	0,00000	7	1,000000
N3SDA75P N3SDA85P	2,220000* 1,605000*	,394462* ,695845*	8*	,615000*	,606536*	2,86790*	7*	,024064*
N3SDA75P N3SDA100	2,220000 1,827500	,394462 ,673769	8	,392500	,887255	1,25123	7	,251046
N3SDA85P N3SDA75P	1,605000* 2,220000*	,695845* ,394462*	8*	-,615000*	,606536*	-2,86790*	7*	,024064*
N3SDA85P N3SDA85P	1,605000 1,605000	,695845 ,695845	8	0,000000	0,000000	0,00000	7	1,000000
N3SDA85P N3SDA100	1,605000 1,827500	,695845 ,673769	8	-,222500	,921718	-,68277	7	,516701
N3SDA100 N3SDA75P	1,827500 2,220000	,673769 ,394462	8	-,392500	,887255	-1,25123	7	,251046
N3SDA100 N3SDA85P	1,827500 1,605000	,673769 ,695845	8	,222500	,921718	,68277	7	,516701
N3SDA100 N3SDA100	1,827500 1,827500	,673769 ,673769	8	0,000000	0,000000	0,00000	7	1,000000

STAT. BASIC STATS	T-test for Dependent Samples (statis01.sta) Marked differences are significant at p < ,05000							
Variable	Mean	Std.Dv.	N	Diff.	Std.Dv. Diff.	t	df	p
N6SDA75P N6SDA75P	3,011250 3,011250	,553106 ,553106	8	0,00000	0,000000	0,00000	7	1,000000
N6SDA75P N6SDA85P	3,011250* 4,556250*	,553106* ,663797*	8*	-1,54500*	,912751*	-4,78764*	7*	,001995*
N6SDA75P N6SDA100	3,011250 3,875000	,553106 ,852459	8	-,86375	1,050183	-2,32631	7	,052900
N6SDA85P N6SDA75P	4,556250* 3,011250*	,663797* ,553106*	8*	1,54500*	,912751*	4,78764*	7*	,001995*
N6SDA85P N6SDA85P	4,556250 4,556250	,663797 ,663797	8	0,00000	0,000000	0,00000	7	1,000000
N6SDA85P N6SDA100	4,556250* 3,875000*	,663797* ,852459*	8*	,68125*	,414537*	4,64823*	7*	,002347*
N6SDA100 N6SDA75P	3,875000 3,011250	,852459 ,553106	8	,86375	1,050183	2,32631	7	,052900
N6SDA100 N6SDA85P	3,875000* 4,556250*	,852459* ,663797*	8*	-,68125*	,414537*	-4,64823*	7*	,002347*
N6SDA100 N6SDA100	3,875000 3,875000	,852459 ,852459	8	0,00000	0,000000	0,00000	7	1,000000

STAT. BASIC STATS	T-test for Dependent Samples (statis01.sta) Marked differences are significant at p < ,05000							
Variable	Mean	Std.Dv.	N	Diff.	Std.Dv. Diff.	t	df	p
N9SDA75P N9SDA75P	6,985000 6,985000	,585345 ,585345	8	0,000000	0,000000	0,00000	7	1,000000
N9SDA75P N9SDA85P	6,985000 6,678750	,585345 ,863307	8	,306250	,899364	,96313	7	,367565
N9SDA75P N9SDA100	6,985000 7,557500	,585345 ,816854	8	-,572500	,756094	-2,14163	7	,069467
N9SDA85P N9SDA75P	6,678750 6,985000	,863307 ,585345	8	-,306250	,899364	-,96313	7	,367565
N9SDA85P N9SDA85P	6,678750 6,678750	,863307 ,863307	8	0,000000	0,000000	0,00000	7	1,000000
N9SDA85P N9SDA100	6,678750* 7,557500*	,863307* ,816854*	8*	-,878750*	,626086*	-3,96987*	7*	,005393*
N9SDA100 N9SDA75P	7,557500 6,985000	,816854 ,585345	8	,572500	,756094	2,14163	7	,069467
N9SDA100 N9SDA85P	7,557500* 6,678750*	,816854* ,863307*	8*	,878750*	,626086*	3,96987*	7*	,005393*
N9SDA100 N9SDA100	7,557500 7,557500	,816854 ,816854	8	0,000000	0,000000	0,00000	7	1,000000

STAT. BASIC STATS	T-test for Dependent Samples (statis01.sta) Marked differences are significant at p < ,05000							
Variable	Mean	Std.Dv.	N	Diff.	Std.Dv. Diff.	t	df	p
N12SDA75 N12SDA75	7,725000 7,725000	1,265058 1,265058	8	0,00000	0,000000	0,00000	7	1,000000
N12SDA75 N12SDA85	7,725000 8,663750	1,265058 ,974635	8	-,93875	1,602243	-1,65717	7	,141453
N12SDA75 N12SDA10	7,725000* 9,692500*	1,265058* ,936220*	8*	-1,96750*	1,483247*	-3,75186*	7*	,007151*
N12SDA85 N12SDA75	8,663750 7,725000	,974635 1,265058	8	,93875	1,602243	1,65717	7	,141453
N12SDA85 N12SDA85	8,663750 8,663750	,974635 ,974635	8	0,00000	0,000000	0,00000	7	1,000000
N12SDA85 N12SDA10	8,663750 9,692500	,974635 ,936220	8	-1,02875	1,259846	-2,30960	7	,054219
N12SDA10 N12SDA75	9,692500* 7,725000*	,936220* 1,265058*	8*	1,96750*	1,483247*	3,75186*	7*	,007151*
N12SDA10 N12SDA85	9,692500 8,663750	,936220 ,974635	8	1,02875	1,259846	2,30960	7	,054219
N12SDA10 N12SDA10	9,692500 9,692500	,936220 ,936220	8	0,00000	0,000000	0,00000	7	1,000000

STAT. BASIC STATS	T-test for Dependent Samples (statis01.sta) Marked differences are significant at p < ,05000							
Variable	Mean	Std.Dv.	N	Diff.	Std.Dv. Diff.	t	df	p
N15SDA75 N15SDA75	9,25750 9,25750	1,474282 1,474282	8	0,00000	0,000000	0,00000	7	1,000000
N15SDA75 N15SDA85	9,25750 10,21625	1,474282 ,765617	8	-,95875	1,394586	-1,94449	7	,092919
N15SDA75 N15SDA10	9,25750* 13,59500*	1,474282* 1,869706*	8*	-4,33750*	1,652727*	-7,42307*	7*	,000147*
N15SDA85 N15SDA75	10,21625 9,25750	,765617 1,474282	8	,95875	1,394586	1,94449	7	,092919
N15SDA85 N15SDA85	10,21625 10,21625	,765617 ,765617	8	0,00000	0,000000	0,00000	7	1,000000
N15SDA85 N15SDA10	10,21625* 13,59500*	,765617* 1,869706*	8*	-3,37875*	2,133210*	-4,47989*	7*	,002867*
N15SDA10 N15SDA75	13,59500* 9,25750*	1,869706* 1,474282*	8*	4,33750*	1,652727*	7,42307*	7*	,000147*
N15SDA10 N15SDA85	13,59500* 10,21625*	1,869706* ,765617*	8*	3,37875*	2,133210*	4,47989*	7*	,002867*
N15SDA10 N15SDA10	13,59500 13,59500	1,869706 1,869706	8	0,00000	0,000000	0,00000	7	1,000000

STAT. BASIC STATS	T-test for Dependent Samples (statis01.sta) Marked differences are significant at p < ,05000							
Variable	Mean	Std.Dv.	N	Diff.	Std.Dv. Diff.	t	df	p
N18SDA75 N18SDA75	9,53000 9,53000	,957437 ,957437	8	0,00000	0,000000	0,00000	7	1,000000
N18SDA75 N18SDA85	9,53000* 11,20500*	,957437* ,846354*	8*	-1,67500*	1,058071*	-4,47760*	7*	,002875*
N18SDA75 N18SDA10	9,53000* 15,08625*	,957437* 1,364488*	8*	-5,55625*	1,615151*	-9,73002*	7*	,000026*
N18SDA85 N18SDA75	11,20500* 9,53000*	,846354* ,957437*	8*	1,67500*	1,058071*	4,47760*	7*	,002875*
N18SDA85 N18SDA85	11,20500 11,20500	,846354 ,846354	8	0,00000	0,000000	0,00000	7	1,000000
N18SDA85 N18SDA10	11,20500* 15,08625*	,846354* 1,364488*	8*	-3,88125*	1,123228*	-9,77347*	7*	,000025*
N18SDA10 N18SDA75	15,08625* 9,53000*	1,364488* ,957437*	8*	5,55625*	1,615151*	9,73002*	7*	,000026*
N18SDA10 N18SDA85	15,08625* 11,20500*	1,364488* ,846354*	8*	3,88125*	1,123228*	9,77347*	7*	,000025*
N18SDA10 N18SDA10	15,08625 15,08625	1,364488 1,364488	8	0,00000	0,000000	0,00000	7	1,000000

APPENDIX 11

Student t-test analysis of diamond bead wear rates over elapsed time

STAT. BASIC STATS	T-test for Dependent Samples (bead-p~2.sta) Marked differences are significant at p < ,05000							
Variable	Mean	Std.Dv.	N	Diff.	Std.Dv. Diff.	t	df	p
N3SDA75P	,531250	,049552						
N3SDA75P	,531250	,049552	8	0,000000	0,000000	0,00000	7	1,000000
N3SDA75P	,531250	,049552						
N3SDA85P	,462500	,179284	8	,068750	,170477	1,14065	7	,291535
N3SDA75P	,531250*	,049552*						
N3SDA100	,278125*	,113733*	8*	,253125*	,095840*	7,47023*	7*	,000141*
N3SDA85P	,462500	,179284						
N3SDA75P	,531250	,049552	8	-,068750	,170477	-1,14065	7	,291535
N3SDA85P	,462500	,179284						
N3SDA85P	,462500	,179284	8	0,000000	0,000000	0,00000	7	1,000000
N3SDA85P	,462500*	,179284*						
N3SDA100	,278125*	,113733*	8*	,184375*	,133589*	3,90370*	7*	,005871*
N3SDA100	,278125*	,113733*						
N3SDA75P	,531250*	,049552*	8*	-,253125*	,095840*	-7,47023*	7*	,000141*
N3SDA100	,278125*	,113733*						
N3SDA85P	,462500*	,179284*	8*	-,184375*	,133589*	-3,90370*	7*	,005871*
N3SDA100	,278125	,113733						
N3SDA100	,278125	,113733	8	0,000000	0,000000	0,00000	7	1,000000

STAT. BASIC STATS	T-test for Dependent Samples (bead-p~2.sta) Marked differences are significant at p < ,05000							
Variable	Mean	Std.Dv.	N	Diff.	Std.Dv. Diff.	t	df	p
N6SDA75P N6SDA75P	2,187500 2,187500	,232916 ,232916	8	0,00000	0,000000	0,00000	7	1,000000
N6SDA75P N6SDA85P	2,187500* 1,540000*	,232916* ,409878*	8*	,64750*	,505816*	3,62070*	7*	,008502*
N6SDA75P N6SDA100	2,187500* ,962500*	,232916* ,247487*	8*	1,22500*	,376032*	9,21417*	7*	,000037*
N6SDA85P N6SDA75P	1,540000* 2,187500*	,409878* ,232916*	8*	-,64750*	,505816*	-3,62070*	7*	,008502*
N6SDA85P N6SDA85P	1,540000 1,540000	,409878 ,409878	8	0,00000	0,000000	0,00000	7	1,000000
N6SDA85P N6SDA100	1,540000* ,962500*	,409878* ,247487*	8*	,57750*	,426204*	3,83247*	7*	,006437*
N6SDA100 N6SDA75P	,962500* 2,187500*	,247487* ,232916*	8*	-1,22500*	,376032*	-9,21417*	7*	,000037*
N6SDA100 N6SDA85P	,962500* 1,540000*	,247487* ,409878*	8*	-,57750*	,426204*	-3,83247*	7*	,006437*
N6SDA100 N6SDA100	,962500 ,962500	,247487 ,247487	8	0,00000	0,000000	0,00000	7	1,000000

STAT. BASIC STATS	T-test for Dependent Samples (bead-p~2.sta) Marked differences are significant at p < ,05000							
Variable	Mean	Std.Dv.	N	Diff.	Std.Dv. Diff.	t	df	p
N9SDA75P N9SDA75P	8,103375 8,103375	1,430268 1,430268	8	0,00000	0,000000	0,0000	7	1,000000
N9SDA75P N9SDA85P	8,103375* 5,835375*	1,430268* ,997220*	8*	2,26800*	1,186772*	5,4053*	7*	,001003*
N9SDA75P N9SDA100	8,103375* 3,260250*	1,430268* ,560209*	8*	4,84313*	,984343*	13,9163*	7*	,000002*
N9SDA85P N9SDA75P	5,835375* 8,103375*	,997220* 1,430268*	8*	-2,26800*	1,186772*	-5,4053*	7*	,001003*
N9SDA85P N9SDA85P	5,835375 5,835375	,997220 ,997220	8	0,00000	0,000000	0,0000	7	1,000000
N9SDA85P N9SDA100	5,835375* 3,260250*	,997220* ,560209*	8*	2,57513*	,891869*	8,1666*	7*	,000080*
N9SDA100 N9SDA75P	3,260250* 8,103375*	,560209* 1,430268*	8*	-4,84313*	,984343*	-13,9163*	7*	,000002*
N9SDA100 N9SDA85P	3,260250* 5,835375*	,560209* ,997220*	8*	-2,57513*	,891869*	-8,1666*	7*	,000080*
N9SDA100 N9SDA100	3,260250 3,260250	,560209 ,560209	8	0,00000	0,000000	0,0000	7	1,000000

STAT. BASIC STATS	T-test for Dependent Samples (bead-p~2.sta) Marked differences are significant at p < ,05000							
Variable	Mean	Std.Dv.	N	Diff.	Std.Dv. Diff.	t	df	p
N12SDA75 N12SDA75	27,72630 27,72630	5,385860 5,385860	8	0,0000	0,000000	0,00000	7	1,000000
N12SDA75 N12SDA85	27,72630* 16,55640*	5,385860* 2,848253*	8*	11,1699*	4,707320*	6,71152*	7*	,000275*
N12SDA75 N12SDA10	27,72630* 7,82460*	5,385860* 1,920640*	8*	19,9017*	6,024701*	9,34329*	7*	,000033*
N12SDA85 N12SDA75	16,55640* 27,72630*	2,848253* 5,385860*	8*	-11,1699*	4,707320*	-6,71152*	7*	,000275*
N12SDA85 N12SDA85	16,55640 16,55640	2,848253 2,848253	8	0,0000	0,000000	0,00000	7	1,000000
N12SDA85 N12SDA10	16,55640* 7,82460*	2,848253* 1,920640*	8*	8,7318*	4,162612*	5,93312*	7*	,000580*
N12SDA10 N12SDA75	7,82460* 27,72630*	1,920640* 5,385860*	8*	-19,9017*	6,024701*	-9,34329*	7*	,000033*
N12SDA10 N12SDA85	7,82460* 16,55640*	1,920640* 2,848253*	8*	-8,7318*	4,162612*	-5,93312*	7*	,000580*
N12SDA10 N12SDA10	7,82460 7,82460	1,920640 1,920640	8	0,0000	0,000000	0,00000	7	1,000000

STAT. BASIC STATS	T-test for Dependent Samples (bead-p~2.sta) Marked differences are significant at p < ,05000							
Variable	Mean	Std.Dv.	N	Diff.	Std.Dv. Diff.	t	df	p
N15SDA75 N15SDA75	72,46260 72,46260	7,974482 7,974482	8	0,0000	0,000000	0,0000	7	1,000000
N15SDA75 N15SDA85	72,46260* 43,99920*	7,974482* 6,541912*	8*	28,4634*	9,830077*	8,1898*	7*	,000078*
N15SDA75 N15SDA10	72,46260* 21,65940*	7,974482* 4,155545*	8*	50,8032*	8,862214*	16,2141*	7*	,000001*
N15SDA85 N15SDA75	43,99920* 72,46260*	6,541912* 7,974482*	8*	-28,4634*	9,830077*	-8,1898*	7*	,000078*
N15SDA85 N15SDA85	43,99920 43,99920	6,541912 6,541912	8	0,0000	0,000000	0,0000	7	1,000000
N15SDA85 N15SDA10	43,99920* 21,65940*	6,541912* 4,155545*	8*	22,3398*	7,604688*	8,3089*	7*	,000072*
N15SDA10 N15SDA75	21,65940* 72,46260*	4,155545* 7,974482*	8*	-50,8032*	8,862214*	-16,2141*	7*	,000001*
N15SDA10 N15SDA85	21,65940* 43,99920*	4,155545* 6,541912*	8*	-22,3398*	7,604688*	-8,3089*	7*	,000072*
N15SDA10 N15SDA10	21,65940 21,65940	4,155545 4,155545	8	0,0000	0,000000	0,0000	7	1,000000

STAT. BASIC STATS	T-test for Dependent Samples (bead-p~2.sta) Marked differences are significant at p < ,05000							
Variable	Mean	Std.Dv.	N	Diff.	Std.Dv. Diff.	t	df	p
N18SDA75 N18SDA75	103,6363 103,6363	9,40192 9,40192	8	0,0000	0,00000	0,0000	7	1,000000
N18SDA75 N18SDA85	103,6363* 64,8648*	9,40192* 10,37760*	8*	38,7715*	17,75696*	6,1757*	7*	,000456*
N18SDA75 N18SDA10	103,6363* 40,8353*	9,40192* 6,90383*	8*	62,8009*	9,96243*	17,8298*	7*	,000000*
N18SDA85 N18SDA75	64,8648* 103,6363*	10,37760* 9,40192*	8*	-38,7715*	17,75696*	-6,1757*	7*	,000456*
N18SDA85 N18SDA85	64,8648 64,8648	10,37760 10,37760	8	0,0000	0,00000	0,0000	7	1,000000
N18SDA85 N18SDA10	64,8648* 40,8353*	10,37760* 6,90383*	8*	24,0295*	14,67530*	4,6313*	7*	,002394*
N18SDA10 N18SDA75	40,8353* 103,6363*	6,90383* 9,40192*	8*	-62,8009*	9,96243*	-17,8298*	7*	,000000*
N18SDA10 N18SDA85	40,8353* 64,8648*	6,90383* 10,37760*	8*	-24,0295*	14,67530*	-4,6313*	7*	,002394*
N18SDA10 N18SDA10	40,8353 40,8353	6,90383 6,90383	8	0,0000	0,00000	0,0000	7	1,000000

APPENDIX 12

Relationship between normal force and rotational torque of diamond wire beads

Fn (N)	Fq (N)	T (Nmm)
0	0.00	0.00
3	1.80	4.50
6	2.44	6.10
9	4.38	10.95
12	6.30	15.75
15	7.30	18.25
18	9.40	23.50
Shaft Diameter (mm) =		5

where

Fn is the measured normal force on the bead
Fq is the measured force to rotate the bead
T is the calculated torque to rotate the bead

Regression Output:		
Constant		0
Std Err of Y Est		0.845233
R Squared		0.989746
No. of Observations		7
Degrees of Freedom		6
X Coefficient(s)	1.263004	
Std Err of Coef.	0.029535	

APPENDIX 13

High speed video sequence 1 of diamond wire rotation at 0,75 m^2h^{-1}

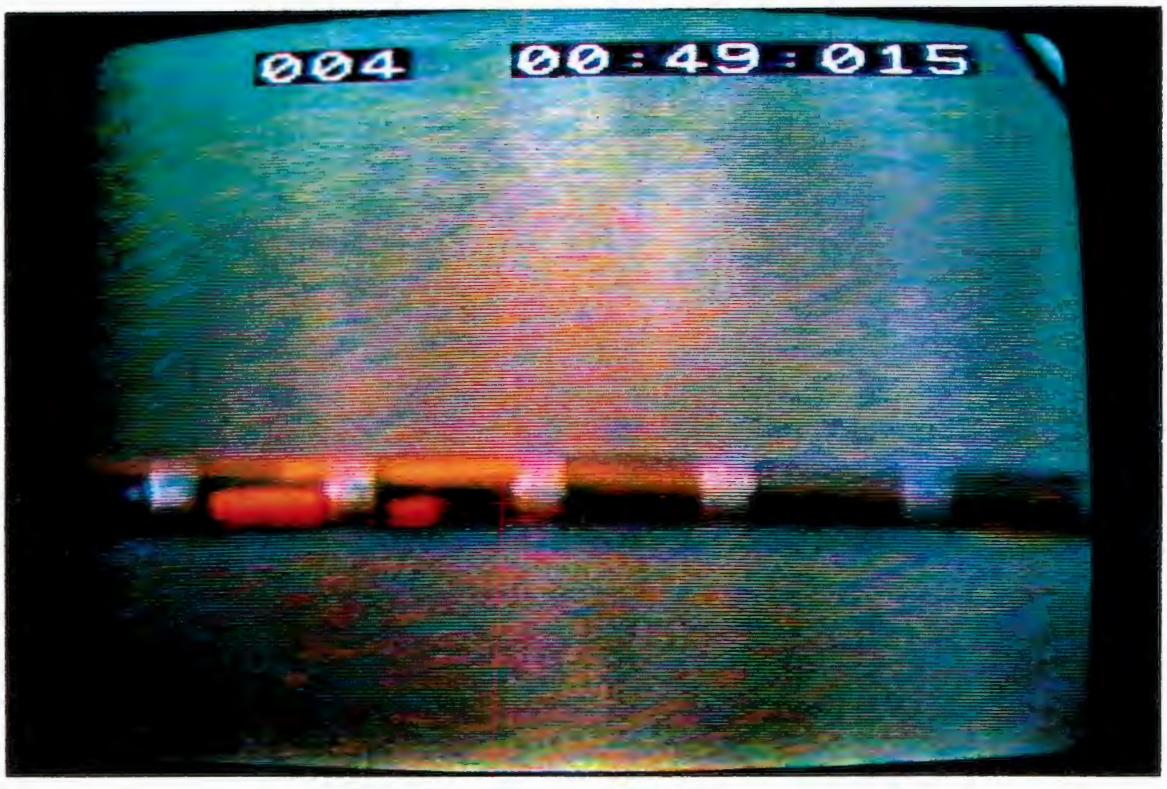

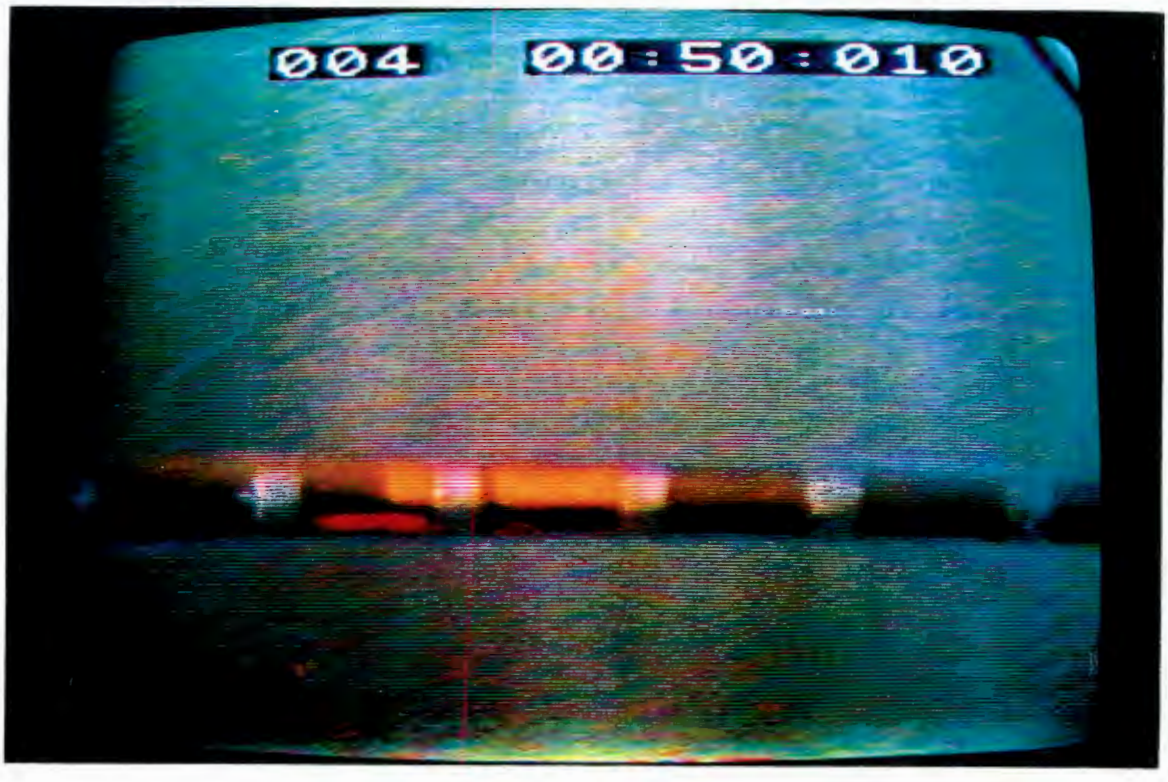

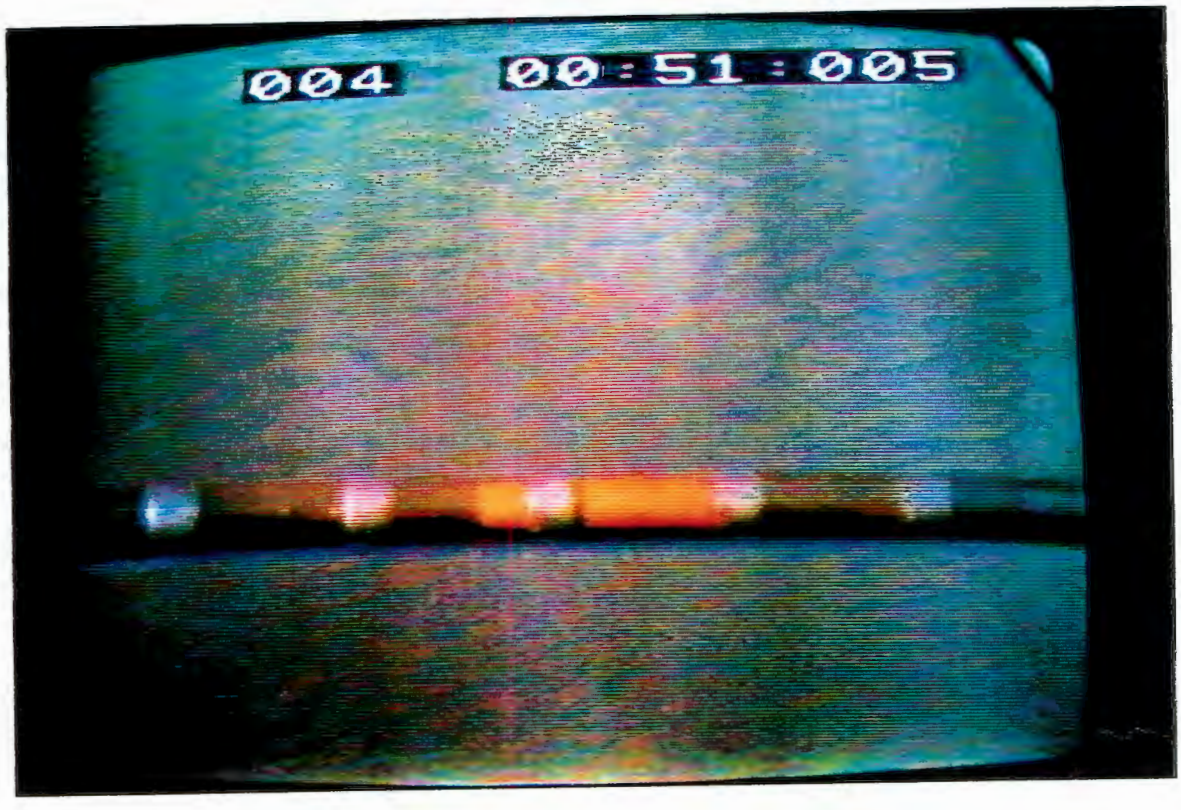
004
00:51:005


004
00:52:000


004
00:52:995


004
00:53:990

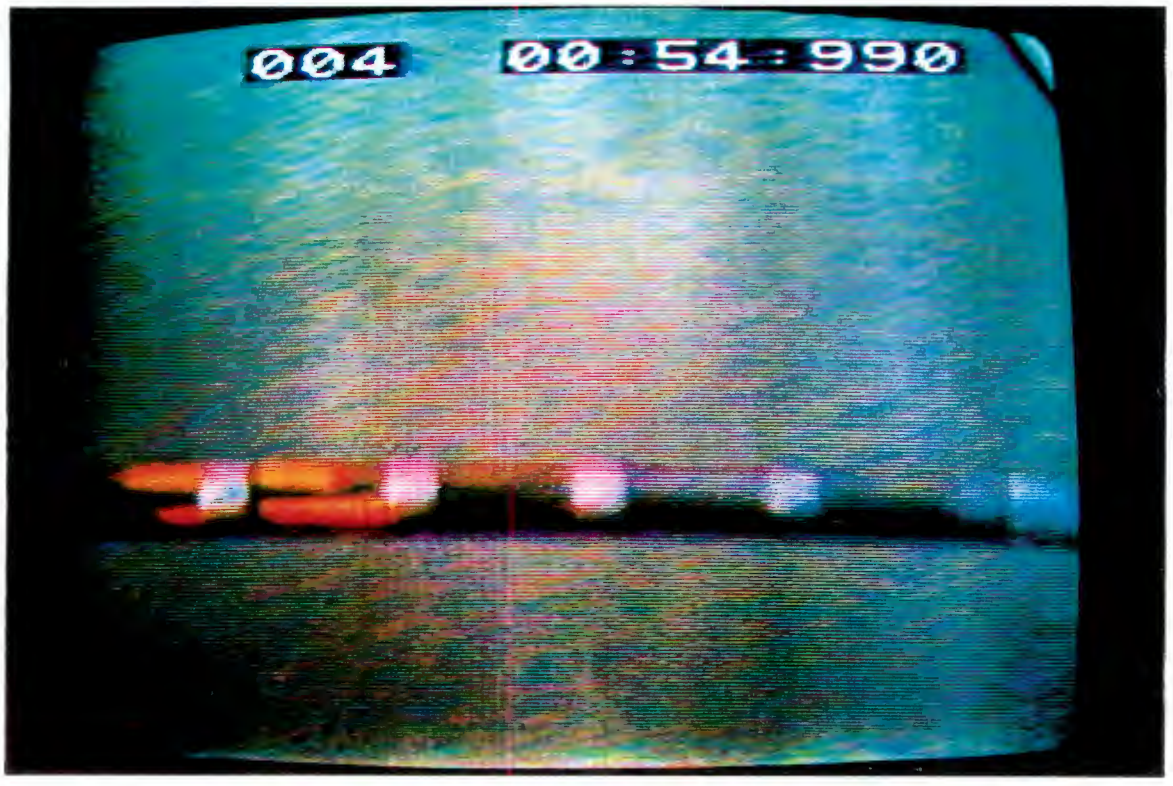
004
00:54:990


004
00:55:985

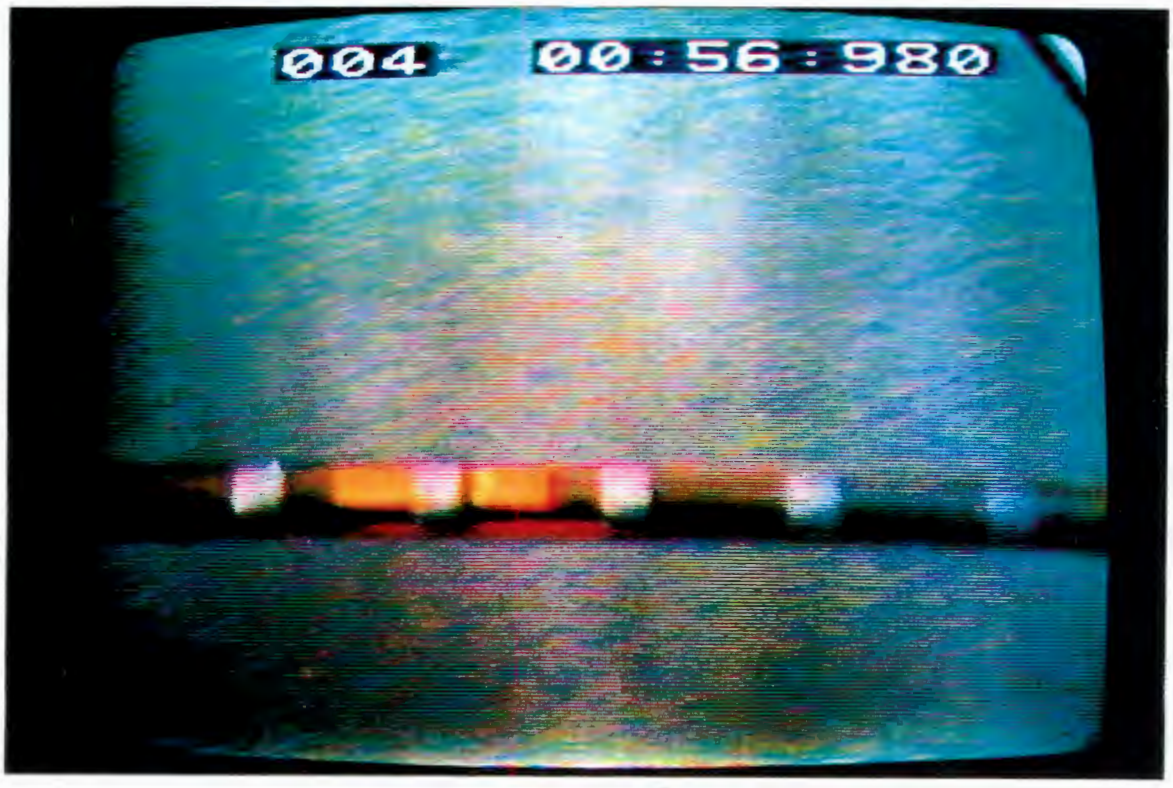
004
00:56:980


004
00:57:975

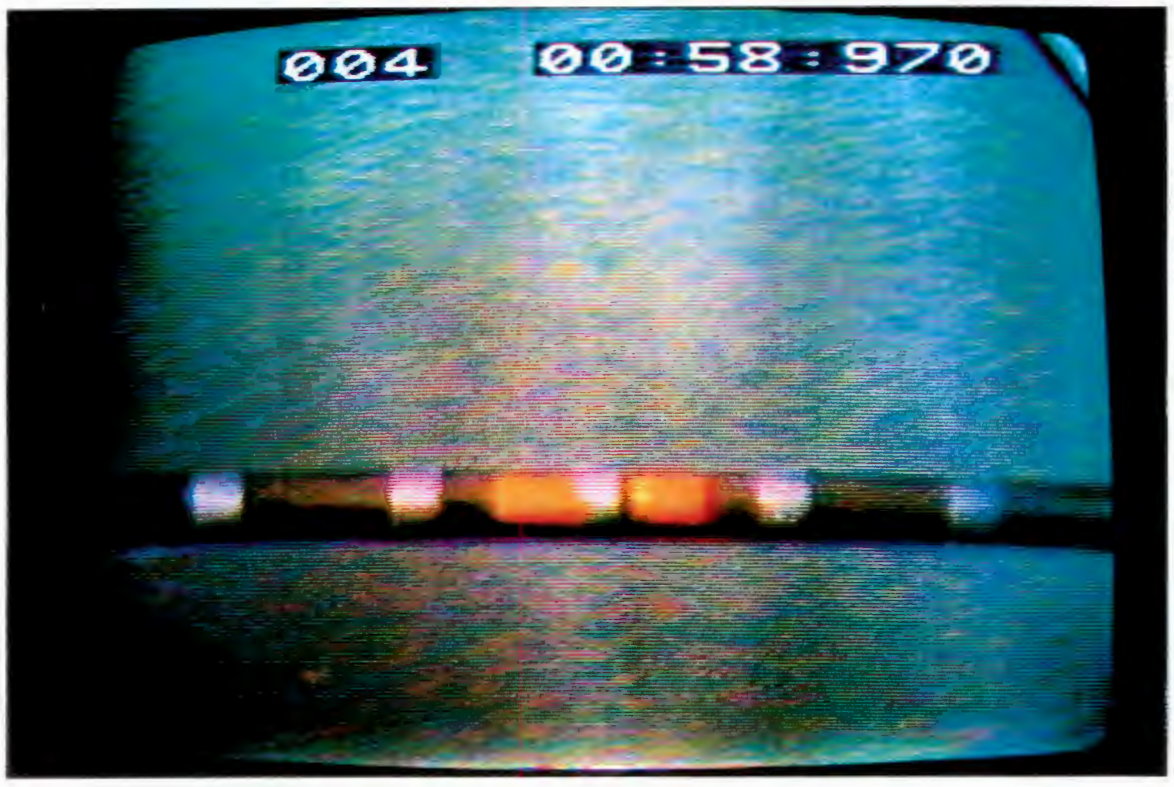
004
00:58:970


004
00:59:965

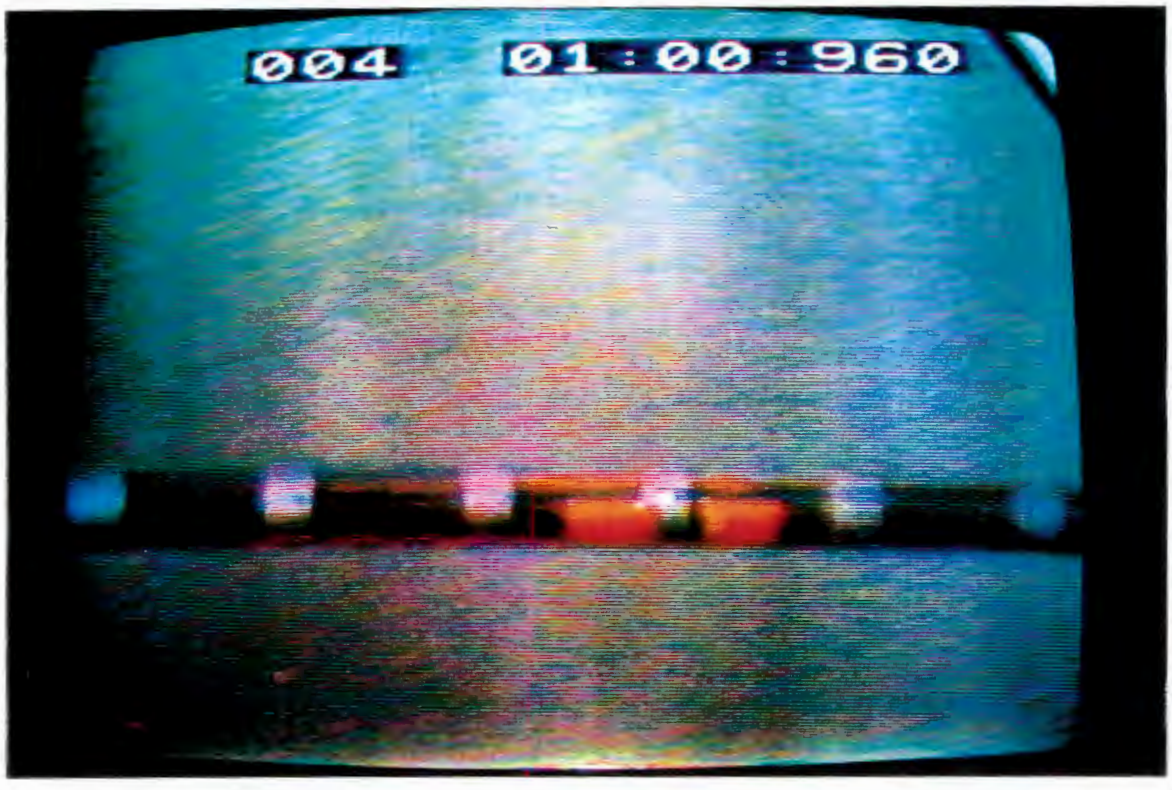
004
01:00:960


004
01:01:955

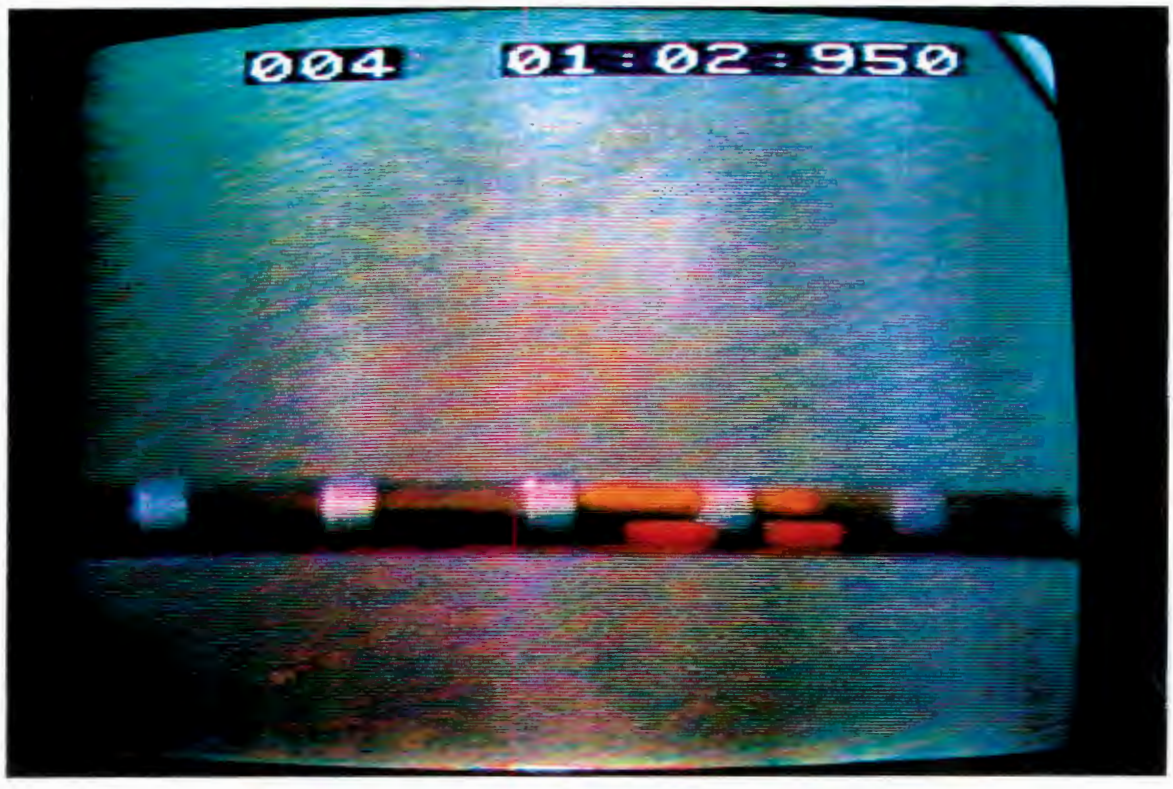
004 01:02:950


004 01:03:945

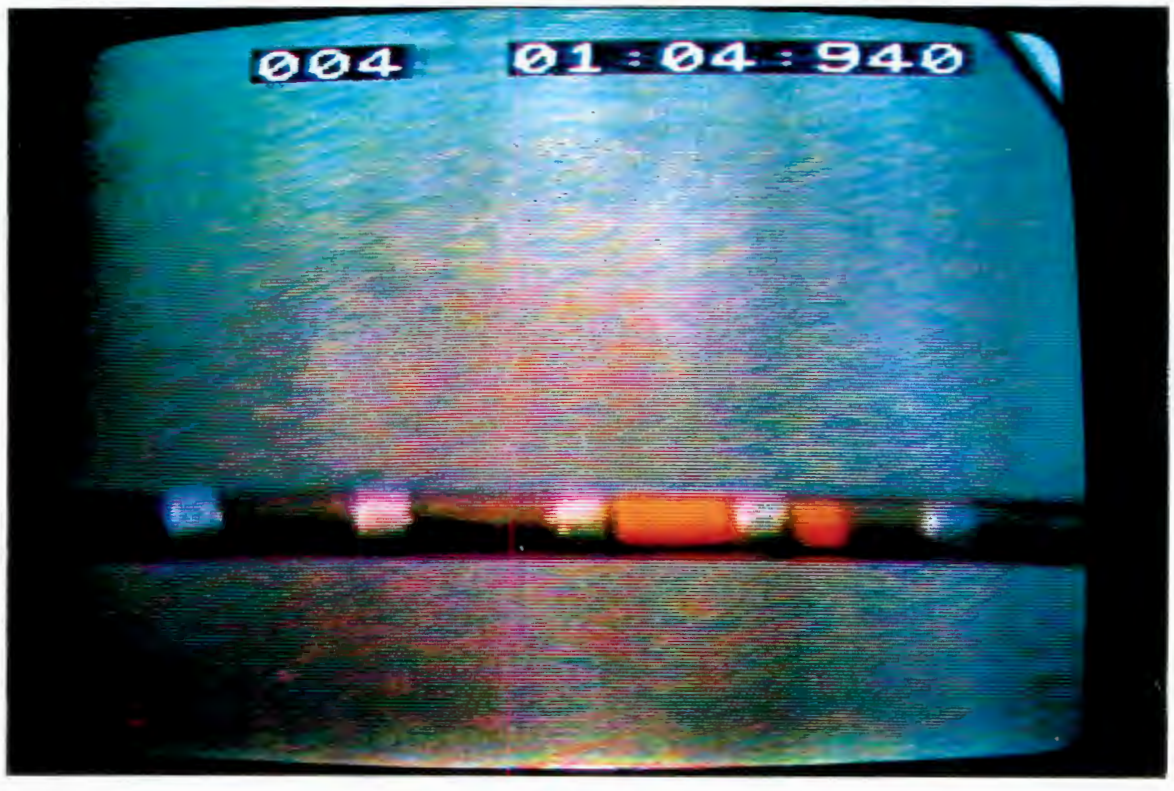
004
01:04:940


004
01:05:935

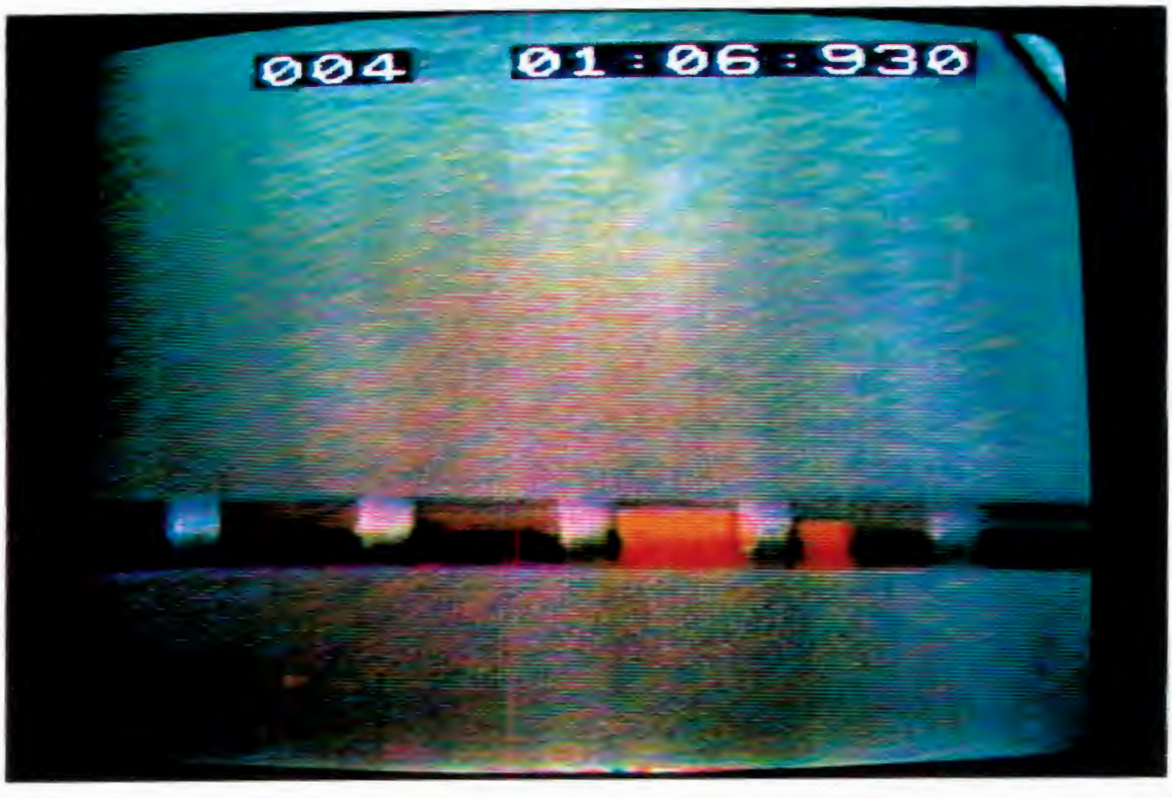
004 01:06:930


004 01:07:925

APPENDIX 13

High speed video sequence 2 of diamond wire rotation at 1,5 m^2h^{-1}

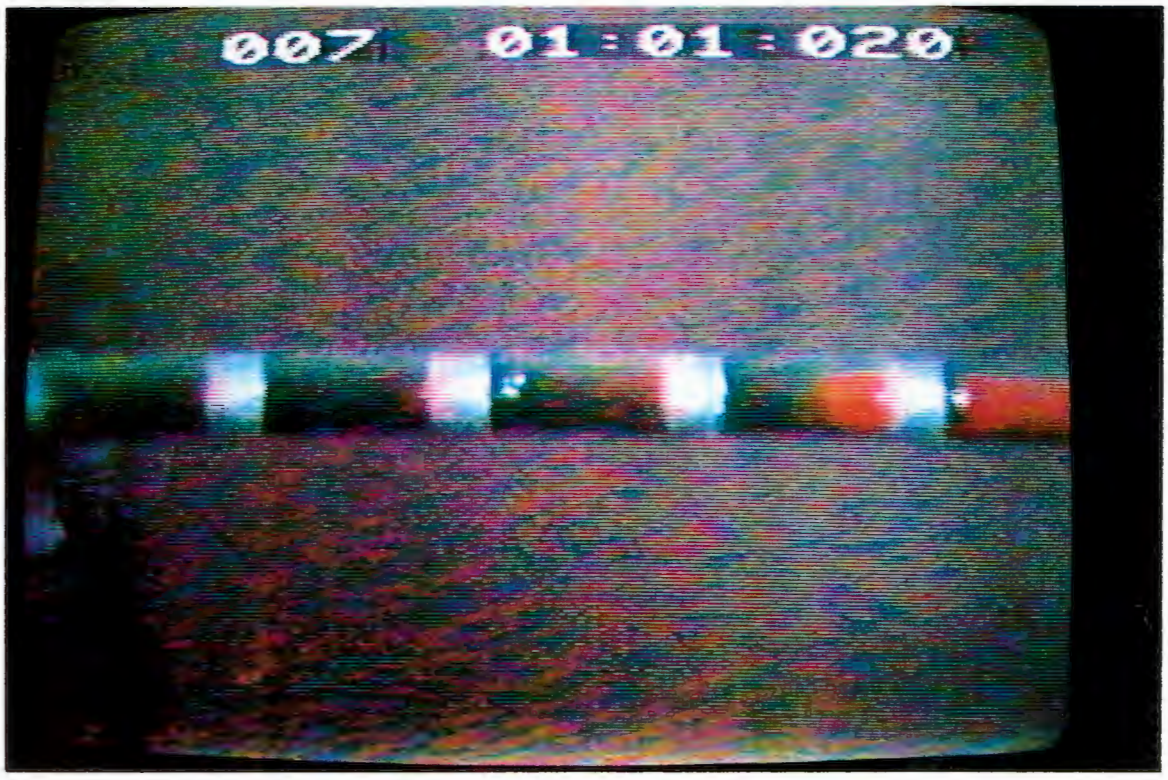

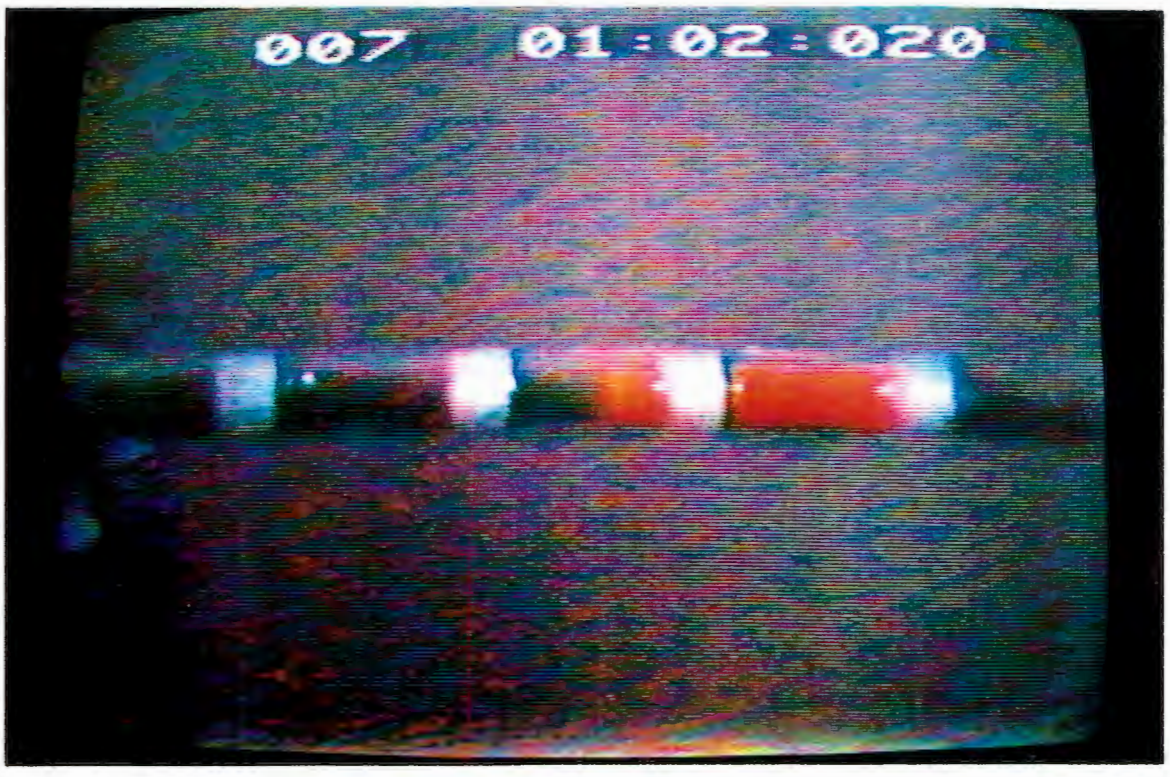

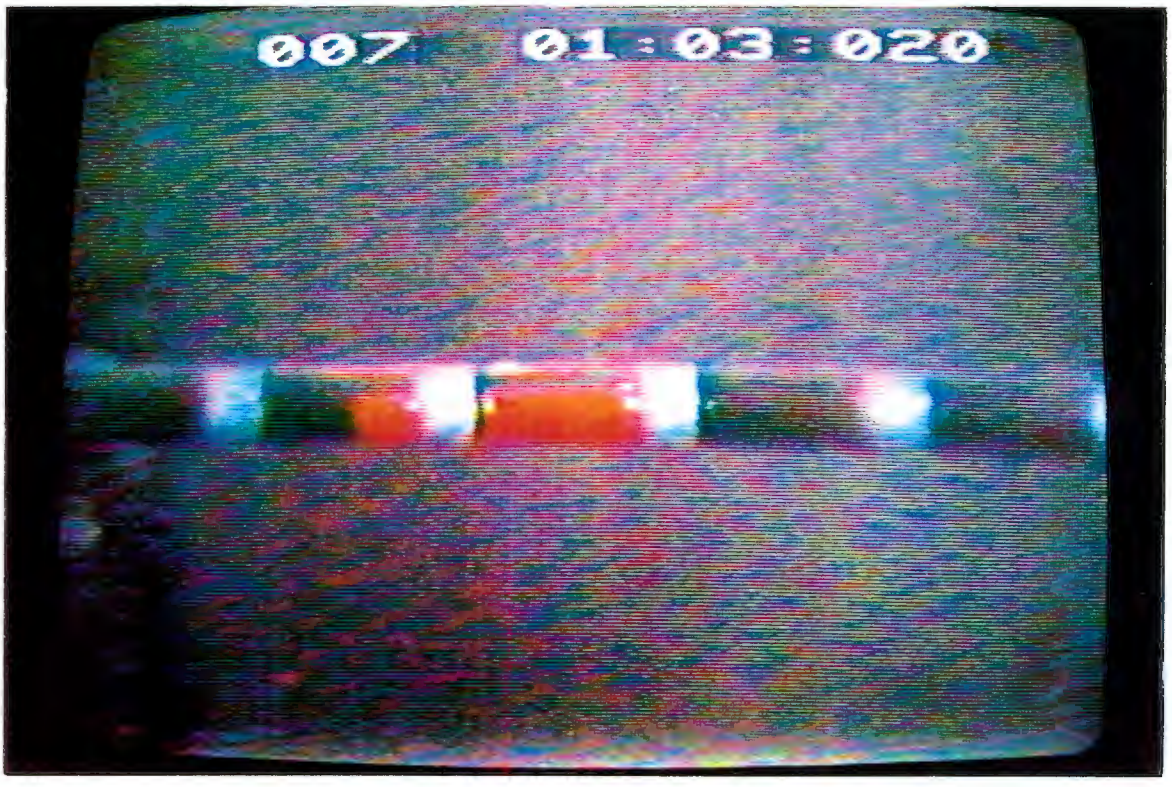
007 01:03:020


007 01:04:020

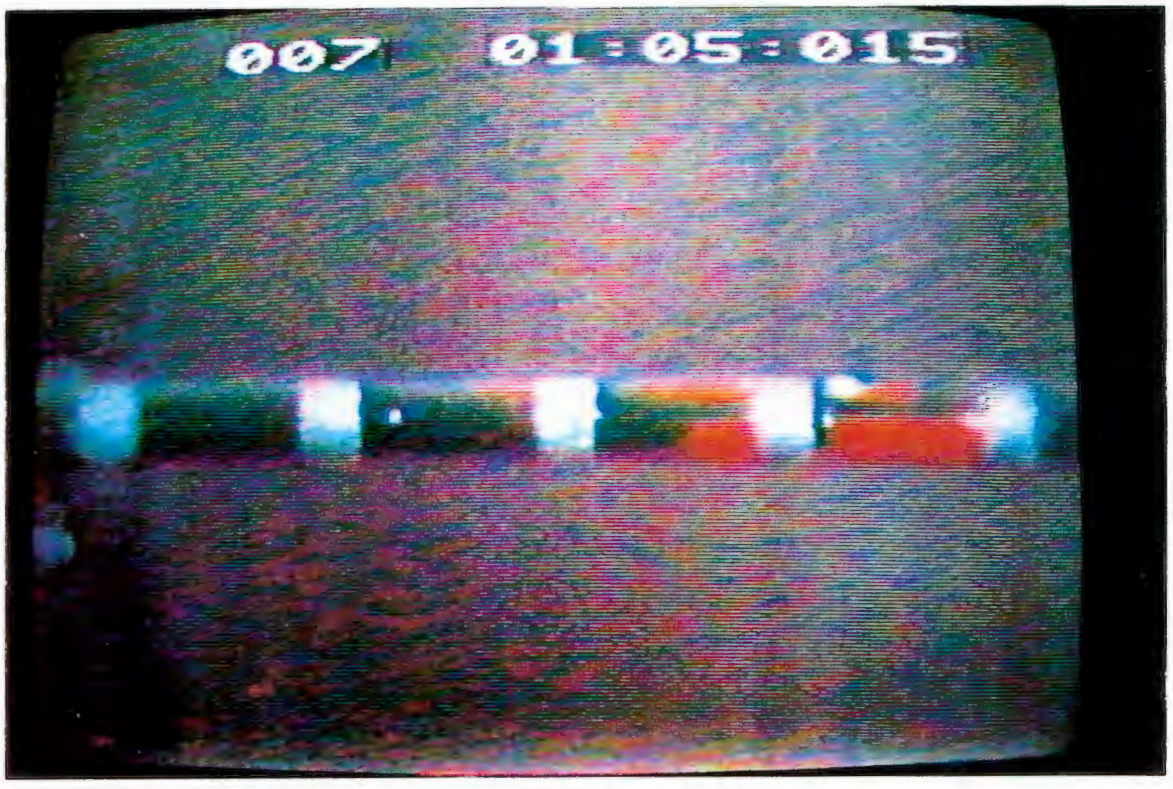
007 01:05:015


007 01:06:015


007 01:07:015

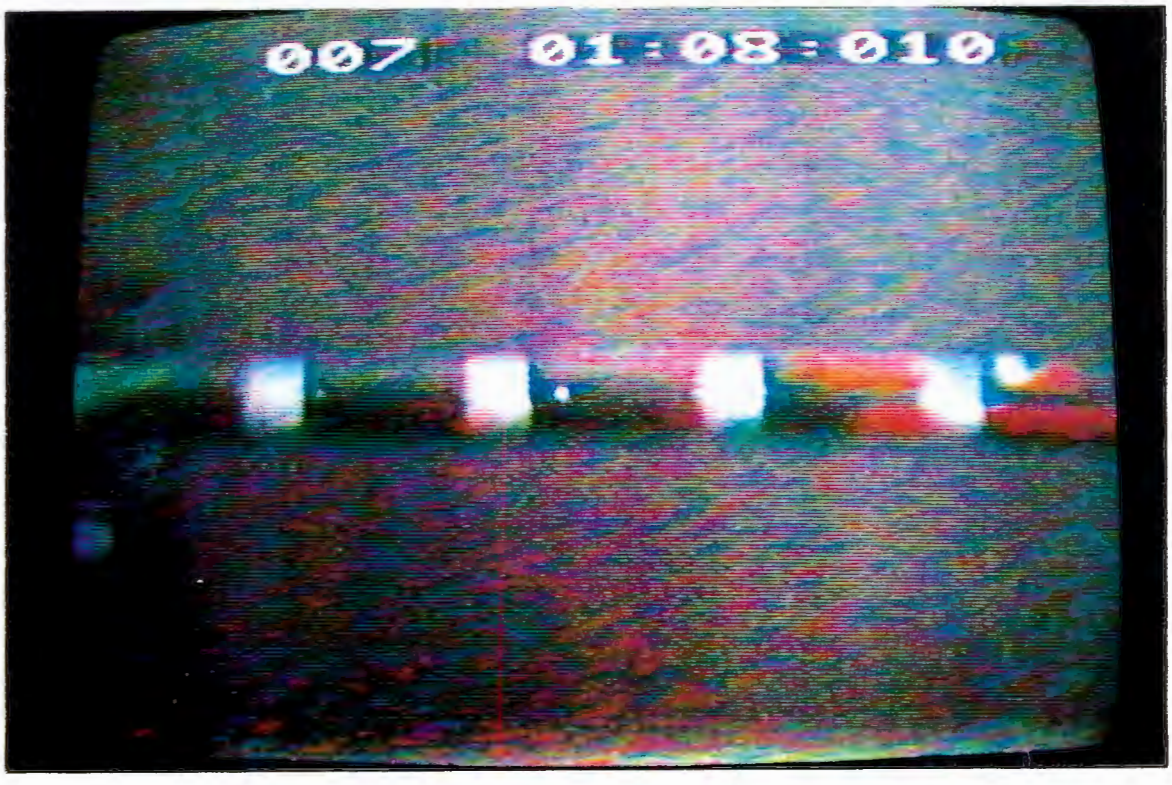
007 01:08:010


007 01:09:010


007 01:10:010


007 01:11:010


007 01:12:005

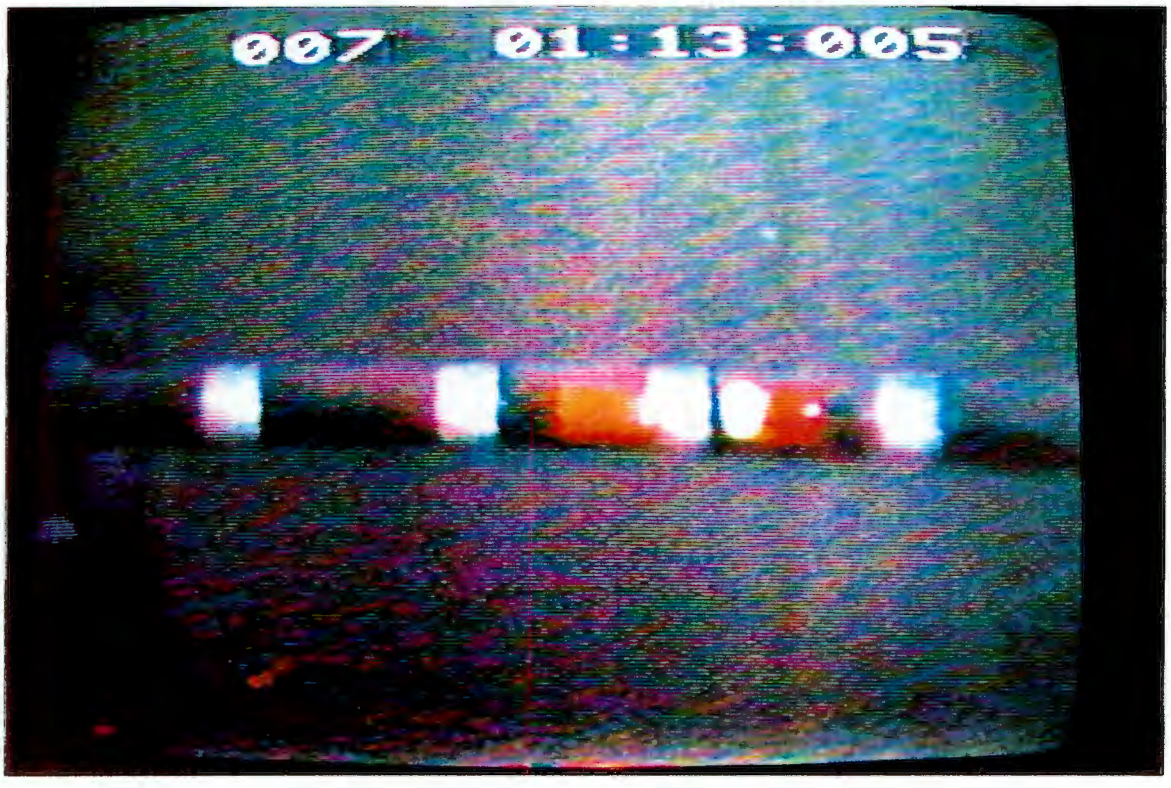
007 01:13:005

APPENDIX 13

High speed video sequence 3 of diamond wire rotation at 2,25 m^2h^{-1}

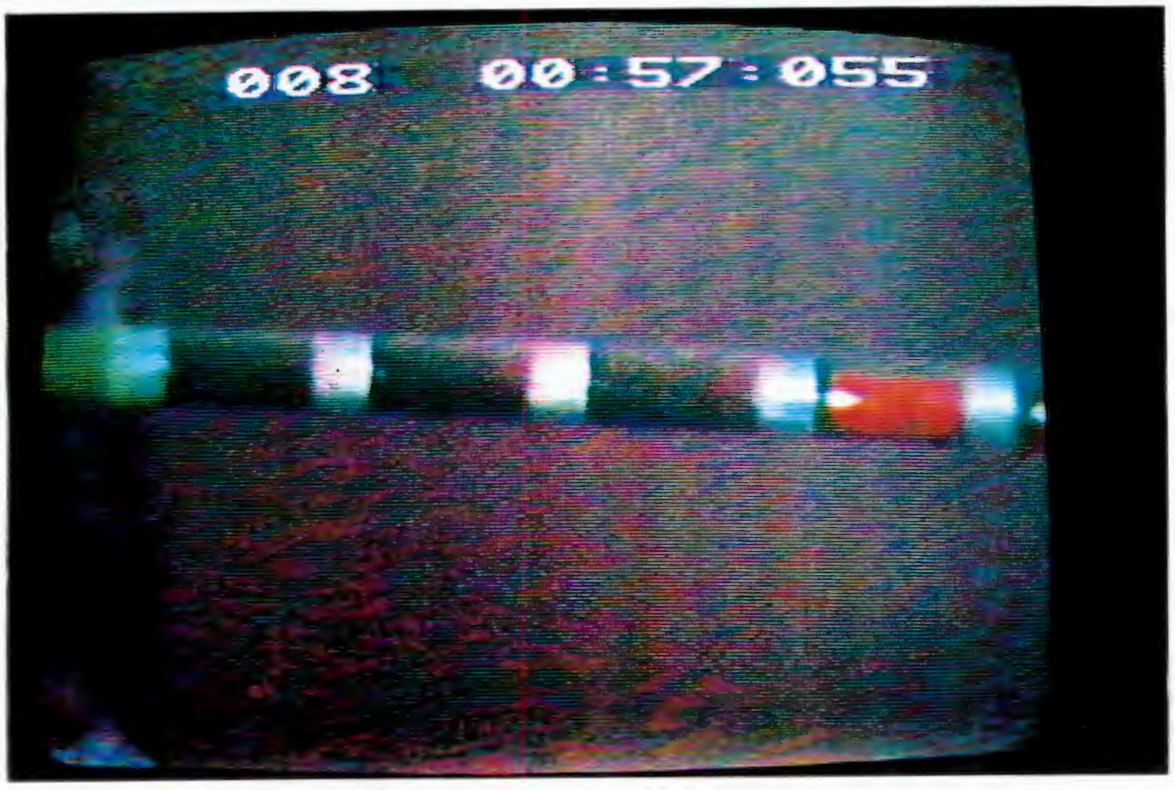
008 00:57:055


008 00:58:055


008 00:59:055


008 01:00:055

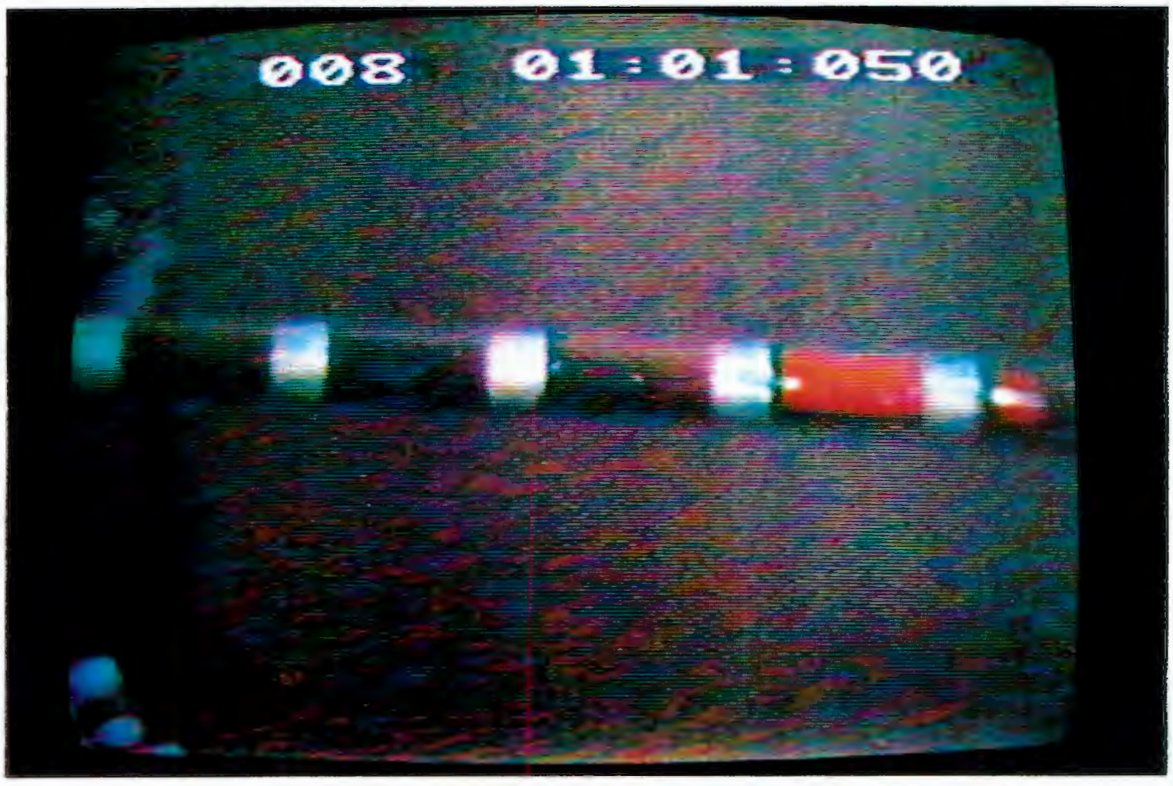
008 01:01:050


008 01:02:050

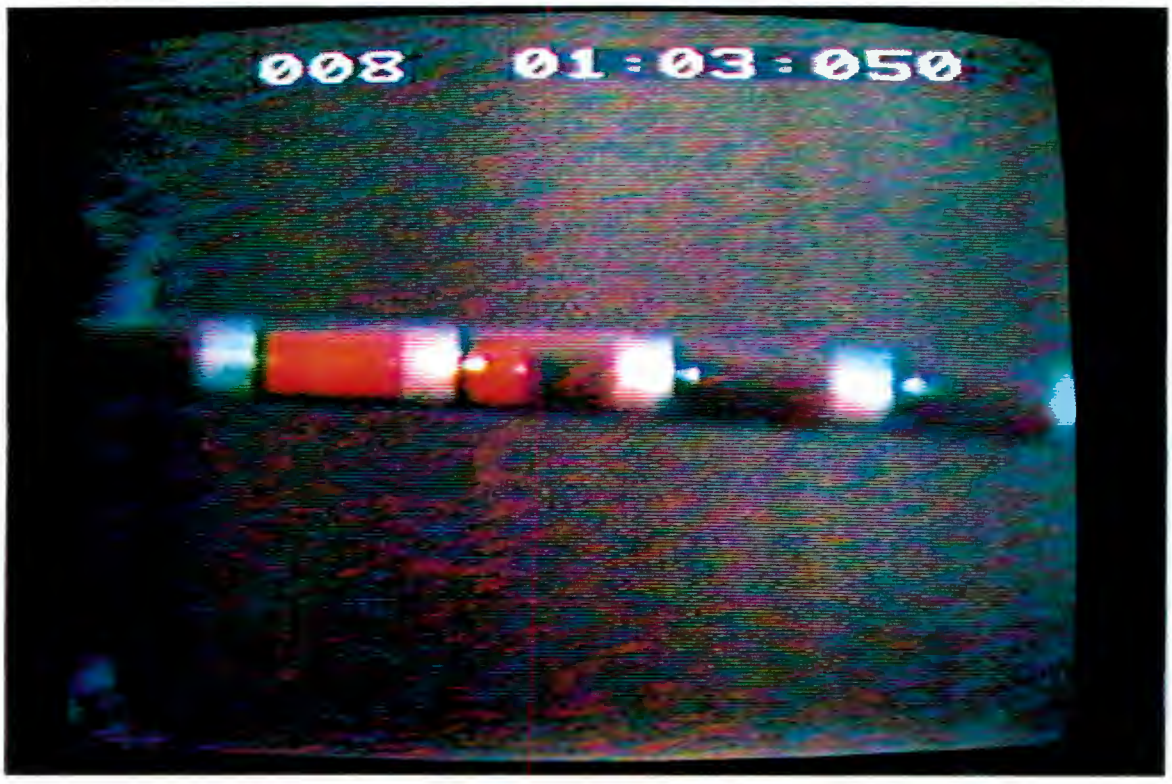
008 01:03:050


008 01:04:045


008 01:05:045


008 01:06:045

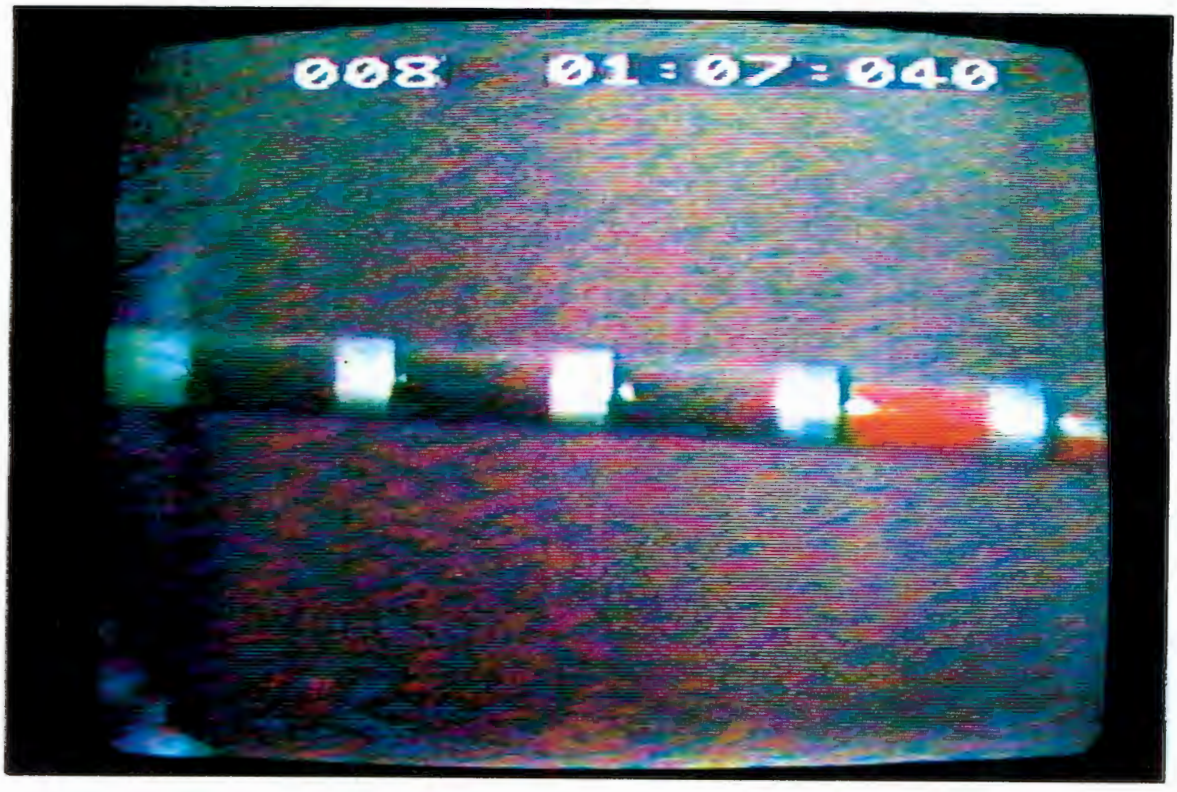
008 01:07:040


008 01:08:040